2002

Analysis of scour of cohesive soils by circular wall jets.

Ye. Liu
University of Windsor

Analysis of Scour of Cohesive Soils by Circular Wall Jets

by

Ye Liu

A Thesis
Submitted to the Faculty of Graduates Studies and Research
through the Department of Civil & Environmental Engineering
in Partial Fulfillment of the Requirements for the Degree of Master of Applied Science
at the University of Windsor

Windsor, Ontario, Canada
2002

ABSTRACT

In this thesis, scour of cohesive soils by submerged circular turbulent wall jets is investigated. Two sets of experimental data obtained by Abt (1980) and Mazurek (unpublished) are analyzed. The first set of data is a series of twelve experiments of 1000 minutes duration, where the scour in one cohesive material downstream of a culvert outlet was observed, with the tailwater mai ntained at a certain height above the culvert invert. The other set of data is an unpublished laboratory study of the scour of clays by a submerged circular wall jet produced in two cohesive soils by flow through a nozzle with a diameter of 4.9, 5.97 or 12.18 mm. Twenty-three experiments were performed to examine the shape and size of the scour holes produced in these materials in the asymptotic state.

In the present study, dimensionless scour hole profiles are developed to give the general shape of the scour holes produced by these jets in cohesive material. It is seen the scour holes have the same dimensionless shape, and this shape is consistent through the scouring process. Using dimensional analysis, a model has been developed to predict the characteristic dimensions of the scour hole, such as the maximum scour depth, the length of the scour hole, and the maximum width. These dimensions are found to correlate well with a dimensionless excess shear stress term found from dimensional analysis.

To My Family

ACKNOWLEDGEMENT

I would like to express my sincere thanks and gratitude to Dr. Kerry Mazurek for her invaluable guidance, instruction and help through the course of this study without which the work would not be accomplished. Her support in both the research funding and my personal life is also great appreciated.

Gratitude is also expressed to Dr. R. Barron, Dr. N. Biswas, Dr. G. Rankin, Dr. S. Reistma, Dr. R. Seth, Dr. E. Tam; all offered much help during my studies at the University of Windsor. Special thanks are expressed to Dr. N. Biswas for his support in the financial aid.

I also want to thank Ms. A. Samson at the Faculty of Graduate Studies and Research, Ms. J. Grondin and my graduate fellows at the Department of Civil and Environmental Engineering for their help in my studies.

Great appreciation is expressed to both my parents and my husband for their continued support and encouragement.

Table of Contents

List of Figures

List of Tables

List of Symbols

a	coefficient used by Abt
A	area of the nozzle
b	slope of the desired characteristic curve used by Abt
b	distance from the nozzle to where the scour is half the maximum scour depth
b_{cl}	distance from the centreline where the scour hole depth is half the centreline scour depth
B	half-width of the scour hole
B_m	maximum half-width of the scour hole
B_0	initial width of the scour hole
c	slope of the desired time relationship used by Abt
c_f	local skin friction coefficient
C_f	global skin friction coefficient
d	diameter of the nozzle
d_{84}	bed material size that 84 % of the soil are finer by weight
d_{16}	bed material size that 16 % of the soil are finer by weight
D	median size of the bed material
D_c	culvert diameter
D.I.	discharge intensity
F_0	densimetric particle Froude number
Fr	Froude number
g	acceleration due to gravity
H	downstream tailwater depth
U_o	velocity of the jet at the nozzle or the culvert outlet
U_m	maximum velocity at a particular distance from the nozzle
V	average fluid velocity
x	distance from the nozzle
x_o	length of the scour hole
x_m	longitudinal distance corresponding to ε_m

x_w	location of the maximum width
R	Reynolds number
Sn_{mod}	Modified Shear Number
t_0	any time less than or equal to 1000 minutes
t	equal to 1000 minutes
V_s	volume of scour hole
w	width of the scour hole
τ_o	bed shear stress
ρ	density of the fluid
$\Delta\rho$	difference between the density of the bed material and the density of the fluid
ε_{cl}	scour hole depth on the centreline
ε_m	maximum depth of scour hole at asymptotic state
σ_g	standard deviation of bed material size
μ	dynamic viscosity of the eroding fluid
λ	jet parameter, equal to ρU_0^2
λ_c	critical value of λ below which no erosion occurs
z	horizontal distance across the jet measured from the jet centreline

CHAPTER 1 INTRODUCTION

1.1 Introduction

Local scour caused by water jets is a problem of considerable importance in hydraulic engineering. Scour by jets occurs downstream of many hydraulic structures, such as submerged sluiced gates, stilling basins, diversion works and outlets of culverts. Scour can undermine the foundation of a structure and thus leads to its failure. In addition to the loss of the structure, the failure may then be followed by flooding and erosion of the surrounding area, which may potentially result in loss of life and damage to the environment (Abida and Townsend, 1991). Restoration costs are high. It is thus an essential feature in the hydraulic design to estimate scour produced downstream of hydraulic structures, so that adequate protection can be provided to reduce these risks.

The term "jet" is used to describe the flow of fluid having a higher velocity emitted into surrounding fluid of lower or no velocity (Rajaratram, 1976). A jet may be two-dimensional or three-dimensional depending on its geometry, and unsubmerged or submerged, depending on the tailwater depth. The location of the jet relative to the undisturbed bed level defines whether it is a wall jet, where it is set so that it flows directly along the boundary; or a horizontal offset jet, where the jet flows parallel to the bed but is set a small distance above the bed; or an impinging jet, where the jet impinges onto the bed or boundary.

Considerable work has been done on the scour of cohesionless materials, whereas, cohesive soils have received little attention. This is despite the fact that there are many cohesive soils of widely varying composition found in practice. The study presented herein focuses on the scour of cohesive soils by submerged circular turbulent wall jets,

which models scour downstream of culverts. Two sets of experimental data obtained by Abt (1980) and Mazurek (unpublished) are analyzed. The first set of data is a series of experiments on scour downstream of culvert outlets in one cohesive material at prototype scale. The other set of data is an unpublished laboratory study of the scour of clays by a submerged circular wall jet produced in two cohesive soils by a nozzle with three different diameters.

1.2 Objectives

The objectives of this study are:

1. To determine the characteristics of scour in cohesive materials by circular wall jets. This includes study of the dimensions of the scour hole and its development with time.
2. To develop a method of predicting the scour hole dimensions from the properties of the jet and the clay.

1.3 Organization of the Thesis

This thesis is organized into five chapters. Chapter 2 is a review of literature, which gives a brief overview of jets and circular wall jets, a summary of the general observations of scour in both cohesionless and cohesive materials and a detailed review of previous studies of scour by circular jets in cohesionless soils (there are no previous studies of erosion in cohesive soils by circular wall jets found in the literature). Chapter 3 discusses experimental setups of Abt (1980) and Mazurek (unpublished). Chapter 4 presents the results and analysis of scour from the two sets of data. Finally, Chapter 5 includes conclusions developed and suggestion for future work.

CHAPTER 2 LITERATURE REVIEW

2.1 Introduction

This chapter includes a review of the behavior of turbulent jets and the characteristics of scour by jets in both cohesionless and cohesive soils. The jet of most interest is the turbulent circular wall jet, as mentioned in chapter 1, because it closely models flow at the outlet of culverts. Although this thesis is focused on scour in cohesive soils by these wall jets, review of scour by jets in cohesionless soils is also discussed because of the important observations of scour that might also be applied to cohesive soils.

2.2 Jets

A jet is defined as a high velocity flow of fluid that enters a lower velocity or stagnant region (Rajaratnam, 1976). The jet may be two-dimensional or three-dimensional, unsubmerged or submerged, depending on the tailwater depth, and of many different geometries. A jet may be impinging, where the jet impinges onto the bed or boundary, or a wall jet, where it flows directly along a boundary, or a horizontal offset jet, where the jet flows parallel to the bed but is set a small distance above the bed. Jets are formed downstream of submerged sluiced gates, stilling basins, diversion works and at outlets of culverts. A circular wall jet is a wall jet produced from a circular origin, such as a nozzle or orifice. The flow at the outlets of culverts and storm drainage pipes are examples of circular wall jets.

Experimental observations on circular wall jets (Abramovich, 1963; Rajaratnam, 1976) show that there is a core of flow with a velocity equal to the velocity at the jet origin referred to as the "potential core". The region from the jet origin or nozzle to the

end of this potential core is known as the flow development region. Beyond this region, away from the end of the potential core, is known as the fully established flow region (Fig. 2.1). The velocity along the jet centreline decays with x (Pani, 1972; Rajaratnam and Pani, 1974), where x is the distance from the nozzle. As well, in the fully established flow zone, it is found that for the velocity profile across the width of the jet at any x-section, the velocity decreases continuously from a maximum velocity on the axis to zero at a large radial distance. The velocity distributions at different x-sections beyond approximately 20 jet diameters also appear to have the same shape. For the vertical velocity profile, these profiles also have the same shape at each x. The bottom part of the profile develops from the growing boundary layer (on the wall) and the upper portion behaves like a free jet (a jet that is not near any boundary) (Rajaratnam, 1976), as seen in Fig. 2.1.

There have been many studies of the boundary shear stresses created by these jets, which is important information for studying erosion, as it is thought that it is the bed shear stresses that control erosion and deposition (for a discussion, one can see Raudkivi, 1998). It was found in experimental observations that the boundary shear stress on the jet centreline decreases with x (Sforza and Herbst 1967; Pani, 1972; Rajaratnam and Pani, 1974), as seen in Fig. 2.2. In Fig. 2.2, the bed or boundary shear stress is represented by the global skin friction coefficient $C_f = \frac{\tau_0}{\frac{1}{2}\rho U_0^2}$, where τ_0 is the bed shear stress, ρ is the density of the fluid, and U_0 is the velocity of the jet at the nozzle, x is the distance from the nozzle and A is the area of the nozzle. In this region $\tau_0 \propto x^2$. It is seen that near the nozzle, the bed shear stresses are maximum and $C_f \approx 0.005$. Figure 2.3 shows the

variation of the shear stress across the width of the jet, where z is the horizontal distance across the jet measured from the jet centreline.

Experimental observations also show that the local skin friction coefficient $c_f = \frac{\tau_0}{\frac{1}{2}\rho U_m^2}$ is constant in the fully developed flow region (Sforza and Herbst 1967; Pani, 1972), where c_f is the local skin friction coefficient and U_m is the maximum velocity at a particular distance x from the nozzle. For various jet shapes (rectangular and circular) and $x/\sqrt{A}$ greater than about 50, where A is the area of the nozzle, the boundary shear stress coefficient c_f was constant around 0.0065 (Pani, 1972).

2.3 Scour by Circular Wall Jets

Most of the studies on scour have been empirical because of the complexity of the physical processes involved. The characteristics of the jet flow, such as velocity and geometry, and that of the bed material, such as particle size and density, are known to affect scour. There have been many attempts to understand the characteristics of scour by circular wall jets in cohesionless materials, such as the scour experiments in sand by Laushey et al. (1967), Rajaratnam and Berry (1977), Rajaratnam (1981), Lim and Chin (1992) and Lim (1995). Some of these studies were made on prototype size culverts, such as those by Laushey et al. (1967), Opie (1967), and Stevens (1969).

Laushey et al. (1967) found that the volume eroded was proportional to the logarithm of time and the equilibrium depth was proportional to the cube root of the volume. Also, in a certain part of the scouring process, the maximum depth of scour or any other significant length scale of the scour process increased linearly with the logarithm of time, where the time was measured from the beginning of scour. This was

confirmed by Rajaratnam and Berry (1977), with the finding that any characteristic dimension of scour also varied linearly with the logarithm of time until near the end of scour, where the variation becomes non-linear and the scouring rate slows to near zero. It was noticed that after a sufficiently long time, the scour hole eventually reaches a size where the rate of change in size is very small (approaching zero). This is called the equilibrium, asymptotic, or ultimate state.

Opie (1967) and Stevens (1969) found that the scour hole parameters were related to material shape, size, culvert diameter and discharges. Bohan (1970) and Fletcher and Grace (1972) correlated the scour hole dimensions with tailwater conditions (both lower and greater than one half of the pipe diameter), culvert diameter, time of discharge, and Froude number (defined as $Fr=Vg^{-0.5}D_c^{-0.5}$, where V is the average fluid velocity, g is the acceleration due to gravity and D_c is the culvert diameter).

Rajaratnam and Berry (1977) found that scour holes are similar in geometric configuration and appearance (the shape is sketched in Fig. 2.4), such as centreline profile, maximum depth, width and length, contours and volume of the scour hole (i.e. the scour holes have the same general shape). Rajaratnam and Diebel (1981) and Lim (1995) also observed this behavior. The characteristic dimensions of the eroded bed, such as the maximum depth of scour, the length of the scour hole and the scour hole width were functions of the densimetric Froude number F_0, defined as $U_0/(gD\Delta\rho/\rho)^{0.5}$, where U_0 is the jet velocity at the outlet, D is the median size of the bed material, $\Delta\rho$ is the difference between the density of the bed material and the density of the fluid and g is the acceleration due to gravity. The densimetric Froude number can be interpreted as the ratio of the shear stress (the driving force of erosion) on the bed to the buoyant unit

weight of particles (the erosion resisting forces). This result was obtained using dimensionless analysis by noting that the maximum depth of scour for the asymptotic state ε_m can be expressed by (Rajaratnam and Berry, 1977):

$$\varepsilon_m = f(U_0, d, D, g\Delta\rho, \rho, \nu)$$

where d is the jet diameter and ν is the kinematic viscosity of the fluid. The densimetric Froude number works well to correlate the scour hole dimensions to the properties of the flow and the soil bed for cohesionless materials.

Lim and Chin (1992) investigated the local scour caused by deeply submerged circular wall jets on uniform and non-uniform sediment beds, where the term "non-uniform" refers to the bed material graduation and is reflected by the grain standard deviation of bed material size σ_g, defined as $\sigma_g = (d_{84}/d_{16})^{0.5}$, where d_{84} refers to the bed material size that 84 % of the soil are finer by weight and d_{16} refers to the bed material size that 16 % of the particles in the soil are finer by weight. It was seen that dunes or ridges formed downstream of the scour hole. As the scour hole increased in size with time, so did the size of the dune. The height of the dune attained an equilibrium height after a certain time. It was also found that the time required for tests with non-uniform sediment to reach the equilibrium scour condition is shorter compared to that with uniform sediment.

The effects of tailwater depth of a culvert were investigated by several researchers. Ali and Lim (1986) reported that asymptotic scour depth was dependent on the tailwater depth and a critical tailwater existed beyond which an increase or a decrease in tailwater causes an increase in the asymptotic scour depth for the range $1<H/D_c<14.5$, where H is the downstream tailwater depth and D_c is diameter of the culvert. They also

indicated that the tailwater effect becomes insignificant for H/d>16. Rajaratnam and Diebel (1981) found that low tailwater and small width of the downstream channel do not affect the maximum depth of erosion significantly while it reduces the value of the distance at which the maximum erosion occurs significantly. Day et al. (2001) found that tailwater depth has an effect on maximum scour depth for $0.5<H/d<2$ and $2.5<F_0<10$, with an increase in F_0 resulting in an increase in scour depth while an increase in tailwater depth caused a reduction in scour depth.

2.4 Scour by Jets in Cohesive Soils

Cohesive soil erosion and scour in cohesive materials has been studied much less than scour and erosion of sand. For sand, the resistance to erosion is primarily due to the buoyant weight of the particle, described by D, $\Delta\rho$ and g. Erosion occurs by removal of individual particles. In clays and cohesive materials, however, the particles "stick together" by electrochemical forces (the balance between the repulsive forces of the clay particles and the Van der Waals forces between the particles) and it is these electrochemical forces that control cohesive soil erosion resistance (Dunn 1959; Partheniades, 1965; Paaswell, 1973). There are many factors that affect these electrochemical forces, such as the density and fabric of the soil and the pore and eroding water chemistry and temperature (Paaswell, 1973). Also, observations show that clay soils do not erode in one manner; instead, they demonstrate a number of different types of erosion depending on the soil properties and the shear stress on the bed (Mazurek et al., 1999). There appears to be two common forms of erosion in cohesive soils. "Surface erosion" is erosion particle by particle or flocs or aggregates and occurs only near the surface of the bed; "mass"or "bulk" erosion removes material in clumps or lumps from

below the surface of the bed. As such, erosion of cohesive soils has been more difficult to understand than the erosion of cohesionless soils.

There have been some studies of scour by jets in cohesive material (Dunn 1959; Moore and Masch, 1962; Abt, 1980; Hedges, 1990; Mazurek, 2001), almost all with impinging jets. Moore and Masch (1962) used a submerged vertical circular impinging jet to examine the evolution of scour in three clays. Results showed that the average scour hole depth grew in a linear relation with the logarithm of time. However, there were discontinuities in the curves when large chunks of clay were suddenly removed. Mazurek (2001) showed that the scour holes grew to an asymptotic or equilibrium state, similar to cohesionless materials.

Abt (1980) and Mazurek (2001) are two of the few studies that examine scour in cohesive soils. Abt (1980) studied the scour produced downstream of culverts (similar to that produced by circular wall jets) in one cohesive soil. Mazurek (2001) studied erosion by plane wall jets, also in one cohesive soil. It was observed by Abt that the scour holes were similar in geometric configuration independent of culvert diameter and discharge and approximately 70 % of the maximum depth, length and width of scour occurred in the initial 3 % of scouring time (Abt, 1980). He also correlated the soil properties of shear strength and plasticity index, the hydraulic properties of fluid density and velocity, and the culvert diameter to the depth, length, width, volume and time of scour in the form of equations to estimate the scour hole characteristics (Abt, 1980). A detailed discussion of Abt's work is given in chapter 4.

Mazurek (2001) found by experiments that the scour holes were formed primarily by mass erosion, however rapid surface erosion was also observed in the very early times.

The dimensionless longitudinal scour hole profiles at equilibrium could be divided into four types based on their shapes. Also, the scour hole dimensions, such as depth and length, appeared to grow in a linear relation with the logarithm of time (Mazurek, 2001). Mazurek correlated the dimensions of the scour hole at equilibrium with the parameter $\lambda = \rho U_o^2$ and reported there was a critical value of λ below which significant erosion did not occur (Mazurek, 2001). This value of λ was then related to the critical shear stress of the soil τ_c. The critical shear stress is defined as the bed shear stress at which the erosion rate goes to zero or below which there is no erosion (also discussed in Raudkivi, 1998).

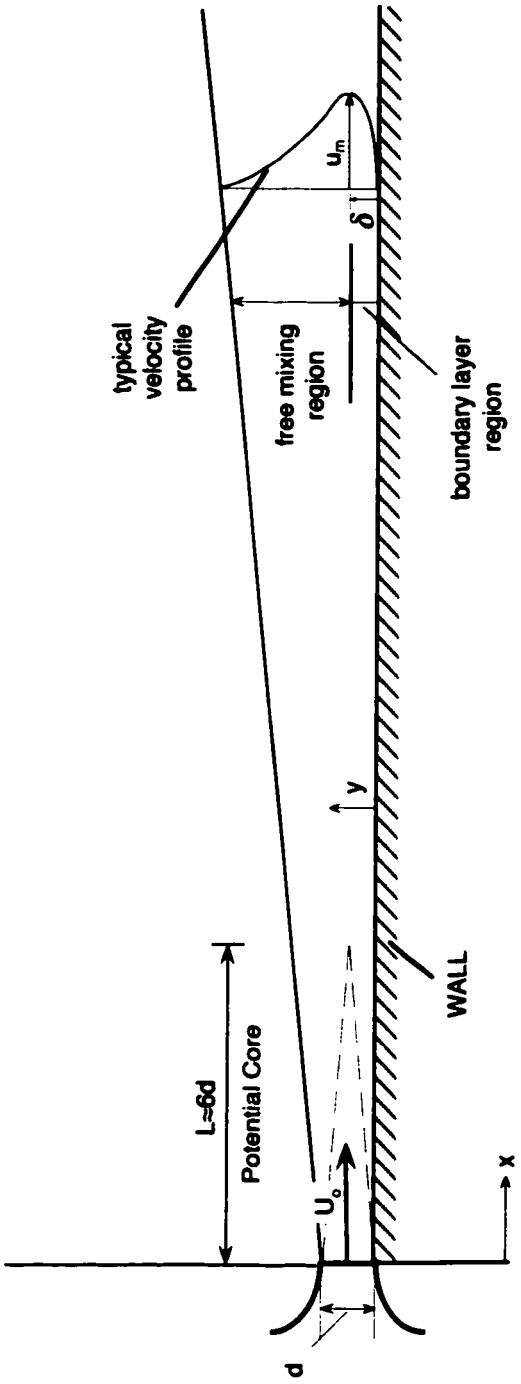

Figure 2.1 Side view of circular turbulent wall jet.

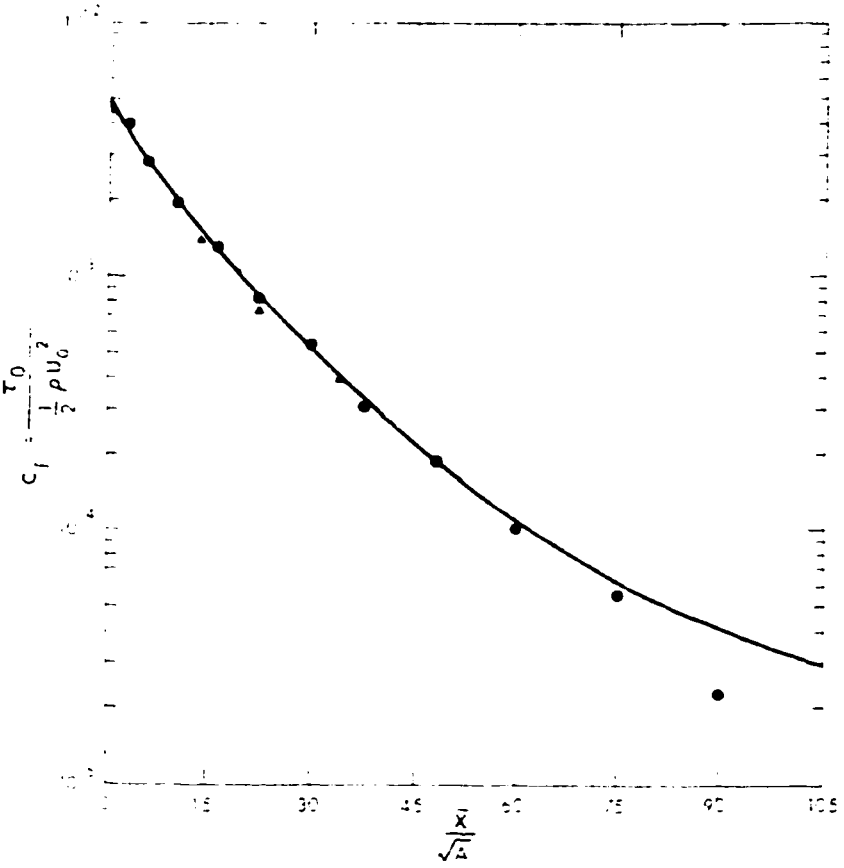

Figure 2.2 Variation of the wall shear stress with distance from the nozzle (adapted from Rajaratnam, 1976).

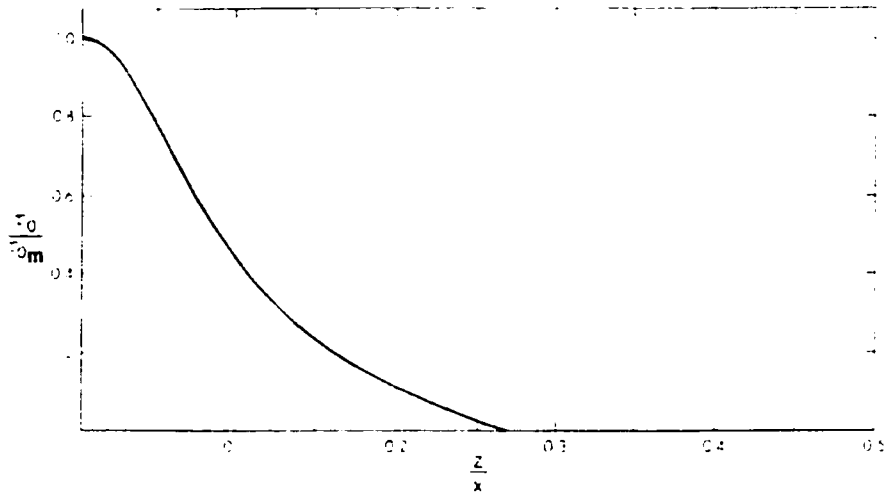

Figure 2.3 Variation of the shear stress across the width of the jet (adapted from Rajaratnam, 1976).

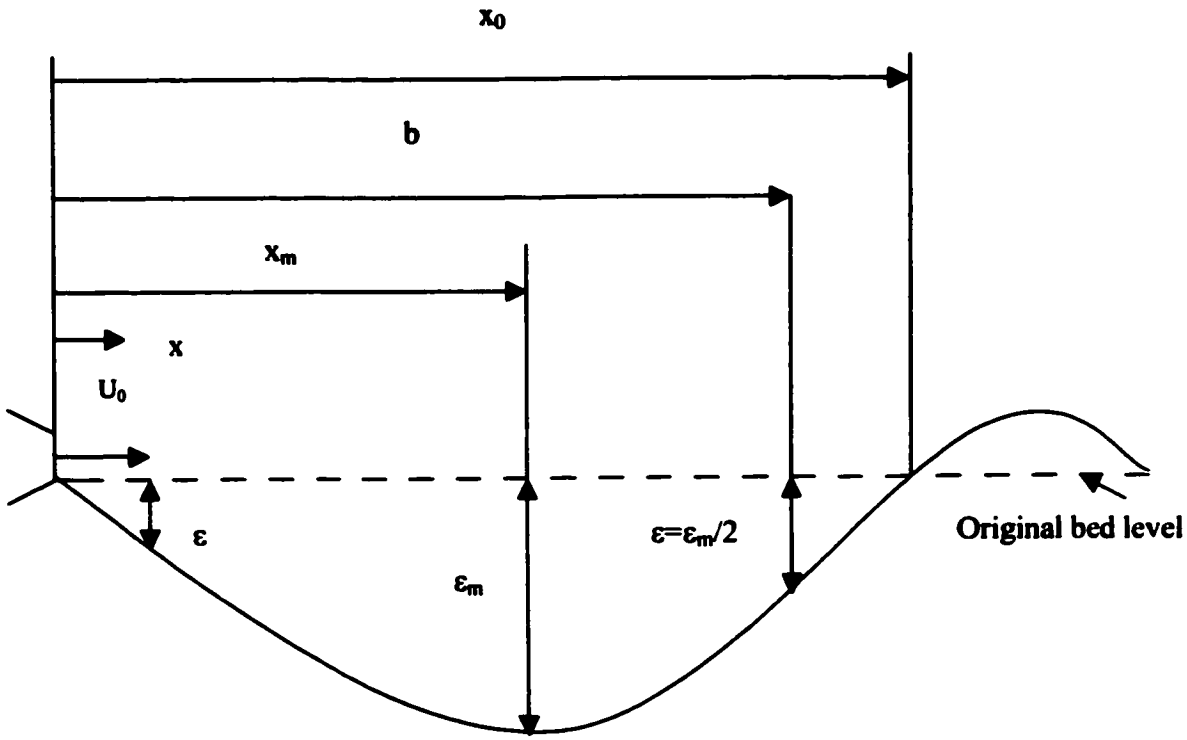

Fig. 2.4 General scour hole shape in cohesionless materials.

CHAPTER 3 EXPERIMENTAL DATA

3.1 Introduction

In this thesis, two sets of experimental data by Abt (1980) and Mazurek (unpublished) are presented and analyzed. The first set of data is a series of experiments on scour downstream of culvert outlets in one cohesive material at prototype scale (which was briefly discussed in the previous chapter). The other set of data is an unpublished and unanalyzed laboratory study of the scour of clays by a submerged circular wall jet produced in two cohesive soils by a flow through a nozzle of three different diameters. The experimental setups, measurements, testing programs, and soil properties are described in this chapter.

3.2 Abt (1980) Experimental Setup and Experiments

3.2.1 Experimental Setup

Abt (1980) performed his tests in an outdoor facility at the Engineering Research Center of Colorado State University. The experiments were conducted in a 30.5 m long, 6.1 m wide and 2.4 m deep flume. The flume contained two reaches, a 19.2 m long upper reach used as the bed material basin, in which the experiments were conducted, and an 11.3 m long lower reach which served as the tailwater basin. A smooth, circular steel culvert was positioned horizontally through the flume headboards with a depth of 1.83 m from the bottom of the flume and extended downstream of the headwall (Fig. 3.1).

Water was pumped from a lake to the outdoor flume. The discharge into the flume was controlled through a pipe network with butterfly valves at the upstream of the flume. The flow rates were monitored with an orifice meter in the pipe network. A gate valve

was installed into the pipe network to facilitate the filling of the tailwater basin. The tailwater depth was controlled with a wall comprised of redwood beams located at the flume outlet, by stacking or removing them depending on requirements.

The scour test was initiated by starting the pump, opening the bypass line, and then adjusting the tailwater control. When the tailwater surface elevation reached $0.45D_c \pm 0.05\ D_c$ above the invert, where D_c is the diameter of the culvert, the bypass line was closed. Then the butterfly valves at the head of the flume were then opened and adjusted to provide the proper discharge. The tailwater control beams were adjusted to maintain the desired tailwater elevation at the same time.

Only one cohesive soil was tested during these experiments. The bed material was placed in the flume using a bucket loader and the scour hole refilled after each test was completed. The soil was compacted to a density of 90 %$\pm$2 % of the optimum density before the scour tests, as determined by a standard proctor test. The maximum dry density was approximately 1824 kg/m^3. The cohesive material used in the scour tests was a mixture of locally derived sands, silts and clays, and was made of up 58 % sand, 28 % clay, 14 % silt, and 1 % organics, and could be classified as sandy clay by unified classification system. It had a plasticity index of 15 and mean grain size of 0.15 mm. The saturation of the material from the bed was determined after scour testing and it was found the material reached 98 % saturation after approximately 22 hours being submerged. Also, a series of vane shear strength tests were performed in the drained scour bed after some selected scour tests.

To assess the possibility of the effects on scour by physical-chemical breakdown of the soil due to particle dispersion, a series of pinhole dispersion tests were performed

on the bed materials. The tests indicated that the soil was not dispersive. Laboratory tests on Cation Exchange Capacity (CEC) gave the value of CEC of the clay material as 17.9 meq/100 g.

3.2.2 Testing Program and Measurements

The discharge ranged from 0.054-0.825 m^3/s. The inside diameter of the culvert was 260, 343, or 445 mm. A series of twelve experiments were performed of 1000-minute duration, the details of which are given in Table 3.1. The tests were stopped and measurements of the scour hole were taken after 31.6, 100, 316, and 1000 min of testing. To measure the scour hole, Abt used a point gauge attached to a motorized carriage equipped with a small cart that traversed the longitudinal axis of the flume on rails mounted on the top of the flume walls. The carriage and cart enabled the collection of data at one-foot scale in the longitudinal direction and one half-foot scale in the transverse direction. At the 1000 minutes duration, the scour cavity was dewatered and photographs were taken for documentation. After each test, the required soil samples were taken and the in situ soil tests performed. The bed was then allowed to air dry for a minimum of 24 hours and then prepared for the next run.

3.3 Mazurek (unpublished) Experimental Setup and Experiments

3.3.1 Experimental Setup

The experimental setup, shown in Figs. 3.2 and 3.3, employed a submerged circular turbulent wall jet to scour the soil samples which were set within a large jet tank 3.5 m long, 1.1 m wide, and 1.2 m deep. The jet was created by flow through a 0.5 m long, 0.15 m diameter plenum, which directed the flow through a circular nozzle with diameter of 4.90, 5.97, or 12.18 mm. City of Edmonton tap water was drawn from the

jet tank and pumped through the plenum using a 1/3 hp jet pump, so that the water in the system was recirculated. An additional supply of water was also constantly added to the tank to make up for leaks in the tank. The water level in the tank was held constant using an overflow set to the desired depth, so that the depth of the submergence of the jet was 0.55 m. The flow rate in the system was measured both by using a rotameter connected near the outlet of the pump and through the use of a pressure tap on the surface of the plenum along with a mercury manometer.

The soil samples were set carefully in the tank so that the soil surface was set at the same height as the bottom of the nozzle. In these tests, 0.25 m long, 0.17 m wide, and 0.11 m deep samples were used, the size of which was setup by the manufacturing process of the samples. The samples were contained within a 2 mm thick metal band to ensure that all samples had the same dimensions. The samples rested within the jet tank on a table, which could be leveled by adjusting the leg length. To prevent the samples from moving with initiation of the flow, the samples were set within a U-shaped holder than could be connected to the jet tank wall (Fig. 3.4).

To set up each test, the metal band for the soil sample was inserted into the sample and the surface was cut with a thin metal wire to ensure an even surface. Water content samples were taken from the excess soil cut from the samples. The samples were then set within the U-shaped holder and onto the table within the jet tank and the holder connected to the jet tank wall. The jet tank was then filled with water to the desired height and the jet flow initiated. The jet flow was initially at a low (non-scouring) velocity and very quickly increased to the desired flow (within about 10 s). Two

different types of soils were used for the tests, with the details of the physical properties given below.

3.3.2 Testing Program and Measurements

For the tests, as discussed, two cohesive soils were used. The velocity of the jet at the nozzle ranged from 2.98 to 15.67 m/s. Three different nozzle diameters 4.90, 5.97, and 12.18 mm were tested. The details of the experiments are given in Table 3.2.

Visual estimates of the length and maximum width of the scour hole were taken at various intervals during the tests until asymptotic scour was considered to be reached. The scour hole was assumed to have reached asymptotic state when the length of the scour hole did not change over 24 h, which generally occurred within 72 h. No physical measurements of the scour hole dimensions were made during the test, as it is known that even a slight disturbance on the surface of a cohesive soil sample may initiate erosion. The condition of the sample was also monitored through a photographic record of the tests.

Once equilibrium had been reached, the jet tank was drained and the jet centreline marked on the metal band containing the sample. The sample was then brought out of the jet tank and a digital point gauge (graded to 0.01 mm) was used to measure the scour in the sample. The scour hole profiles along the plane of symmetry, the width of the scour with distance from the nozzle, and in some tests, the cross-sectional profiles across the width of the sample were measured relative to the unscoured soil surface. The exact location of the cross-sectional profiles was varied so that there they were most representative profiles for each test. After the scour hole profile measurements were complete, vane shear strength tests were carried out on the samples. Samples were then

taken from the area around where the vane shear tests were carried out for water content determination.

The water temperature, pH, and conductivity were recorded for each test. The water sample was taken from the jet tank and tested using a Fisher 101 pH/conductivity meter. Conductivity and pH values were consistent with water chemistry data given by Epcor, the company that supplies water for the City of Edmonton. The water chemistry of the eroding fluid also appears to have been fairly consistent throughout the course of testing.

3.3.3 Soil Samples

The soil samples used in the experiments were manufactured pottery clays obtained from Plainsman Clays Ltd. of Medicine Hat, Alberta, Canada (M390, M332 are the company designations of the clays used). The M390 samples contained about 37 % clay, 48 % silt, and 15 % fine sand, and had an average vane shear strength of 17.9 kPa, a liquid limit of 33.7 %, a plastic limit of 18.1 %, a dry density of about 1547 kg/m^3, and a saturation before and after the tests of 98.4 and 100 % respectively. The water content of the blocks prior to testing averaged 26.2 % and after the test averaged 27.5 %. For the M332 clay, the samples contained about 33 % clay, 39 % silt, and 28 % sand. The M332 soil samples also had an average vane shear strength of 17.9 kPa, a liquid limit of 35.1 %, a plastic limit of 16.9 %, a dry density of 1553 kg/m^3, and saturation before and after the test of 99.7 and 100 % respectively. Electron micrographs produced by a scanning electron microscope of the structure of the clays, given in Figs. 3.5 and 3.6, show that both clays had an aggregated structure with random particle orientations. An X-ray

diffraction test of the soils showed that the clay component of the soils consisted of kaolinite and illite.

Table 3.1: Details of Experiments for Abt

Test No.	U_o (m/s)	D (mm)	Q (m^3/s)	DI*	Note
26	2.60	444.5	0.404	1.0	
28	3.97	444.5	0.404	1.5	
29	1.50	342.9	0.404	2.0	has varied DI
30	2.33	444.5	0.404	1.0	
31	3.49	444.5	0.618	1.5	
32	4.65	444.5	0.618	2.0	
33	1.31	260.4	0.618	0.5	
34	2.03	444.5	0.618	1.0	
35	3.04	247.6	0.824	1.5	
36	4.05	247.6	0.824	2.0	

*DI:Discharge Intensity, $DI=Qg^{-0.5}d^{-2.5}$

Table 3.2: Details of Experiments for Mazurek

Test No.	Test Date	Clay	d (mm)	U_o (m/s)	Q (L/min)	t_d (h)	Temp (°C)	pH	Conductivity (µs/cm)	w_p (%)	w_f (%)	S_v (kPa)	Note
1	28-Feb-01	M390	4.90	13.67	15.5	122.75	12.0	-	-		27.75		*†
2	7-Mar-01	M390	4.90	11.66	13.2		12.5	-	-	26.86			
3	22-Mar-01	M390	4.90	14.97	16.9			-	-	26.24			
4	27-Mar-01	M390	4.90	15.67	17.7	67.60	10.5	-	-	25.61	27.17	19.90	*†+
5	30-Mar-01	M390	4.90	10.28	11.6	73.42	13.0	-	-	25.84	27.53	17.50	*†+
6	2-Apr-01	M390	4.90	8.35	9.4	95.25	9.5	-	-	25.74	27.19	17.20	*†
7	6-Apr-01	M390	4.90	12.18	13.8	68.08	8.0	-	-	26.11	27.73	16.94	*
8	19-Apr-01	M390	5.97	9.58	16.1	93.03	11.0	-	-	26.40	27.59	16.34	*†
9	23-Apr-01	M390	5.97	14.42	24.2	90.70	14.0	-	-	27.23	28.60	13.66	*†
10	27-Apr-01	M332	5.97	14.31	24.0	96.27	16.5	-	-	26.07	27.80	16.93	*†+
11	1-May-01	M390	5.97	4.41	7.4	47.53	14.5	-	-	26.55	27.09	19.32	*†
12	3-May-01	M390	5.97	2.98	5.0	72.50	16.0	-	-	25.70	27.59	-	*
13	7-May-01	M332	5.97	5.74	9.6	92.67	15.5	7.53	338	26.14	27.61	20.21	*†
14	11-May-01	M332	5.97	13.11	22.0	70.17	15.8	7.57	333	26.18	26.77	19.91	*†+
15	14-May-01	M332	5.97	3.75	6.3	67.25	19.9	7.79	336	26.07	26.95	-	*
16	17-May-01	M332	5.97	7.94	13.3	119.23	16.6	7.67	320	25.54	26.60	23.77	*†
17	24-May-01	M332	5.97	13.66	22.9	94.67	19.7	7.68	330	26.67	27.22	16.64	*†
18	4-Jun-01	M332	5.97	8.43	14.2	94.47	17.5	7.67	343	25.78	27.26	14.26	*†
19	8-Jun-01	M390	5.97	10.45	17.6	66.50	18.0	7.73	337	26.42	26.97	16.42	*†
20	12-Jun-01	M390	12.18	5.06	35.4	70.07	21.1	7.66	331	26.62	26.09	16.04	*†
21	15-Jun-01	M390	12.18	7.59	53.1	68.25	18.5	7.62	331	26.34	27.96	14.55	*†
22	18-Jun-01	M390	12.18	11.24	78.6	44.57	17.8	7.63	325	25.74	27.17	19.74	*†+
23	20-Jun-01	M390	12.18	9.79	68.4	43.92	18.6	7.68	318.0	25.95	26.96	18.74	*†

* scour hole profile along the plane of symmetry.
†growth of the width of the scour hole.
+cross-section data

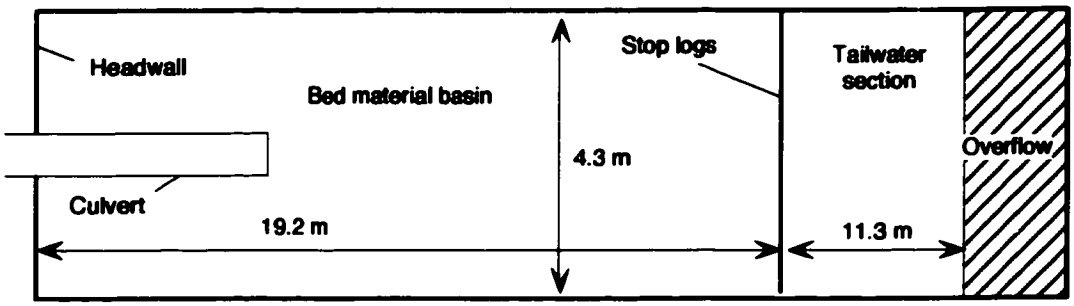

(a)

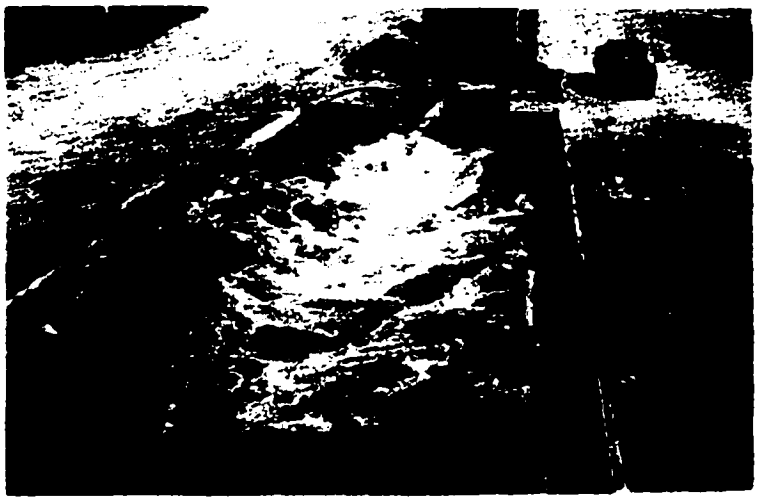

(b)

Figure 3.1 Experimental setup of Abt (a) plan view (b) operating setup (adapted from Abt and Ruff, 1982).

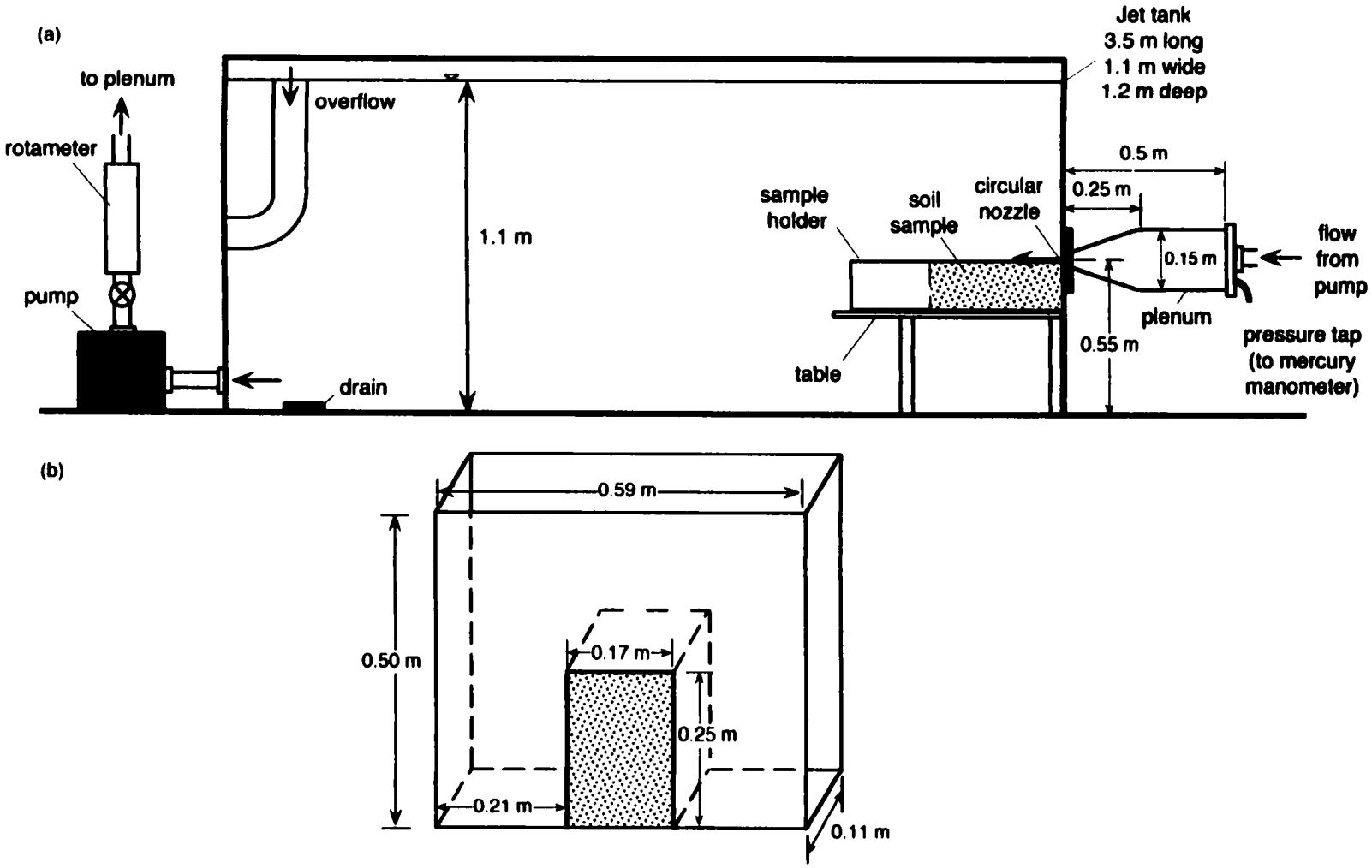

Figure 3.2 Experimental setup of Mazurek (a) general setup (b) dimensions of sample holder.

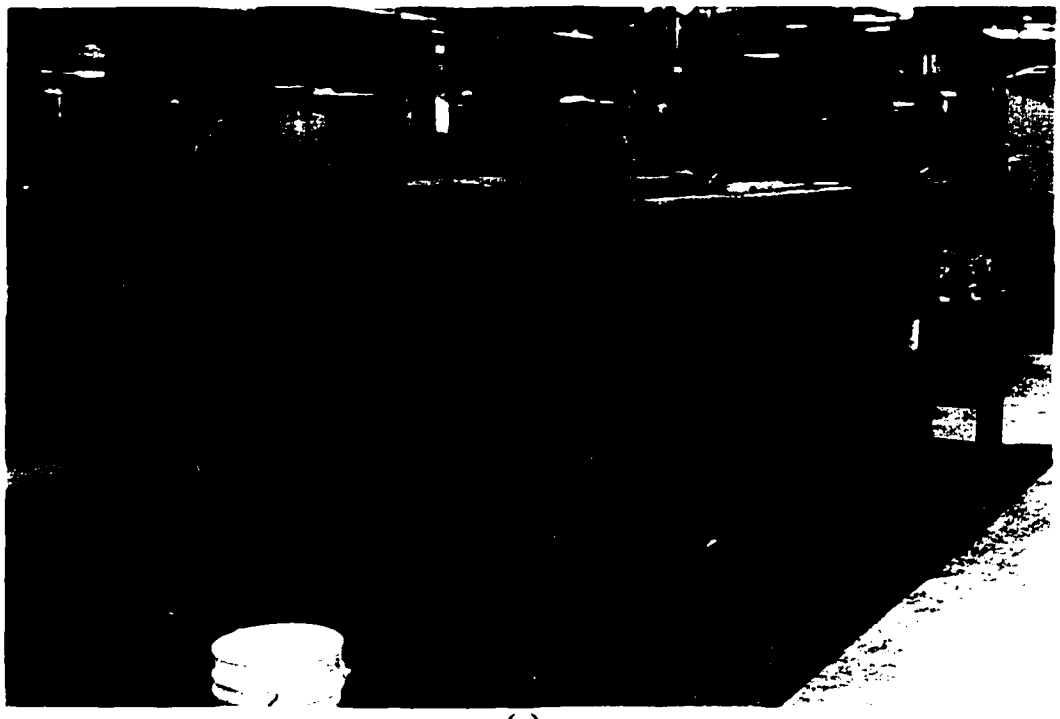

(a)

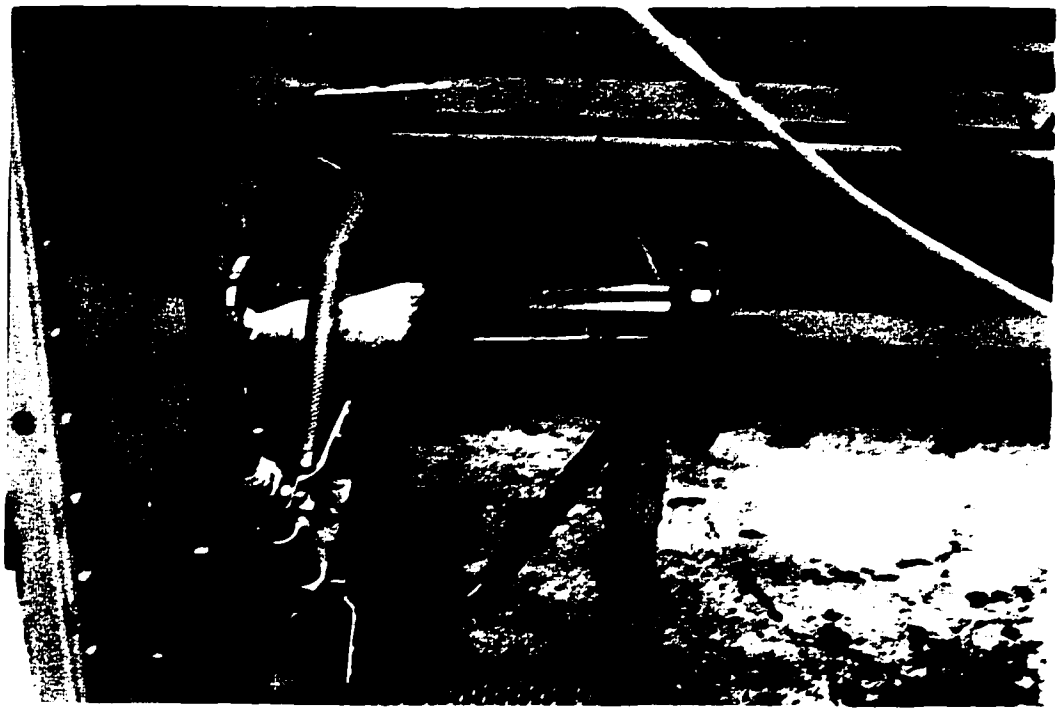

(b)

Figure 3.3 Experimental setup of Mazurek (a) jet tank and pump (b) plenum of jet.

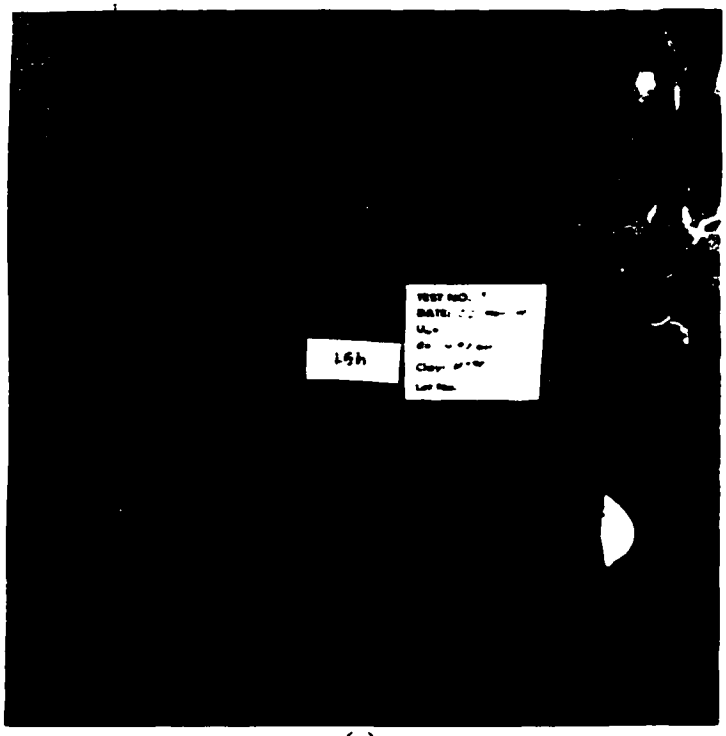

(a)

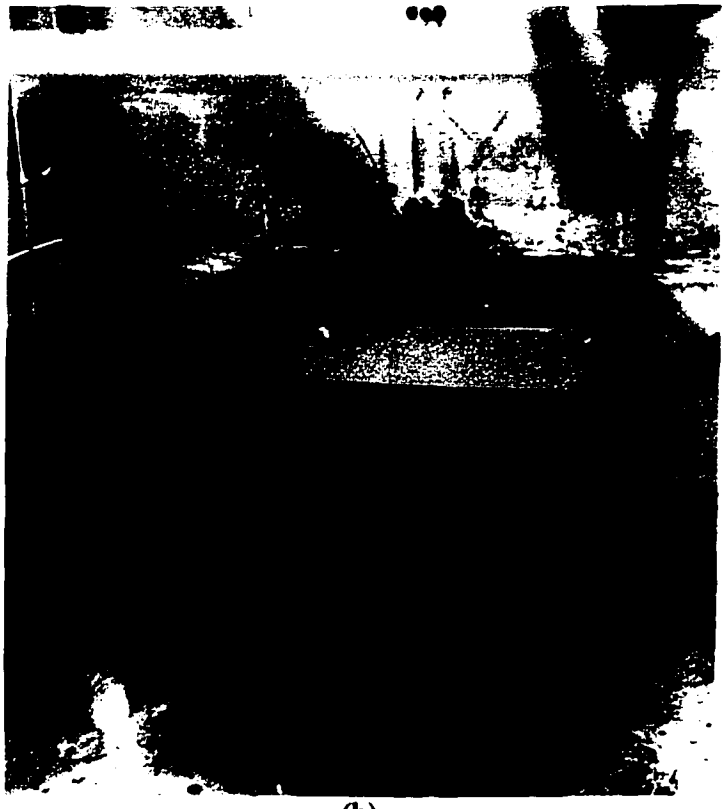

(b)

Figure 3.4 Soil sample set within apparatus (a) side view (b) end view.

(a)

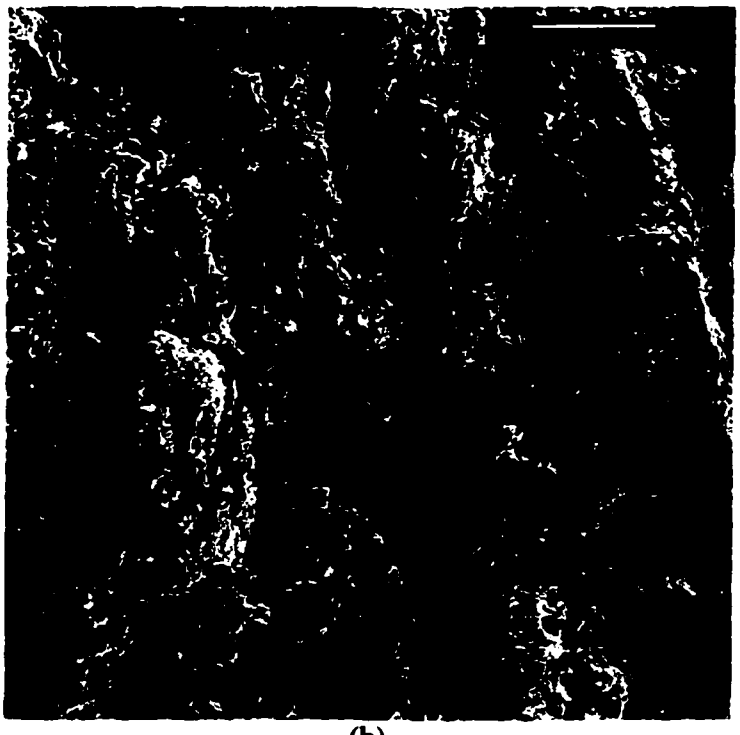

(b)

Figure 3.5 Electron Micrographs of M390 Clay (a) 7500 X magnification (b) 1500 X magnification.

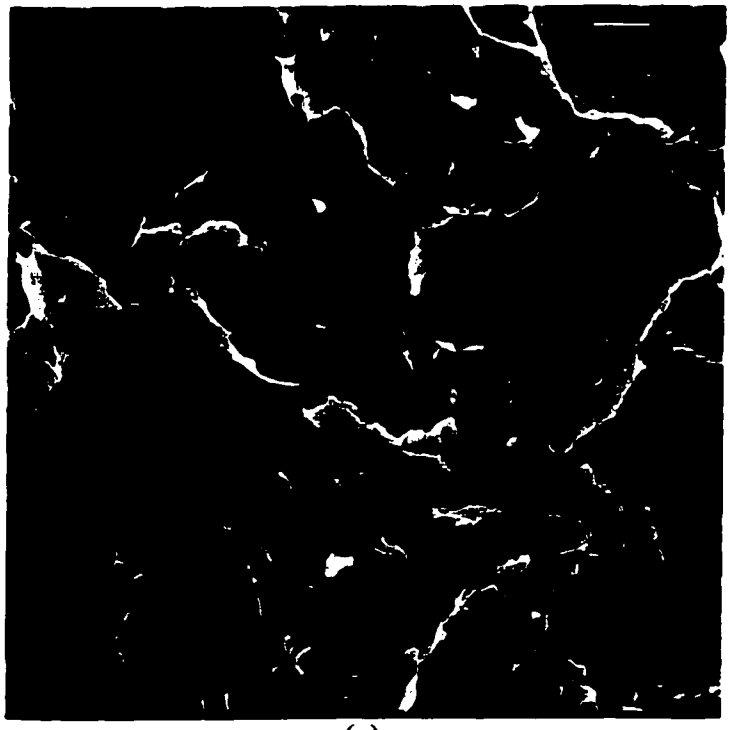

(a)

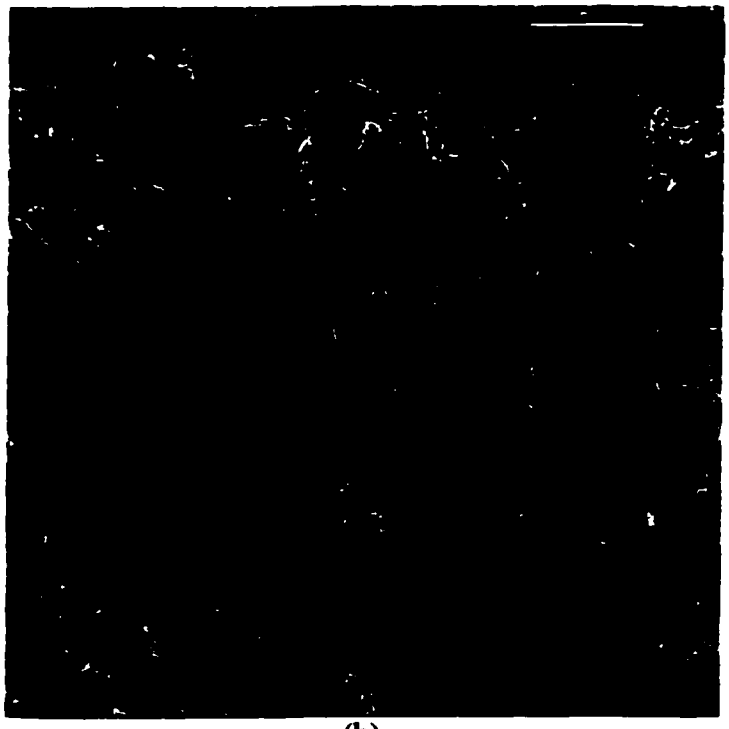

(b)

Figure 3.6 Electron Micrographs of M332 Clay (a) 7500 X magnification (b) 1500 X magnification.

CHAPTER 4 RESULTS AND ANALYSIS

4.1 Introduction

As discussed in the review of the literature on jet erosion of clays, the experimental studies on the flow at the outlets of the culverts by Abt (1980) and the laboratory work by Mazurek (unpublished) appear to be the only studies available on scour of cohesive materials by circular wall jets. Abt did his own analysis of this data, which will be discussed briefly in this chapter; however, there is no previous analysis for the Mazurek data.

In this chapter, observations drawn from the experimental work of both Mazurek and Abt are presented. Dimensional analysis is used to develop parameters and semi-empirical equations that may be appropriate to predict the scour hole dimensions in cohesive soils caused by circular wall jets. The maximum scour depth, distance to the maximum depth from the jet, and the length and width of the scour hole, are correlated with the jet properties and the critical shear stress of the soil to predict the scour hole dimensions. The shape of the scour hole profiles is also analyzed. The data sets are first analyzed separately, as each data set covers different aspects of the problem, and then a comparison of the results is made at the end of the chapter.

4.2 Results and Analysis of Mazurek Data

4.2.1 General Observations from Mazurek Data

A typical scour hole profile observed in Mazurek's experiment is shown in Fig. 4.1, with a dimensional plot of the profile shown in Fig. 4.2. The maximum scour depth tends to occur along the centreline (or plane of symmetry of the jet); however, this was

not always observed to be the case. The shape in plan typically grew linearly with distance from the nozzle in the first part of the scour hole (near the nozzle) and then was more rounded at the end of the scour hole. It is also seen that the maximum depth of erosion occurs some distance away from the origin of the jet at the nozzle, even though the highest shear stresses are initially (at the start of the test) near the nozzle. There was no formation of a mound (made of up eroded material) at the end of the scour hole, such as typically seen in cohesionless soils. A definition sketch of the variables used to describe the scour hole is given in Fig. 4.3. For the scour hole, ε is the depth of erosion at any location in the equilibrium state, ε_m is the maximum depth of erosion, x_m is the longitudinal distance corresponding to ε_m, x_o is the length of the scour hole, and b is the distance at which $\varepsilon = \varepsilon_m/2$ on the part of the scour profile in which $x>x_m$.

In the experiments, the erosion most often occurred by the removal of small chunks, usually 2-3 mm in size (mass erosion). Typical eroded particles are shown in Fig. 4.4. Removal of larger chunks also occurred in some tests, as seen by the relatively large sized chunk shown in Fig. 4.4. There was also the removal of individual particles (surface erosion) at the same time as mass erosion, although mass erosion was the predominant erosion type.

4.2.2 Developing Dimensionless Parameters

To analyze the scour data, dimensionless parameters will be developed by dimensional analysis using the ideas from the previous studies on scour by jets in cohesionless soils and the recent work by Mazurek (2001) in cohesive soils. It is proposed that the maximum depth of scour hole at *equilibrium state* (the end state of scour), ε_m , can be considered to have the following functional dependence

$$\varepsilon_m = f(U_0, d, \rho, \tau_c, \mu) \tag{4.1}$$

where U_0 = velocity of the jet at the nozzle

d = nozzle diameter

ρ = density of the eroding fluid

τ_c = critical shear stress of the soil, which is the shear stress on the bed below which erosion will not occur and is a property of the soil

μ = dynamic viscosity of the eroding fluid

These properties have the dimensions of length (L), mass (M) and time (T) of:

$$U_0 \rightarrow (L/T)$$

$$\varepsilon_m \rightarrow L$$

$$d \rightarrow L$$

$$\rho \rightarrow M/L^3$$

$$\tau_c \rightarrow M/(LT^2)$$

$$\mu \rightarrow M/(LT)$$

Using the Buckingham Pi theorem and selecting U_0, d and ρ as the repeating variables, we have:

$$\pi_1 = \frac{\varepsilon_m}{U_0^{x_1} d^{y_1} \rho^{z_1}} \tag{4.2}$$

$$\pi_2 = \frac{\tau_c}{U_0^{x_2} d^{y_2} \rho^{z_2}} \tag{4.3}$$

$$\pi_3 = \frac{\mu}{U_0^{x_3} d^{y_3} \rho^{z_3}} \tag{4.4}$$

and $$\pi_1 = \pi_2 = \pi_3 = 1 \tag{4.5}$$

From (4.2),

$$\varepsilon_m = U_0^{x_1} d^{y_1} \rho^{z_1} \tag{4.6}$$

$$[L] = [L/T]^{x_1} [L]^{y_1} [M/L^3]^{z_1}$$

From those equations we find that $x_1 = 0$, $y_1 = 1$ and $z_1 = 0$.

Therefore, $$\pi_1 = \varepsilon_m / d \tag{4.7}$$

From (4.3),

$$\tau_c = U_0^{x_2} d^{y_2} \rho^{z_2} \tag{4.8}$$

$$M/(LT^2) = [L/T]^{x_2} [L]^{y_2} [M/L^3]^{z_2}$$

$$T: -x_2 + 2 = 0$$

$$M: z_2 = 1$$

$$L: x_2 + y_2 - 3z_2 = -1$$

Solving these equations gives $x_2 = 2$, $y_2 = 0$, $z_2 = 1$.

Hence, $$\pi_2 = \tau_c / \rho U_0^2 \tag{4.9}$$

From (4.4),

$$\mu = U_0^{x_3} d^{y_3} \rho^{z_3} \tag{4.10}$$

$$M/(LT) = [L/T]^{x_3} [L]^{y_3} [M/L^3]^{z_3}$$

$$T: -x_3 = -1$$

$$M: z_3 = 1$$

$$L: x_3 + y_3 - 3z_3 = -1$$

which implies that $x_3 = y_3 = z_3 = 1$,

Thus, $$\pi_3 = \mu / \rho d U_0 = \nu / U_0 d \tag{4.11}$$

Then, from the Buckingham Pi theorem,

$$\pi_1 = f(\pi_2, \pi_3) \tag{4.12}$$

That is, $$\varepsilon_m/d = f(\rho U_0^2 / \tau_c \,.\, U_0 d/\nu) \tag{4.13}$$

The parameter $\rho U_0^2 / \tau_c$ can be considered as the ratio of the shear stress on the bed to the critical shear stress of the soil, since the shear stress on the bed is $\tau_0 = C_f (\rho U_0^2)/2$, where C_f is the (dimensionless) global skin friction coefficient. As discussed, the critical shear stress τ_c is the value of τ_0 below which no erosion occurs. Thus, τ_c can be related to ρU_0^2 by writing $\tau_c = \frac{C_f}{2}(\rho U_0^2)_c$, where $(\rho U_0^2)_c$ is the value of (ρU_0^2) below which there is no erosion. The parameter π_2^{-1} developed from dimensional analysis is then equivalent to $\frac{\rho U_0^2}{(\rho U_0^2)_c}$. Further, following previous ideas from sediment transport, this term can be written as an "excess stress" in the form of Shields parameter, $\frac{\tau_0 - \tau_c}{\tau_c}$, as $\frac{\rho U_0^2 - (\rho U_0^2)_c}{(\rho U_0^2)_c}$. To simplify this form of relation, the parameter λ is defined as $\lambda = \rho U_0^2$. Thus $\frac{\rho U_0^2 - (\rho U_0^2)_c}{(\rho U_0^2)_c}$ is written as $(\lambda - \lambda_c)/\lambda_c$.

The parameter $U_0 d/\nu$ is the jet Reynolds number, R, where ν is the kinematic viscosity of the eroding fluid. Since the shear stress on the bed has been found to have a weak dependence on R (Rajaratnam, 1976), it is assumed that the effect of the Reynolds number on erosion is small and is neglected. Then we can write

$$\varepsilon_m/d = f_1((\lambda - \lambda_c)/\lambda_c) \tag{4.14}$$

It is assumed, since the other dimensions of the scour hole are also lengths, that they will also follow a similar functional relation as for the maximum scour depth, so that

$$x_m/d = f_2((\lambda-\lambda_c)/\lambda_c) \quad (4.15)$$

$$x_0/d = f_3((\lambda-\lambda_c)/\lambda_c) \quad (4.16)$$

$$x_w/d = f_4((\lambda-\lambda_c)/\lambda_c) \quad (4.17)$$

$$w/d = f_5((\lambda-\lambda_c)/\lambda_c) \quad (4.18)$$

where x_m is the location of the maximum depth of scour hole, x_0 is the length of the scour hole, w is the maximum width of the scour hole and x_w is the location of the maximum width.

4.2.3 Characteristics of the Scour Hole

4.2.3.1 Dimensions of the Scour Hole at Equilibrium State

The Mazurek data are for scour holes in the equilibrium or asymptotic state of scour. As discussed, the equilibrium state of scour occurs when the rate of scour slows so much that any further growth in the scour hole is negligible. For Mazurek this occurred after about 72 h of testing.

The dimensionless maximum scour depth $\frac{\varepsilon_m}{d}$ at the equilibrium state was first plotted against λ as shown in Fig. 4.5. It is seen that the dimensionless maximum scour depth appears to grow in a linear relation with λ for both clays tested. For each clay, a line was drawn through the $\frac{\varepsilon_m}{d}$ vs. λ data to determine the critical value of λ, i.e. λ_c, for each soil. λ_c was found to be 17000 Pa for clay M390 and 21000 Pa for clay M332. To help determine a good value of λ_c, one can also use the location of maximum depth x_m and scour hole length data given in Figs. 4.6 and 4.7. Using C_f=0.005 (as discussed in chapter 2) these λ_c are equivalent to critical shear stress values of 42 Pa for clay M390 and 52 Pa for clay M332. The scour hole dimension measurements are given in Table 4.1,

with the complete scour hole dimension data given in Appendix A, and plots of scour hole profiles along the plane of symmetry for all tests given in Appendix B.

Using the critical value of λ_c =17000 Pa for clay M390 and λ_c =21000 Pa for clay M332, the maximum depth of scour was plotted against $(\lambda-\lambda_c)/\lambda_c$ as shown in Fig. 4.8. An equation was then developed to predict the maximum depth of scour:

$$\varepsilon_m/d = 0.231\ \{(\lambda-\lambda_c)/\lambda_c\} \tag{4.19}$$

This equation gave a correlation coefficient r^2 of 0.71. A similar analysis was carried out for the variation of the location of the maximum scour depth, x_m, the length of the scour hole, x_0, the maximum width of the scour hole, w, and the location of the maximum width, x_w. Figures. 4.9 to 4.12 show the variation of these dimensions with $(\lambda-\lambda_c)/\lambda_c$. It was found that the data could be fit best by the equations:

$$x_m/d = 1.07\{(\lambda-\lambda_c)/\lambda_c\} \tag{4.20}$$

$$x_0/d = 14.3\{(\lambda-\lambda_c)/\lambda_c\}^{0.38} \tag{4.21}$$

$$w/d = 1.007\ \{(\lambda-\lambda_c)/\lambda_c\} + 2.0 \tag{4.22}$$

$$x_w/d = 1.98\ \{(\lambda-\lambda_c)/\lambda_c\} + 3.0 \tag{4.23}$$

which gives r^2 of 0.51, 0.75, 0.84 and 0.96 respectively. The correlation coefficient of Eqn. (4.20) seems low, however since x_m is small. There is more error in those values and larger eroded chunks might affect this value.

For the maximum width, w/d does not tend to zero as $(\lambda-\lambda_c)/\lambda_c$ decreases as for the other dimensions, which was shown in Fig. 4.11. This is likely because the minimum width of the scour hole is near the nozzle and this width would form upon initiation of erosion. This behavior is also seen for x_w (Fig 4.12). As well, from general jet behavior, it is known that the "virtual origin" or true origin of the jet, where the jet diameter

approaches zero, is back by the nozzle by some distance. Perhaps because we are measuring from the nozzle and not the virtual origin, there is some effect on the analysis of the data.

4.2.3.2 Scour Hole Profiles at Equilibrium State

Some typical scour hole profiles along the plane of symmetry were shown in Fig. 4.2. From Fig. 4.2, it appears that the depth profiles are similar in shape and an attempt is made here to develop a dimensionless profile that will fit all the scour holes. To do this, the scour hole profiles along the jet centreline are made dimensionless by using suitable scales. Abt (1980) used the length of the scour hole, x_o, to nondimensionalize the horizontal distance along the jet centreline x, however he had much scatter in the results. Mazurek (2001), in her work with plane wall jet scour in cohesive material, used the distance from the nozzle, b, at which $\varepsilon = \varepsilon_m/2$ on the part of the scour profile in which $x>x_m$ to normalize the horizontal distance x, with a better result. In both cases, the maximum scour hole depth ε_m was used as the scale for nondimensionalizing the scour depth along the profile. Using b and ε_m as the scales, the dimensionless scour profiles are shown in Fig. 4.13.

Dimensional analysis was also carried out for the variation of b. The value of b was plotted against $(\lambda-\lambda_c)/\lambda_c$ as shown in Fig. 4.14. An equation was developed to predict b with a correlation coefficient r^2 of 0.84:

$$b/d = 6.57\{(\lambda-\lambda_c)/\lambda_c\}^{0.42} \qquad (4.24)$$

Typical cross-sectional profiles are shown in Fig. 4.15. The cross-sectional profiles also appear to have a similar shape. Typically, the maximum scour depth along the cross-sectional profile occurs at the jet centreline, however, this was not always the

case. To normalize the data, the scour hole depth on the certreline is used as a scale to nondimensionalize the scour depth. The half-width b_{cl}, which is the distance from the certreline where the scour hole depth is half the certreline scour depth, is used to nondimensionalize the distance from certreline. Typical dimensionless cross-sectional profiles are shown in Fig. 4.16. For all the cross-section data, the dimensionless profiles agree with each other very well. A quadratic curve is used to fit the general shape (Fig. 4.16):

$$\varepsilon/\varepsilon_{cl} = 0.44\,(y/b_{cl})^2 - 0.0032(y/b_{cl}) - 0.99 \qquad (4.25)$$

with an $r^2 = 0.93$. A Gaussian curve has been frequently used to fit cross-sectional data in cohesionless material (Aderibigbe, 1996), and it is included here for comparison (Fig. 4.16). The Gaussian equation is given by:

$$\varepsilon/\varepsilon_{cl} = \exp\{-0.693\,(y/b_{cl})^2\} \qquad (4.26)$$

The typical shape of the scour hole when looking in plan view also appears to have some similar shape (Fig. 4.17). The half-width is used here to show the growth of the scour hole in the traverse direction with x. The growth of the half-width with x was made dimensionless by using the maximum half-width B_m to normalize the width. Two scales were tried to nondimensionalize the distance from the nozzle. One is x_0, the length of the scour hole; the other is x_w, the location of x corresponding to the maximum width. Dimensionless width profiles using those two different scales are shown in Fig. 4.18 and Fig. 4.19. It can be seen that the scale x_w works much better for the dimensionless profiles.

4.3 Analysis of Abt's Data

4.3.1 Original Observations and Analysis of Abt's Data

A series of twelve scour cavities were observed in the Abt tests. The scour cavities were generally similar in geometric configuration and appearance. Scour cavities were circular in shape at low discharges and oval in shape at higher discharges. Typical scour hole profiles are shown in Fig. 4.20.

Abt observed that larger diameter materials, sands and clods, were deposited at the downstream end of the scour hole. Also, a mound was formed downstream of the cavity. Smaller material, clay, and silt particles were entrained by the flow and transported to the settling basin or trapped in void spaces in the mound. At the end of each experiment, considerable deposition of sands and clods was found around the cavity. Large particles were deposited around the cavity in the mound while fine particles were transported into the settling basin.

To analyze the scour hole dimension data, Abt first performed dimensional analysis by using the Buckingham Pi theorem. A dimensionless parameter, the *Discharge Intensity* D.I. (defined as $Qg^{-0.5}d^{-2.5}$) was found by the Pi theorem. From dimensional analysis he also found the *Modified Shear Number*, Sn_{mod}, (defined as $\tau_c \rho^{-1} U_0^{-2}$). He used the diameter of the culvert, D_c to nondimensionalize the maximum depth ε_m, length x_0, width w and volume of scour V_s (for V_s he used D_c^3). In his analysis, those dimensionless parameters (ε_m/D_c, x_0/D_c, w/D_c or V_s/D_c^3) were found related to the *Discharge Intensity* D.I and the *Modified Shear Number*, Sn_{mod}. Abt also noticed that the length x_0, width w and volume of scour V_s could be correlated to the maximum depth ε_m in the dimensionless form of x_0/D_c, w/D_c or V_s/D_c^3 versus ε_m/D_c. Those parameters were used

together to estimate the scour dimensions. Abt's dimensionless analysis of the scour hole brought out the two dimensionless forms which were also found here: for Abt ε_m/D_c is equivalent to ε_m/d, and the *Modified Shear Number*, Sn_{mod}, is equivalent to $(\rho U_0^2)/\tau_c$.

Finally, the time scale was taken into account in the prediction formula

$$y=a\,x^b\,(t_0/t)^c \tag{4.27}$$

where

a = coefficient

b = slope of the desired characteristic curve

c = the slope of the desired time relationship

t_0 = any time less than or equal to 1000 minute

t = 1000 minutes

$x = Qg^{-0.5}d^{-2.5}$, $\tau_c\rho^{-1}U_0^{-2}$, or ε_m/D_c

$y = \varepsilon/D_c$, w/D_c, x_0/D_c, or V_s/D_c^3

Abt suggested that equation (4.27) could be used for estimating the dimensions of a scour cavity at a culvert in a silt clay (SC by unified classification system) cohesive material knowing any single cavity characteristics (i.e. depth, length, width or volume).

4.3.2 Re-analysis of Abt's Data

Abt's data is reanalyzed here following the methods used for the Mazurek data.

4.3.2.1 Growth of Scour Hole Dimensions with Time

Typical plots of the growth of the maximum scour depth ε_m and the scour hole length, x_0, versus time are given in Fig. 4.21 and 4.22. It should be noted that this data does not correspond to equilibrium state. As discussed previously, other researchers (Mazurek, 2001) have found that the scour hole dimensions of a plane wall jet in

cohesive materials and for circular wall jet in cohesionless materials (Rajaratnam and Berry, 1977) grow in a linear relation with the logarithm of time until the equlibrium or asymptotic state of scour is reached. This trend is likely not seen in the Abt data because the limitation of the data (measurement were taken at only four times) and the short duration of the tests.

4.3.2.2 Dimensions of the Scour Hole at 1000 Minute

To examine the influence of the parameter $\lambda=\rho U_0^2$ (introduced in section 4.2.1) on the scour hole, the dimensionless scour depth and scour hole length are plotted in Figs. 4.23 and 4.24. As Abt's tests run to a maximum duration of 1000 min, only the data at this time is considered. There does not appear to be any signinificant trend for increasing maximum scour depth with λ (Fig. 4.23). However, since the scour holes are not at equilibrium, the different data represent scour holes at different parts of the scouring process. There is a definite trend for increasing scour hole length with increasing λ (Fig. 4.24). The data cannot adequately be compared with Mazurek data, however, because the test did not reach equilibrium.

4.3.2.3 Scour Hole Profiles

The typical dimensional profiles along the plane of symmetry of Abt's data are shown in Fig. 4.25. Scour hole profiles throughout the scouring process are shown in Figs. 4.25 and 4.26. It is seen that they appear to have the same general shape with time. The scour hole profiles for each time for each test are given in Appendix C.

The dimensional profiles at the centreline of Abt's data are normalized to develop dimensionless profiles using the same parameters discussed in Section 4.2.3.2. Typical dimensionless profiles are shown in Figs. 4.27 and 4.28. For each test run, the scour hole

profiles at different times (31.6 min, 100 min, 316 min and 1000 min) all appear to have the same dimensionless shape, i.e. that the scour hole has the same (dimensionless) shape throughout the scouring process. The dimensionless scour hole profiles at the four different times for each test are given in Appendix D.

Dimensionless scour hole profiles of all tests for each test duration are also plotted in Figs. 4.29-4.32. It is seen that the dimensionless profiles are consistent between tests. The dimensionless scour hole profiles at the same time scale are also approximately the same in shape for different test runs. Thus, the scour hole profile is similar in shape for all tests at all times with all different times, as seen in Fig. 4.33. Polynomials with different power were tried to fit the scour hole profile. Results show that a fifth power polynomial fit the general shape best with the highest correlation coefficient (Fig. 4.33):

$$\varepsilon/\varepsilon_m = 1.52(x/b)^5 - 7.02(x/b)^4 + 9.82(x/b)^3 - 2.73(x/b)^2 - 1.94(x/b) - 0.23 \quad (4.28)$$

with an $r^2 = 0.95$.

The ratio of b/D_c at the four times vs. the parameter λ was plotted in Fig. 4.34. An equation was developed to predict b for the longest time of 1000 min and is given as

$$b_{1000}/D_c = 1.76\lambda^{0.22} \quad (4.29)$$

Equation (4.29) has a correlation coefficient for the 1000 min data of 0.37 , which seems not high enough to give an accurate prediction of b.

Typical cross-section profiles of Abt's data are showed in Fig. 4.35. Using the scour hole depth on the centreline and the half-width b_{cl} to nondimensionlize the parameters, the dimensionless cross-section profiles are shown in Fig. 4.36. The scour hole cross-sectional profiles also appear to have a similar general shape.

4.4 Comparison of Abt's and Mazurek's Data

In this section, a comparison is made between Abt data and Mazurek data. Using the dimensionless parameters developed in section 4.2.2, Mazurek's data has an apparent relationship with the parameter $(\lambda-\lambda_c)/\lambda_c$, and equations have been developed to predict the scour hole dimensions. However, Abt's data did not reach equilibrium state and thus only the data at 1000 min are analyzed. For Abt, there was a less strong correlation with λ, likely because the scour holes were not at equilibrium.

For the dimensionless scour profiles, Abt's data are similar in shape for all tests at all times with all different time scales (Fig. 4.33). A fifth power polynomial (Eqn. 4.28) fits the general shape very well. This polynomial fits the Mazurek data (Fig. 4.13) in the range below $x/b<1.5$ quite well.

The dimensionless profiles of Abt's data appear to have less symmetry than that of Mazurek's results. However, Abt measured at 1 ft intervals and this may not give an accurate good enough description at the scour holes.

4.5 Discussion

Experiments on scour by circular wall jet of clay materials (Mazurek, unpublished) show that the scour hole dimensions at equilibrium state are correlated with the properties of the jet, the fluid and the characteristics of the clay. Dimensional analysis suggests the parameter λ for the relationship. For the Mazurek data, there appears to be a critical value of λ, λ_c, below which no significant erosion occurs. λ is estimated to be about 17000 Pa for clay M390 and 21000 Pa for clay M332. These λ_c give a critical shear stress value of 42 Pa for clay M390 and 52 Pa for clay M332. Equations developed using the parameter λ can be used to predict the scour hole dimensions at equilibrium state.

The flow in the culvert can be considered as a circular wall jet. The parameter λ does not work well for the 1000 min duration culvert tests by Abt (1980), which may be too short to reach the equilibrium state. Using the proper dimensionless scales discussed, Abt's data are similar in shape for all tests at all times with all different time scales for the dimensionless scour profiles. A fifth power polynomial fits the general shape very well. The polynomial also fits Mazurek's data in the range below $x/b<1.5$ quite well.

The cross-section profiles for both tests are similar in general shape, while Abt's data appear to have less symmetry than that of Mazurek's data.

The equations developed herein are limited to cohesive materials that are not dispersive (where there is no critical shear stress), fissured or otherwise disturbed, or where there are layers or lenses of sand or silt They also only apply to the range of shear stresses tested, for jet Reynolds number R greater than about 10,000, and only for jets that are not offset from or inclined to impinge on the bed.

Table 4.1: Details of Experiments for Circular Wall Jet in Cohesive Soil of Mazurek

Test No.	Test Date	Clay	d (mm)	U_o (m/s)	ε_m (mm)	x_m (mm)	x_0 (mm)	B_0 (mm)	B_{max} (mm)	x_w (mm)	b (mm)		Note
1	28-Feb-01	M390	4.90	13.67	9.40	55.0	190	8.0	61.0	120	92.00	*†	
2	7-Mar-01	M390	4.90	11.66	-	-	-	-	-	-	-		flow rate not stable
3	22-Mar-01	M390	4.90	14.97	-	-	-	-	-	-	-		flow rate not stable
4	27-Mar-01	M390	4.90	15.67	14.30	67.0	195	10.0	72.0	130	101.97	*†+	
5	30-Mar-01	M390	4.90	10.28	6.80	38.0	152	8.0	38.5	80	73.00	*†+	
6	2-Apr-01	M390	4.90	8.35	4.99	14.0	109	10.5	26.0	50	51.23	*†	
7	6-Apr-01	M390	4.90	12.18	7.31	36.0	184	-	-	-	63.16	*	
8	19-Apr-01	M390	5.97	9.58	8.36	0.0	127	20.0	45.5	70	48.28	*†	
9	23-Apr-01	M390	5.97	14.42	14.12	63.0	230	20.5	81.0	146	99.80	*†	
10	27-Apr-01	M332	5.97	14.31	13.94	42.0	216	14.0	64.0	122	99.20	*†+	
11	1-May-01	M390	5.97	4.41	2.79	0.0	33	8.5	13.0	19	17.78	*†	
12	3-May-01	M390	5.97	2.98	1.47	0.0	21	-	-	-	18.14	*	had unstable flow rate, but constant at end of test
13	7-May-01	M332	5.97	5.74	4.03	5.0	100	12.5	20.5	38	21.92	*†	large chunk removed near nozzle affected profile
14	11-May-01	M332	5.97	13.11	10.7	62.5	214	11.0	58.5	110	108.10	*†+	
15	14-May-01	M332	5.97	3.75	1.37	0.0	15	-	-	-	14.27	*	
16	17-May-01	M332	5.97	7.94	8.96	44.0	99	7.0	15.5	40	68.24	*†	had removal of large chunk that disturbed scour hok
17	24-May-01	M332	5.97	13.66	10.20	27.0	204	18.0	58.0	90	78.57	*†	
18	4-Jun-01	M332	5.97	8.43	3.53	45.0	154	9.5	34.0	86	94.51	*†	
19	8-Jun-01	M390	5.97	10.45	6.78	31.0	162	14.0	40.0	81	65.00	*†	
20	12-Jun-01	M390	12.18	5.06	3.11	30.0	150	10.0	34.0	50	63.95	*†	
21	15-Jun-01	M390	12.18	7.59	1.90	40.0	220	14.0	52.5	120	-	*†	
22	18-Jun-01	M390	12.18	11.24	20.45	125.0	180	23.0	89.0	160	-	*†	end of block failed
23	20-Jun-01	M390	12.18	9.79	20.64	120.0	220	20.0	95.0	220	-	*†+	

* scour hole profile along the plane of symmetry.
†growth of the width of the scour hole.
+cross-section data

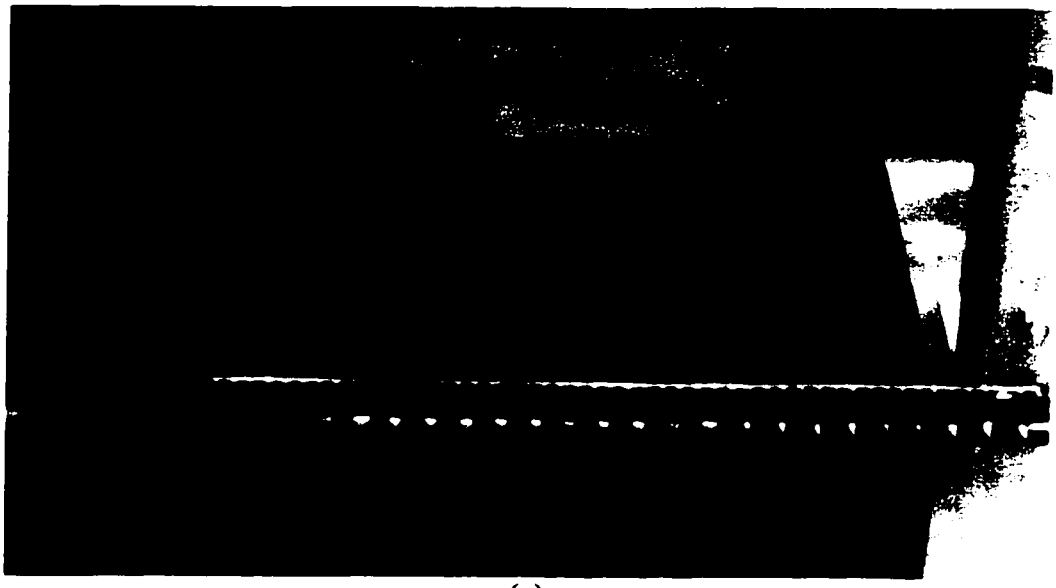

(a)

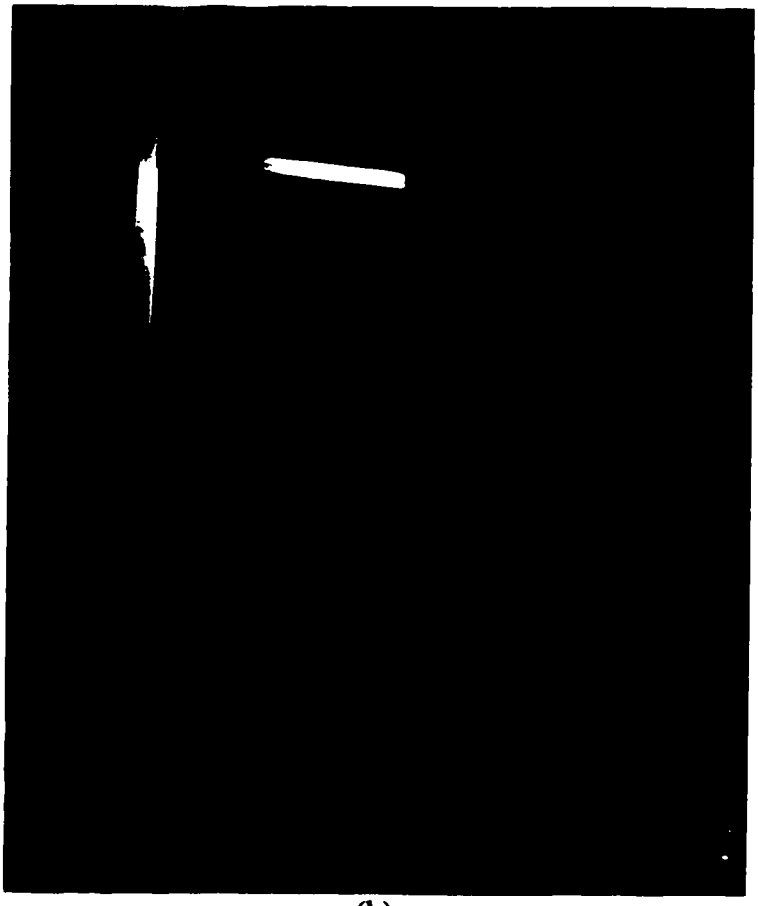

(b)

Figure 4.1 Typical scour hole (a) side view (b) end view (both Test 4).

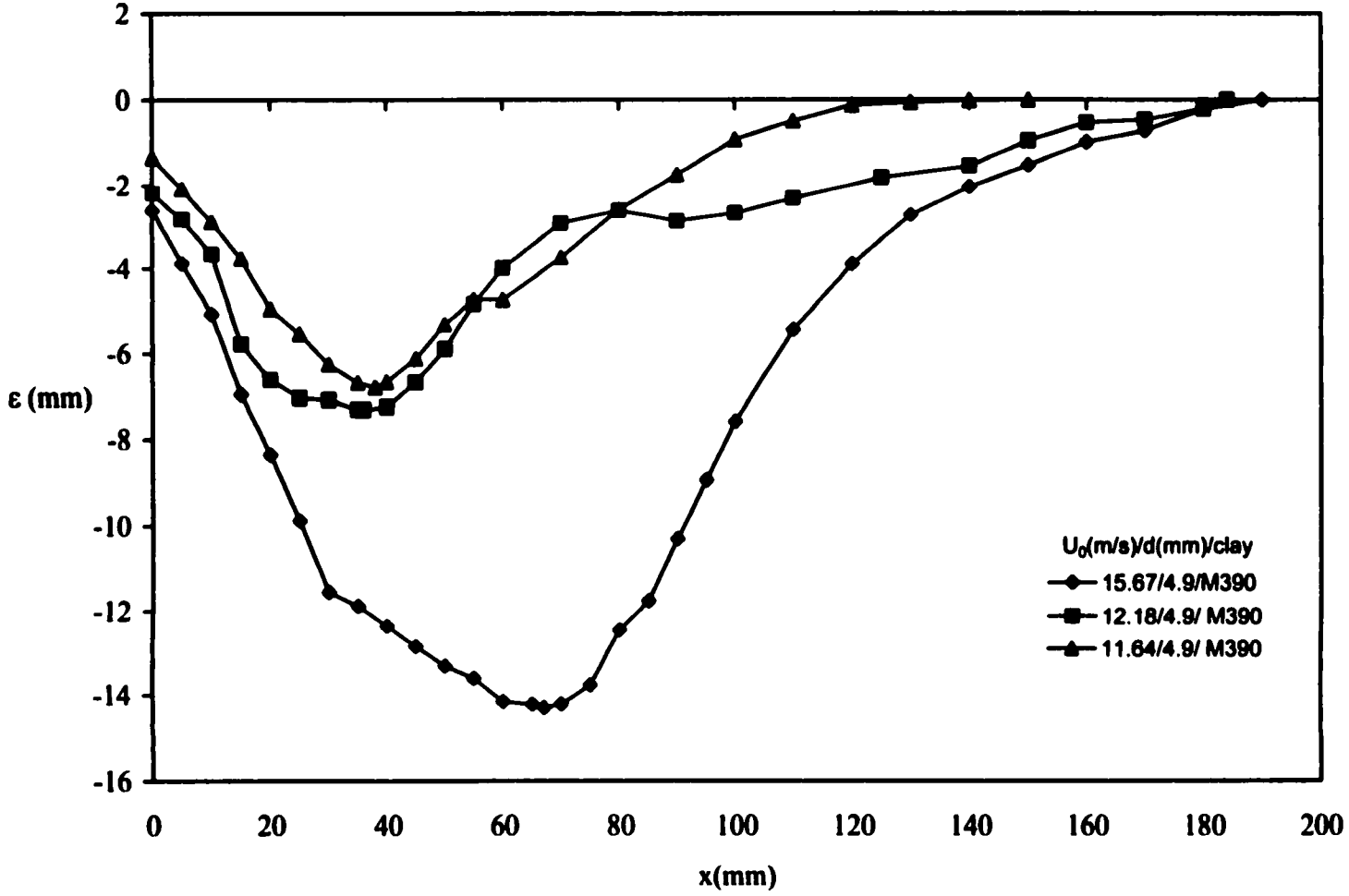

Fig. 4.2 Dimensional scour hole profiles along the plane of symmetry for Mazurek data.

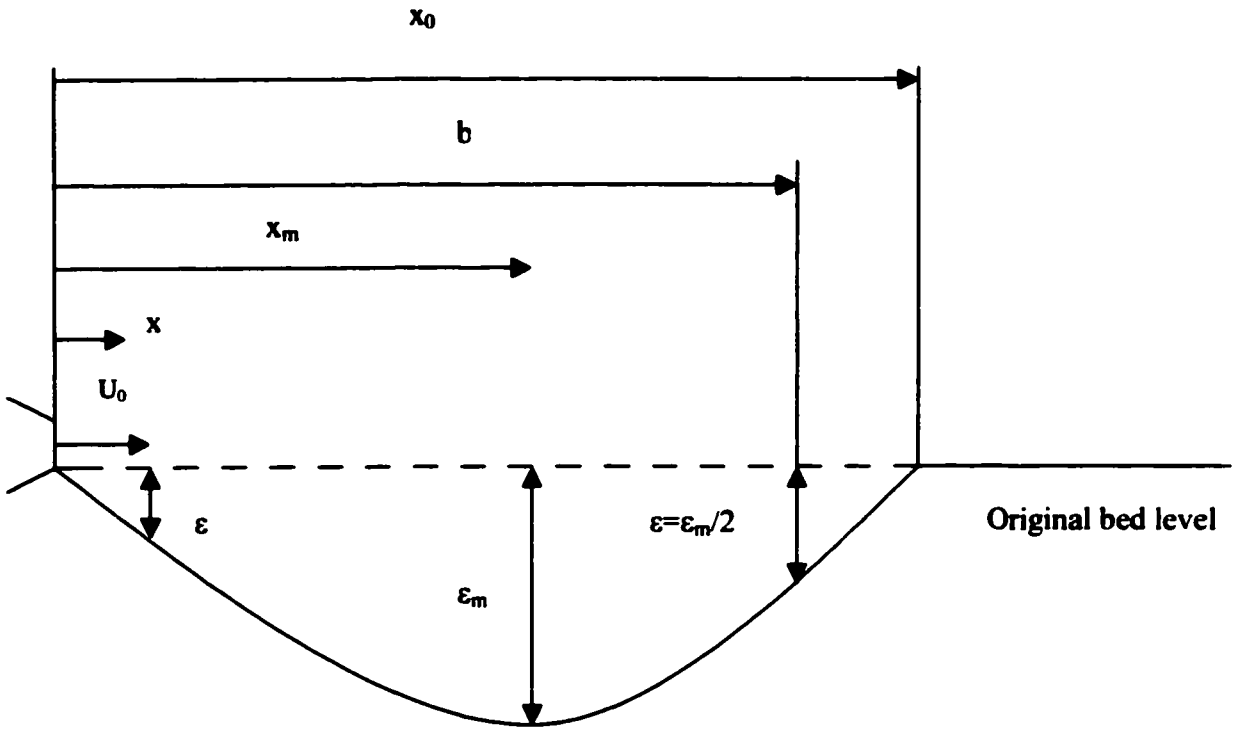

Fig. 4.3 Definition sketch: scour hole profile along the plane of symmetry

Figure 4.4 Typical size of eroded particles.

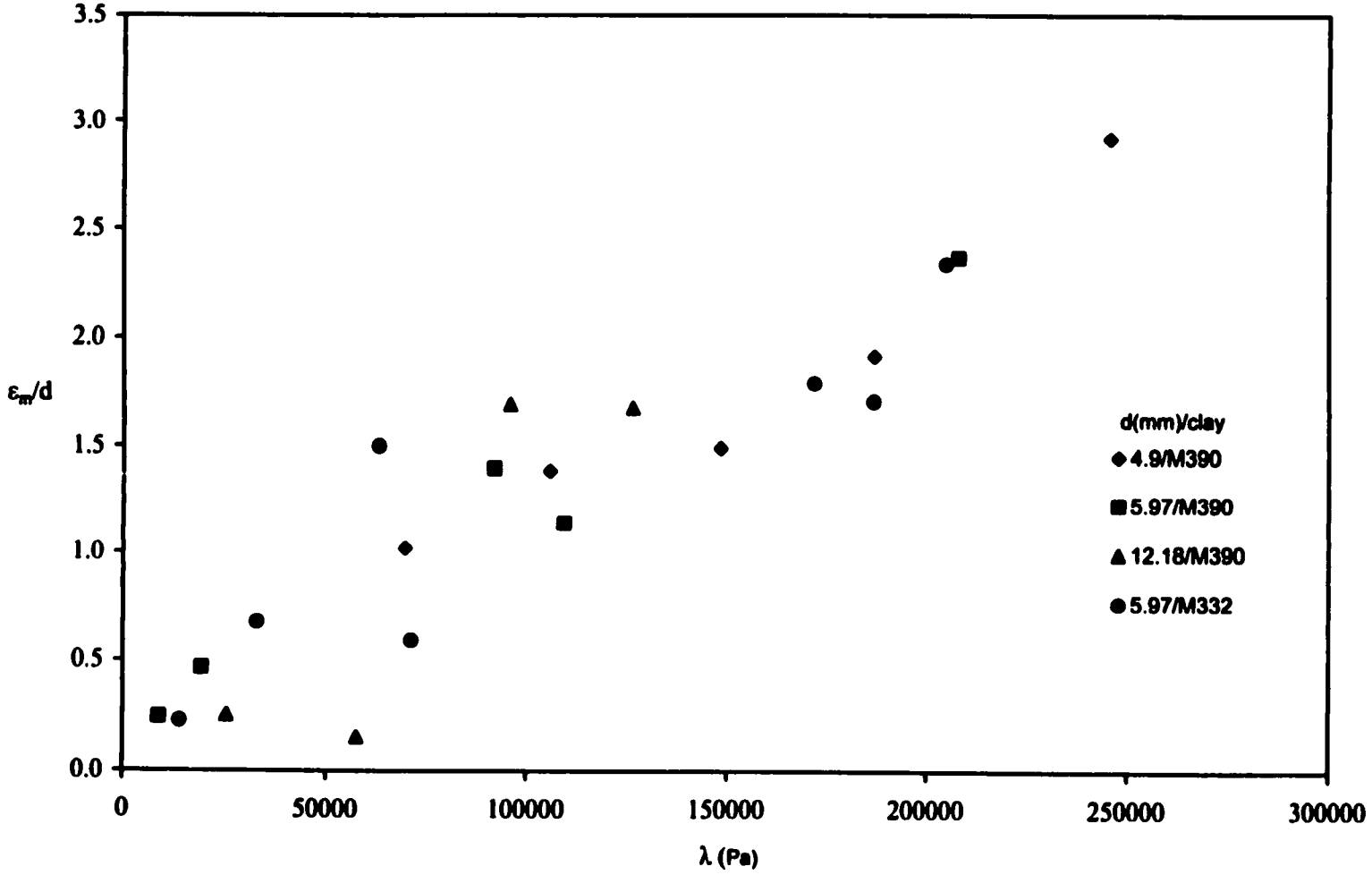

Fig. 4.5 Dimensionless maximum scour hole depth at equilibrium.

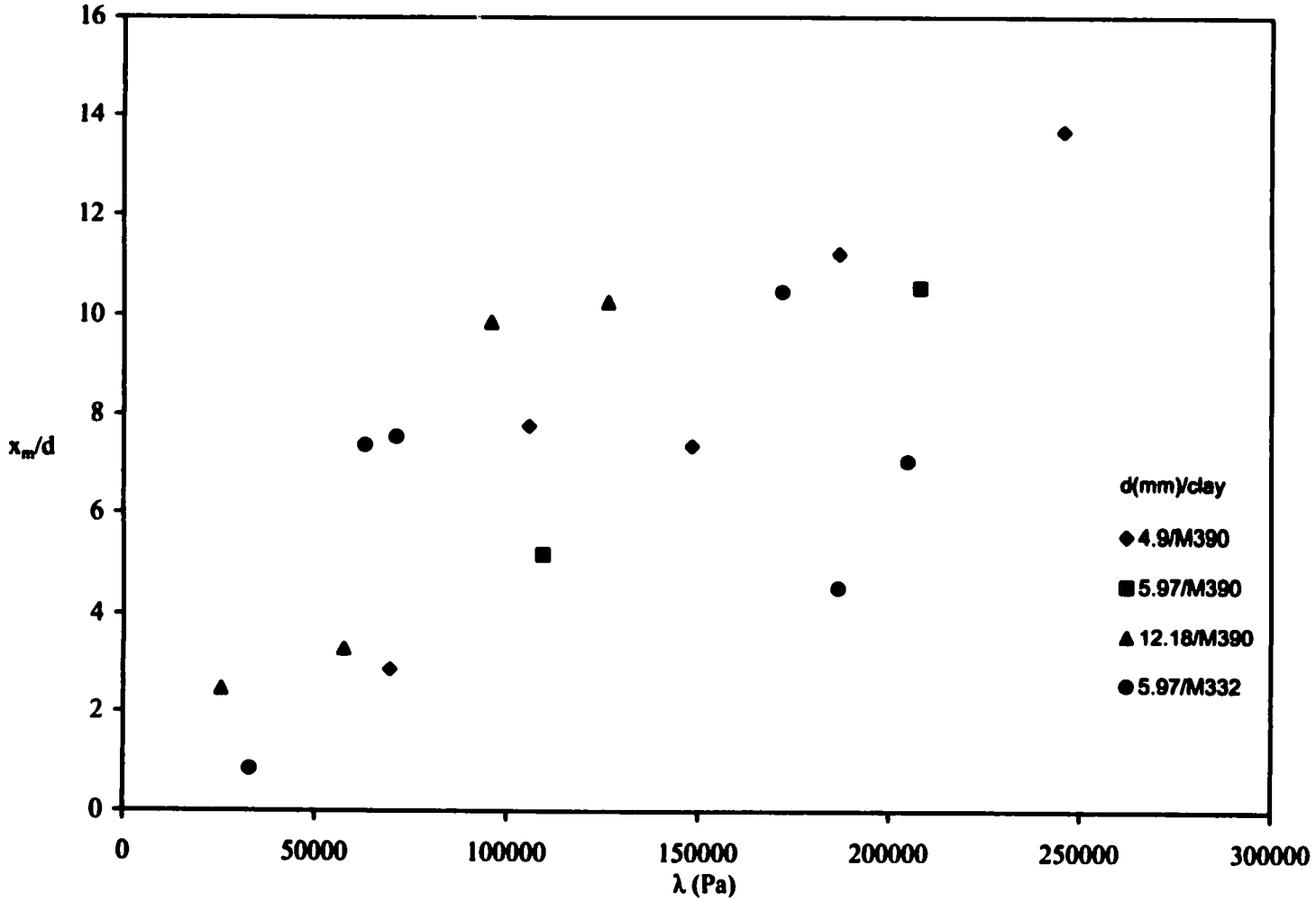

Fig. 4.6 Dimensionless location of maximum scour hole depth at equilibrium.

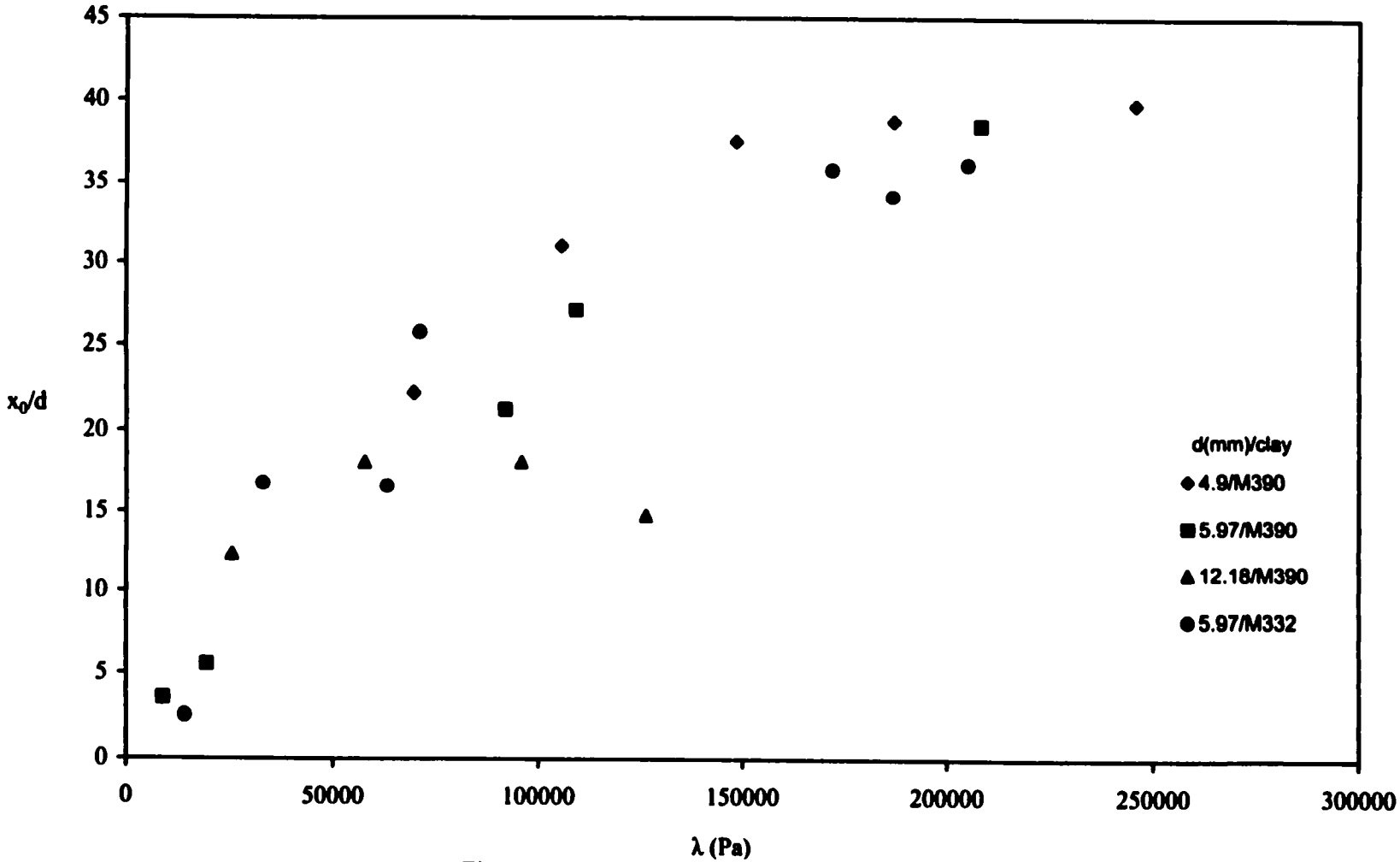

Fig. 4.7 Dimensionless scour hole length at equilibrium.

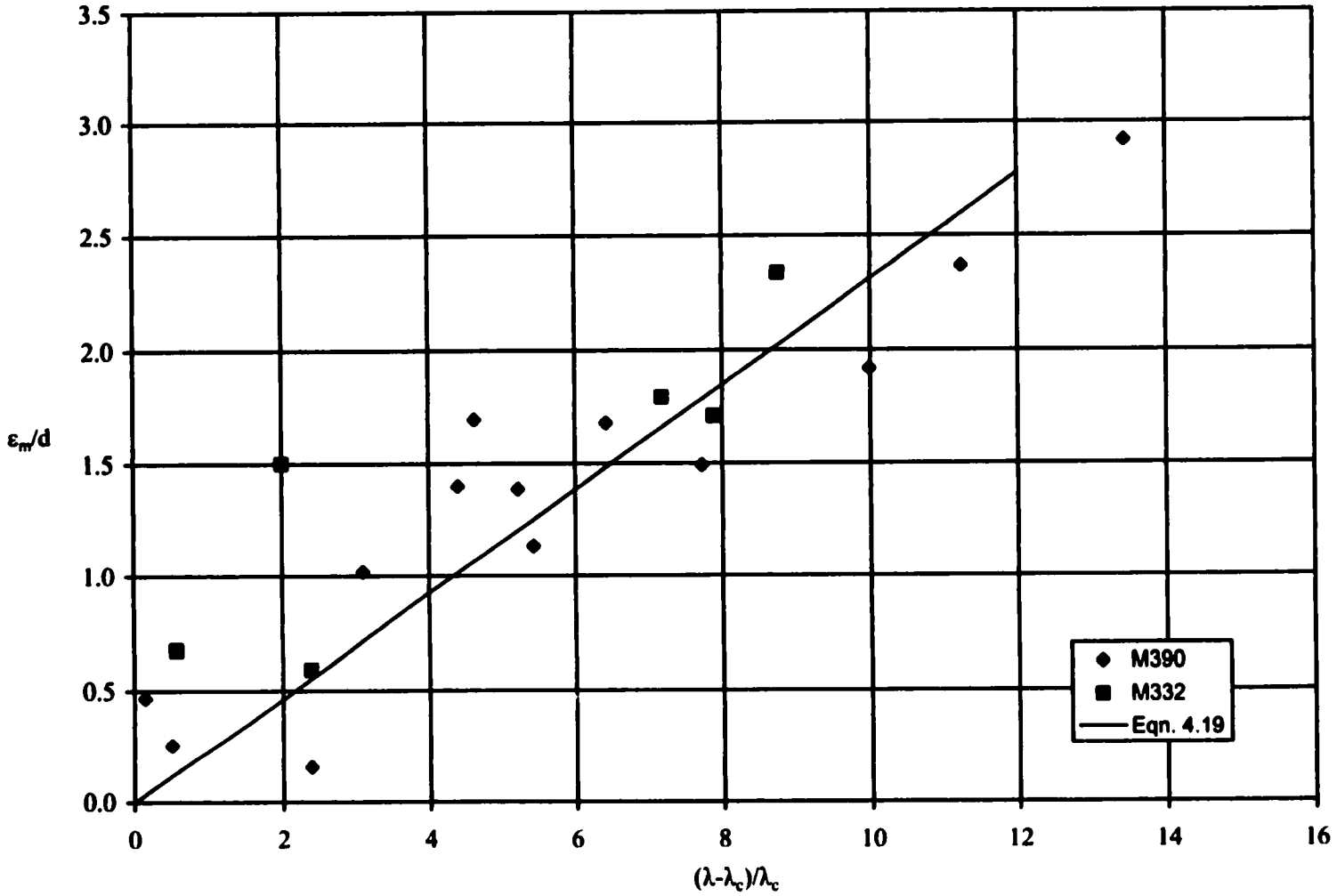

Fig. 4.8 Dimensionless maximum scour hole depth at equilibrium as a fuction of the excess shear stress.

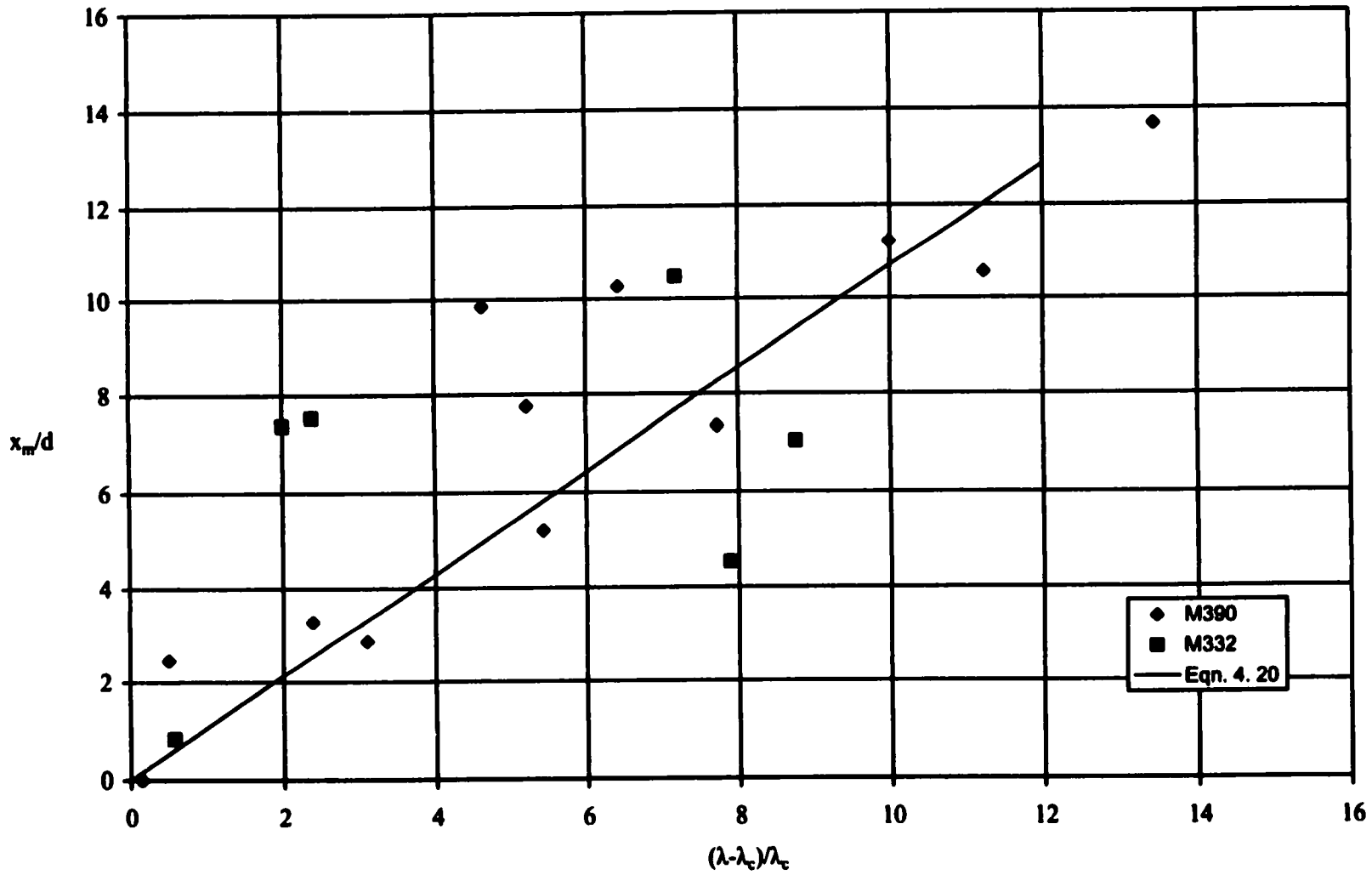

Fig. 4.9 Dimensionless location of the maximum scour hole depth at equilibrium as a function of the excess shear stress.

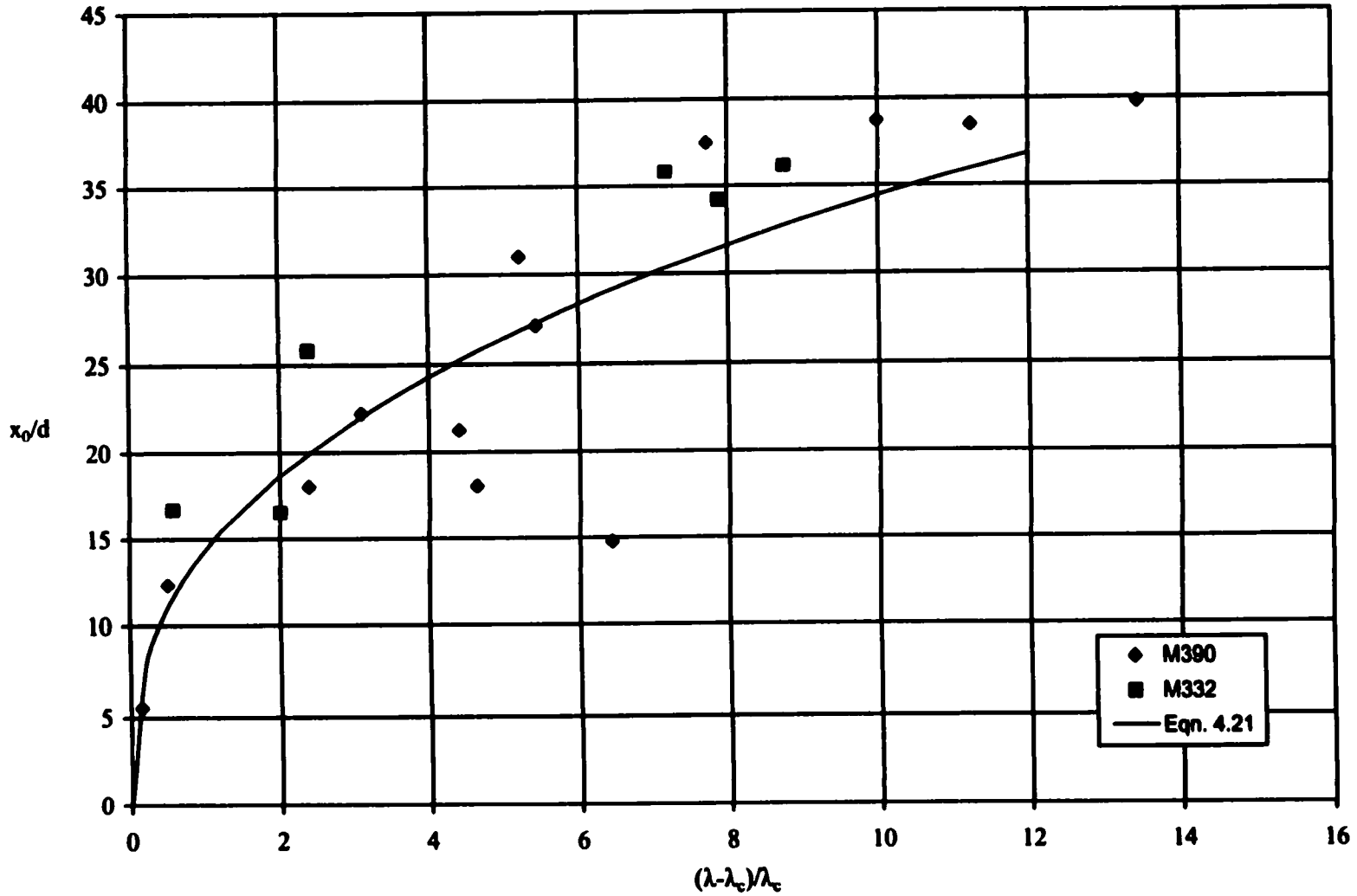

Fig. 4.10 Dimensionless length of the scour hole at equilibrium as a function of the excess shear stress.

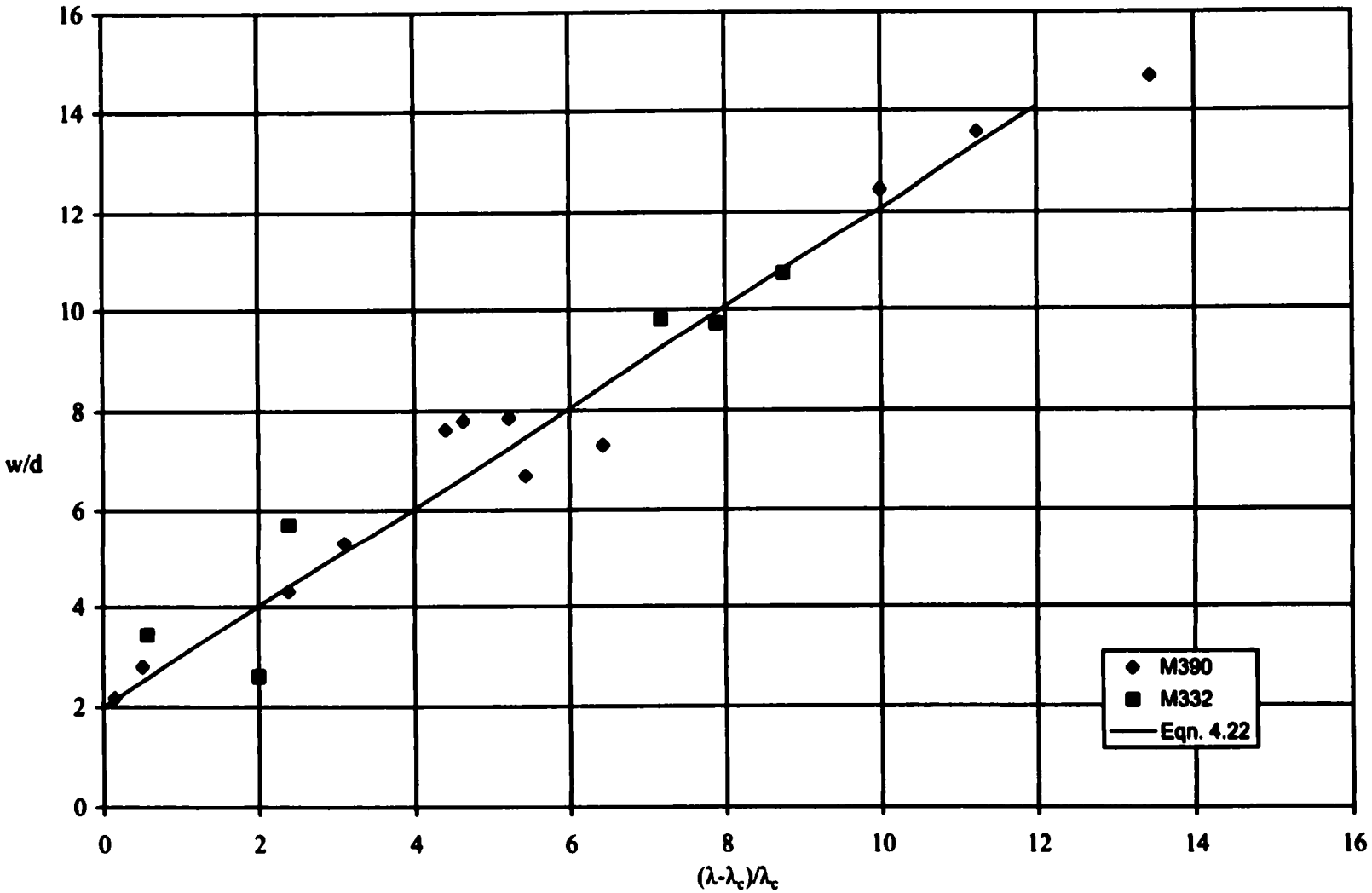

Fig. 4.11 Dimensionless width of the scour hole at equilibrium as a function of the excess shear stress.

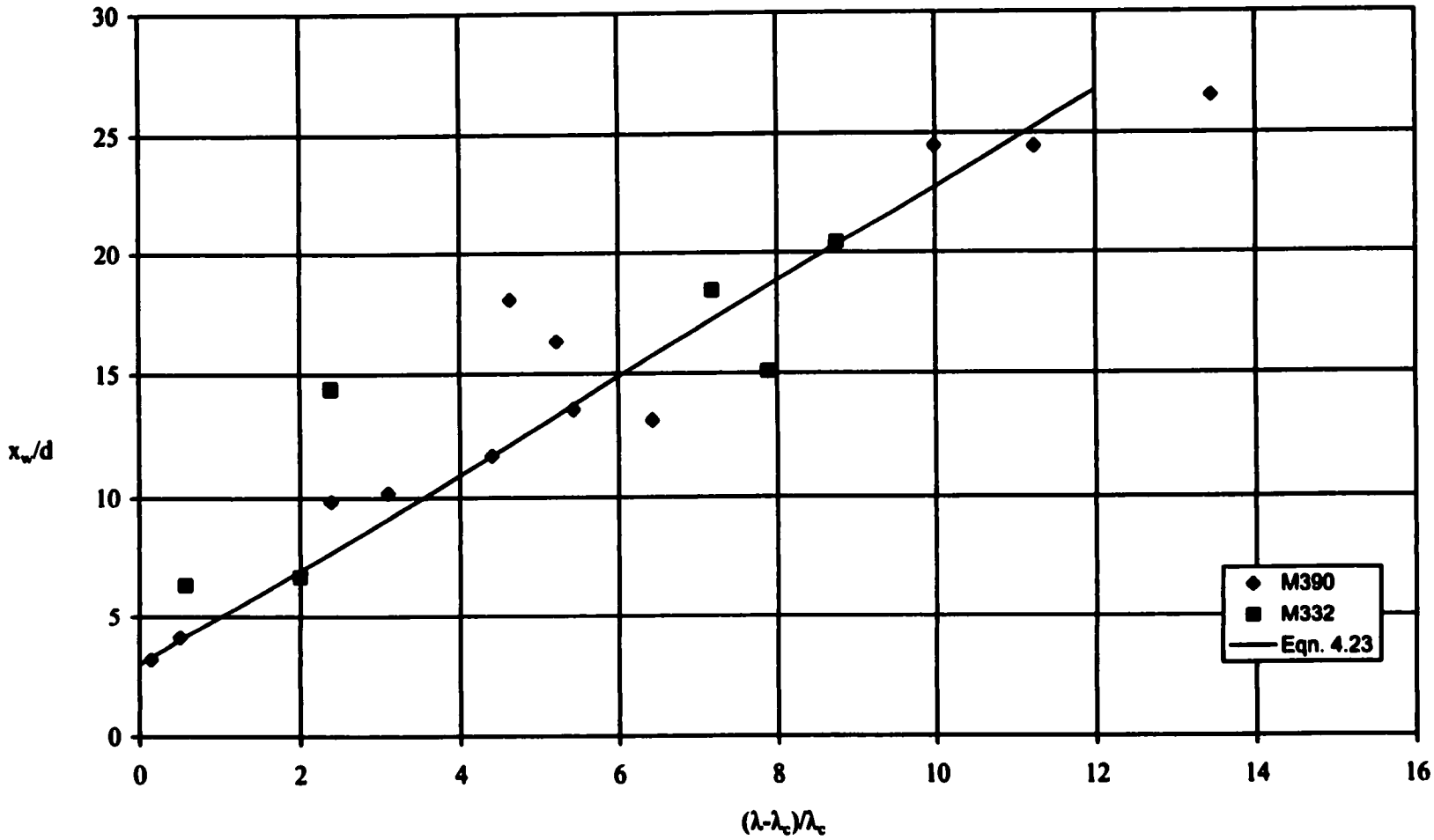

Fig. 4.12 Dimensionless location of maximum width of the scour hole at equilibrium as a function of the excess shear stress.

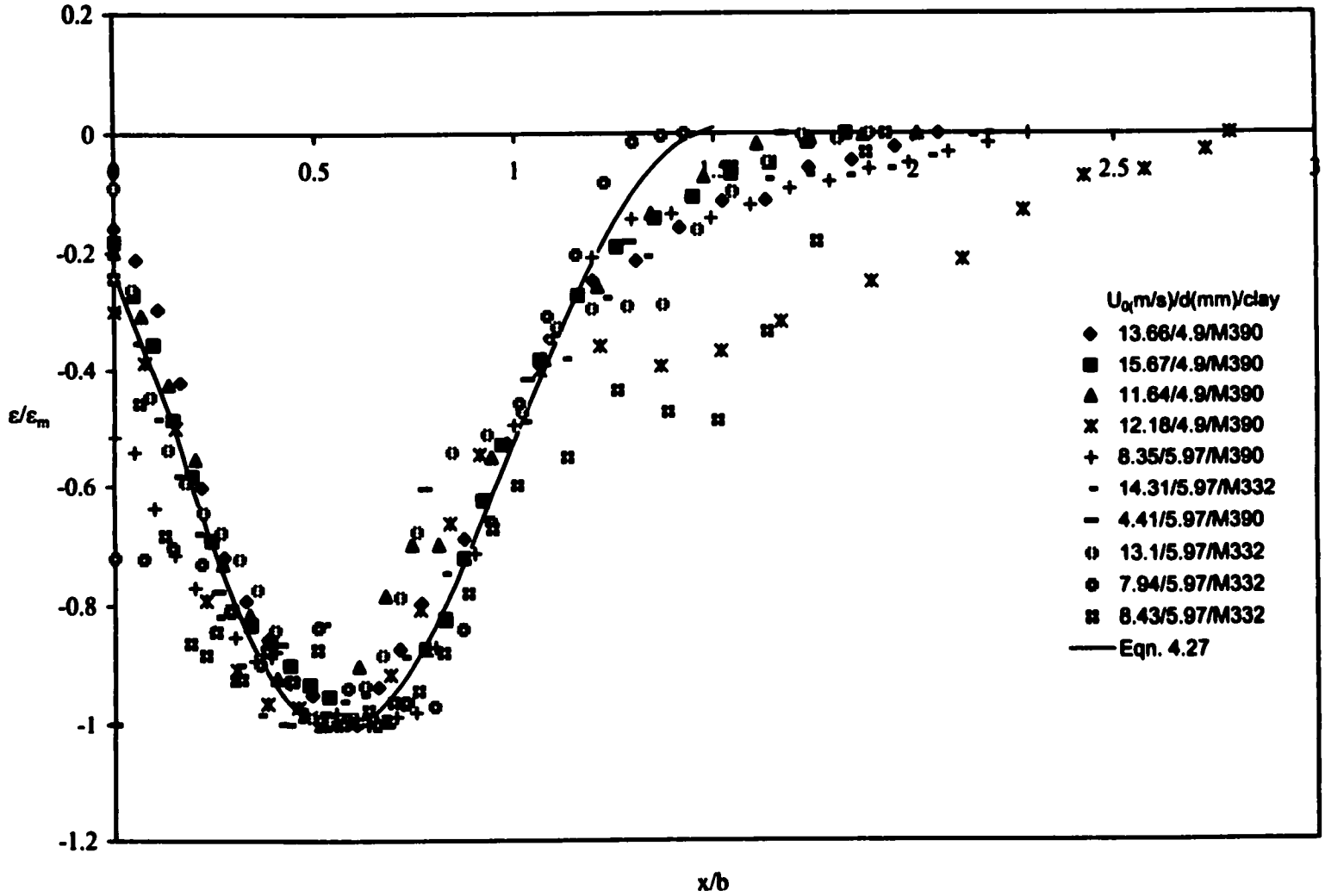

Fig. 4.13 Dimensionless scour hole profile-Mazurek data.

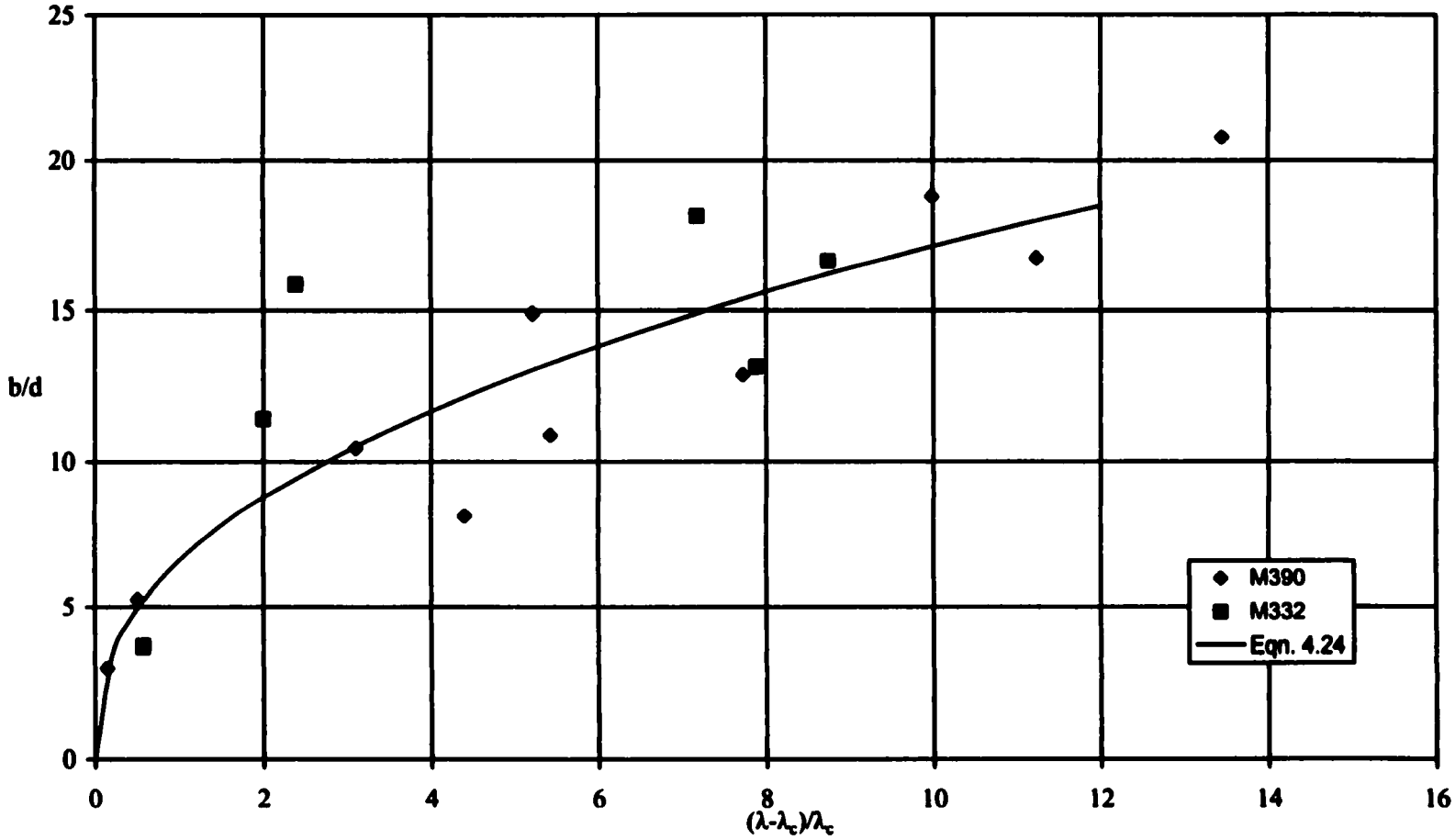

Fig. 4.14 Dimensionless scale b at equilibrium as a function of the excess shear stress.

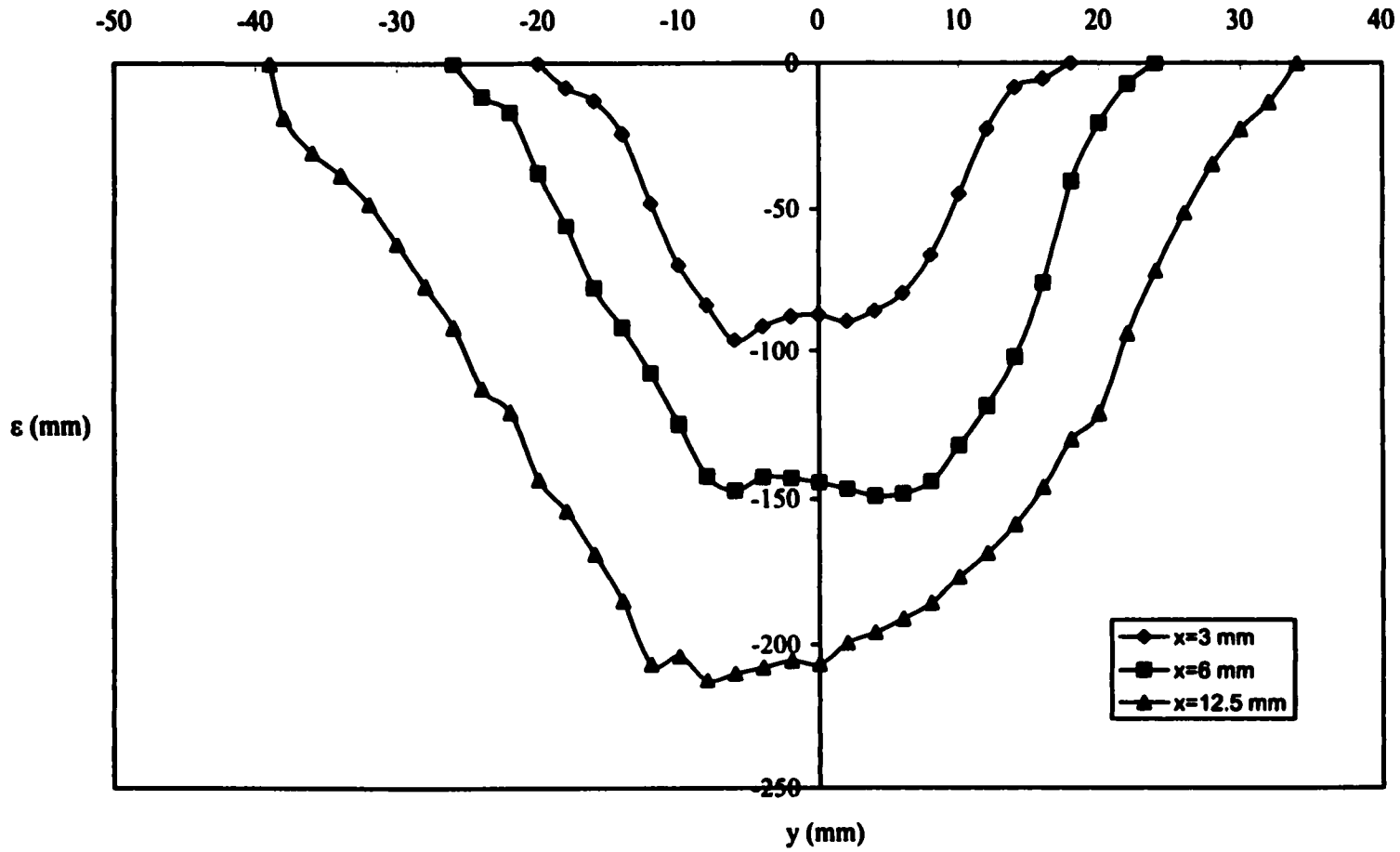

Fig. 4.15 Typical cross section profiles-Mazuerk data.

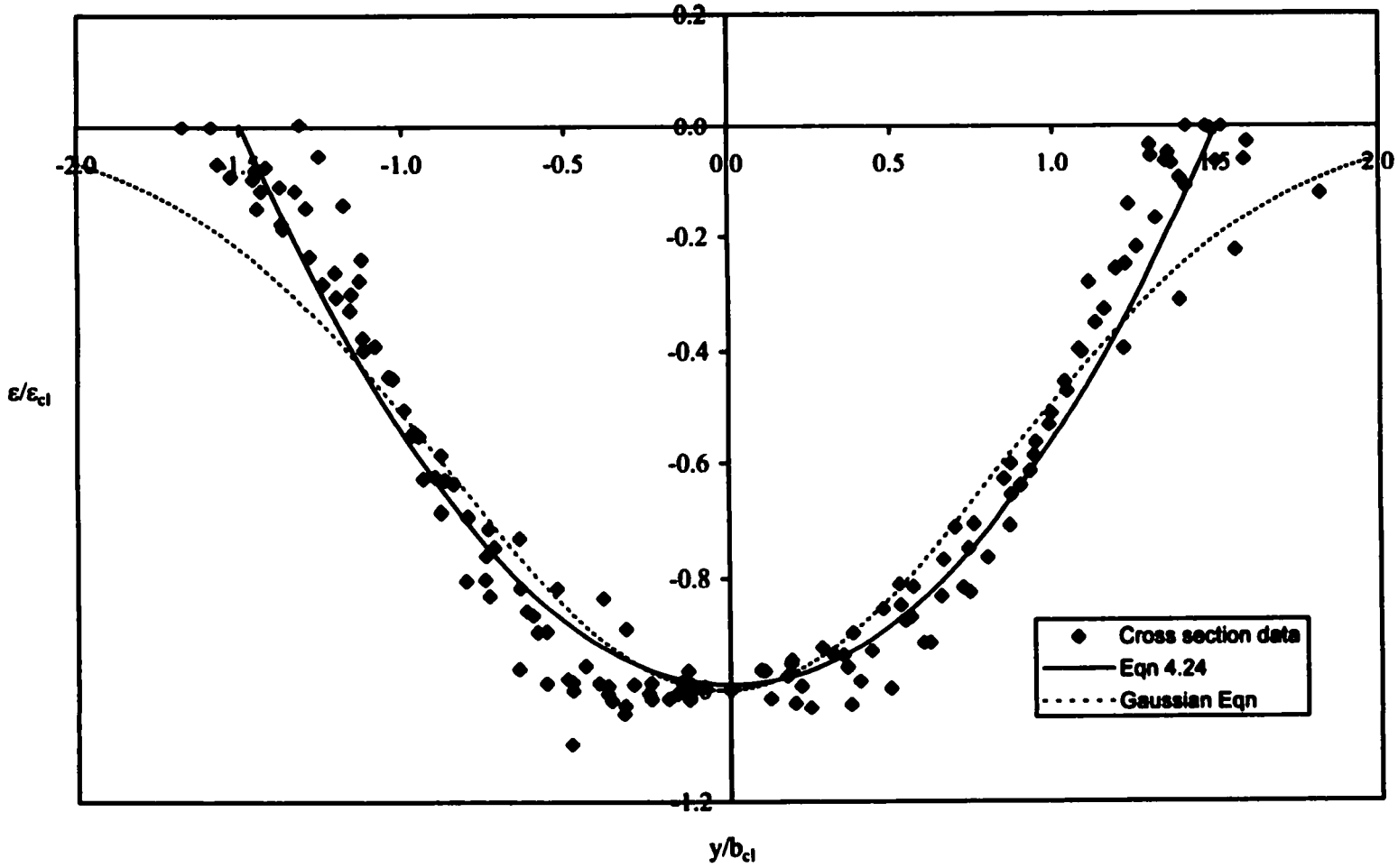

Fig. 4.16 Curve fits for the dimensionless cross section profiles.

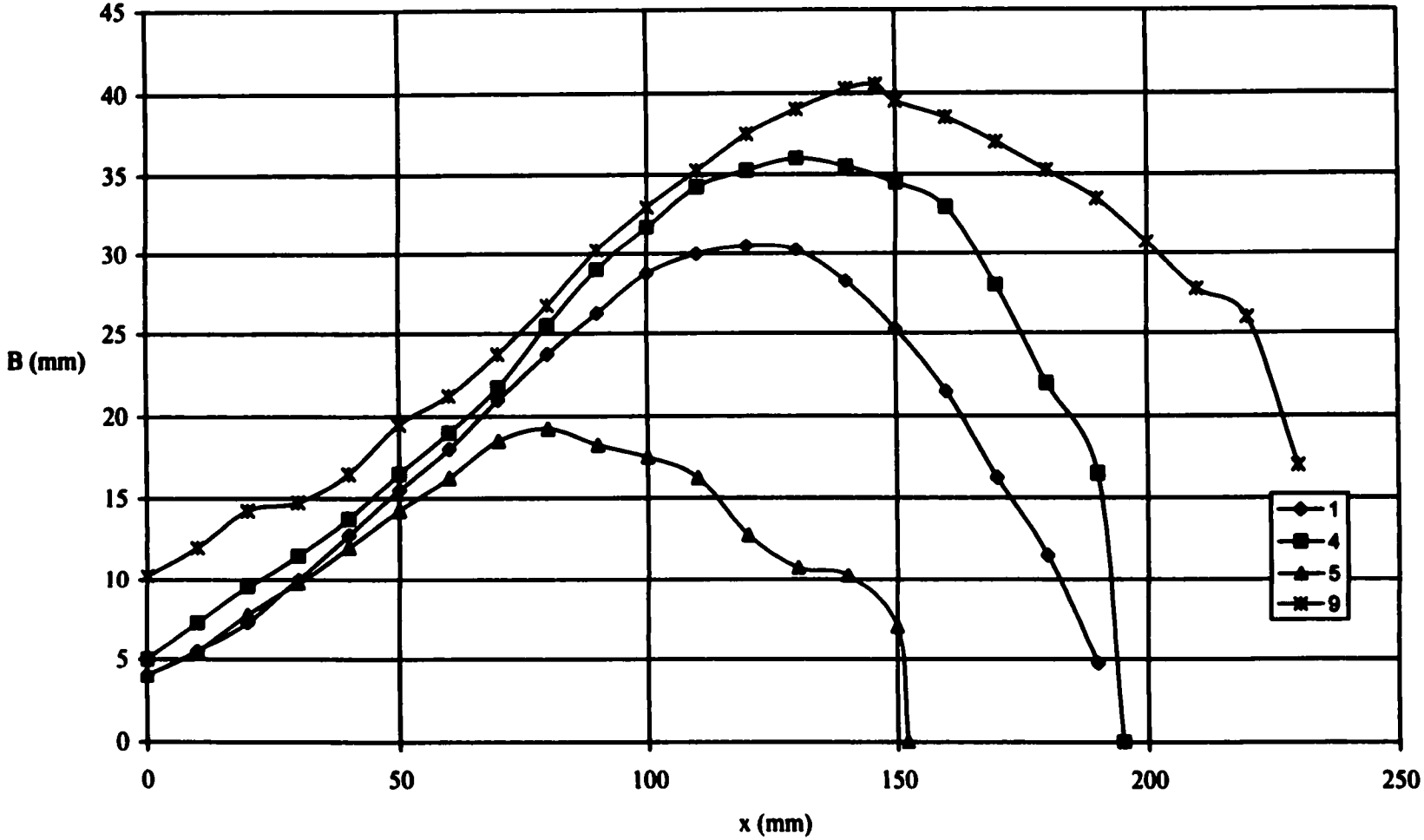

Fig. 4.17 Typical half-width profiles in plan-Mazurek data.

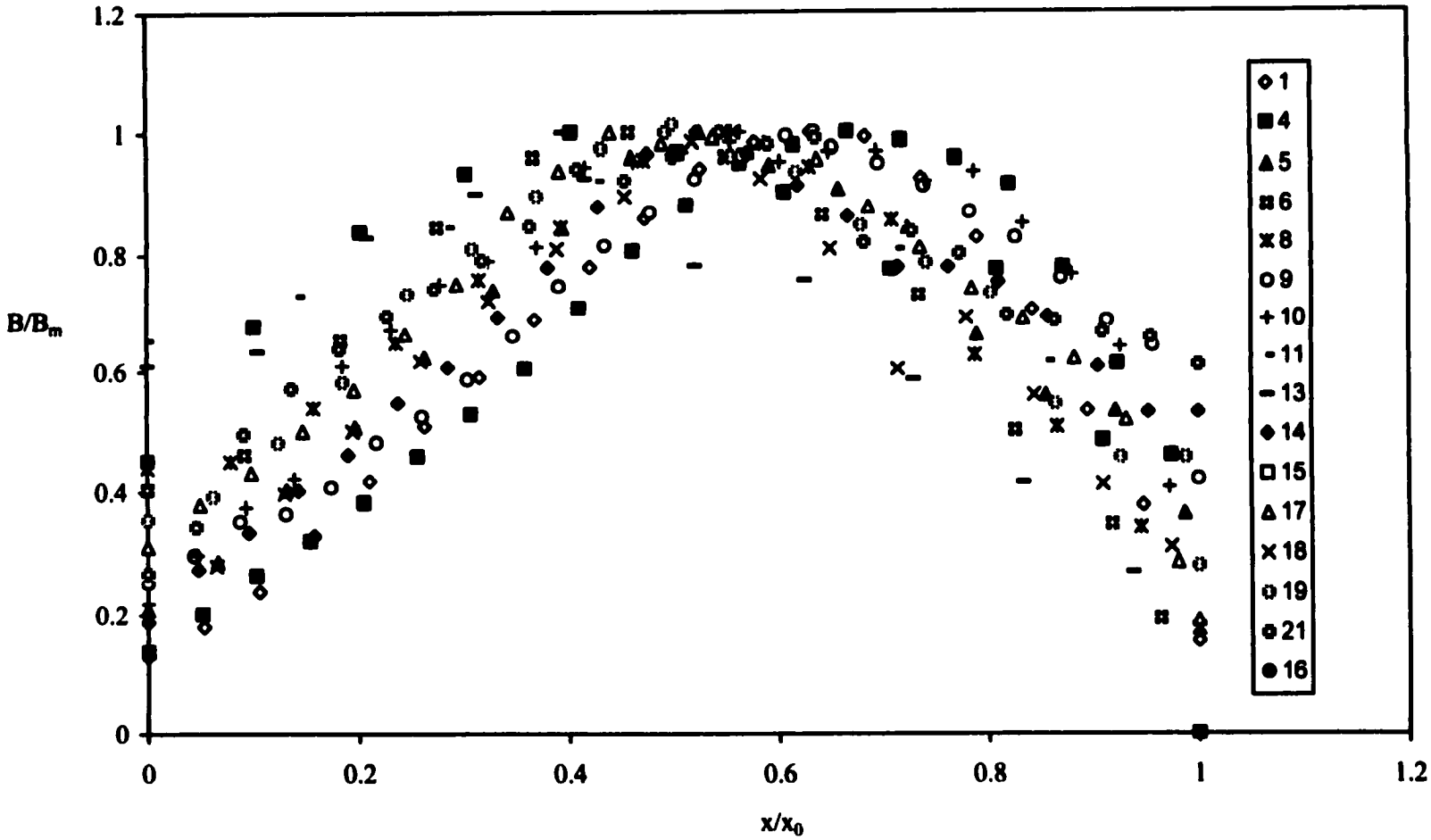

Fig. 4.18 Dimensionless growth profiles of half-width with x_0.

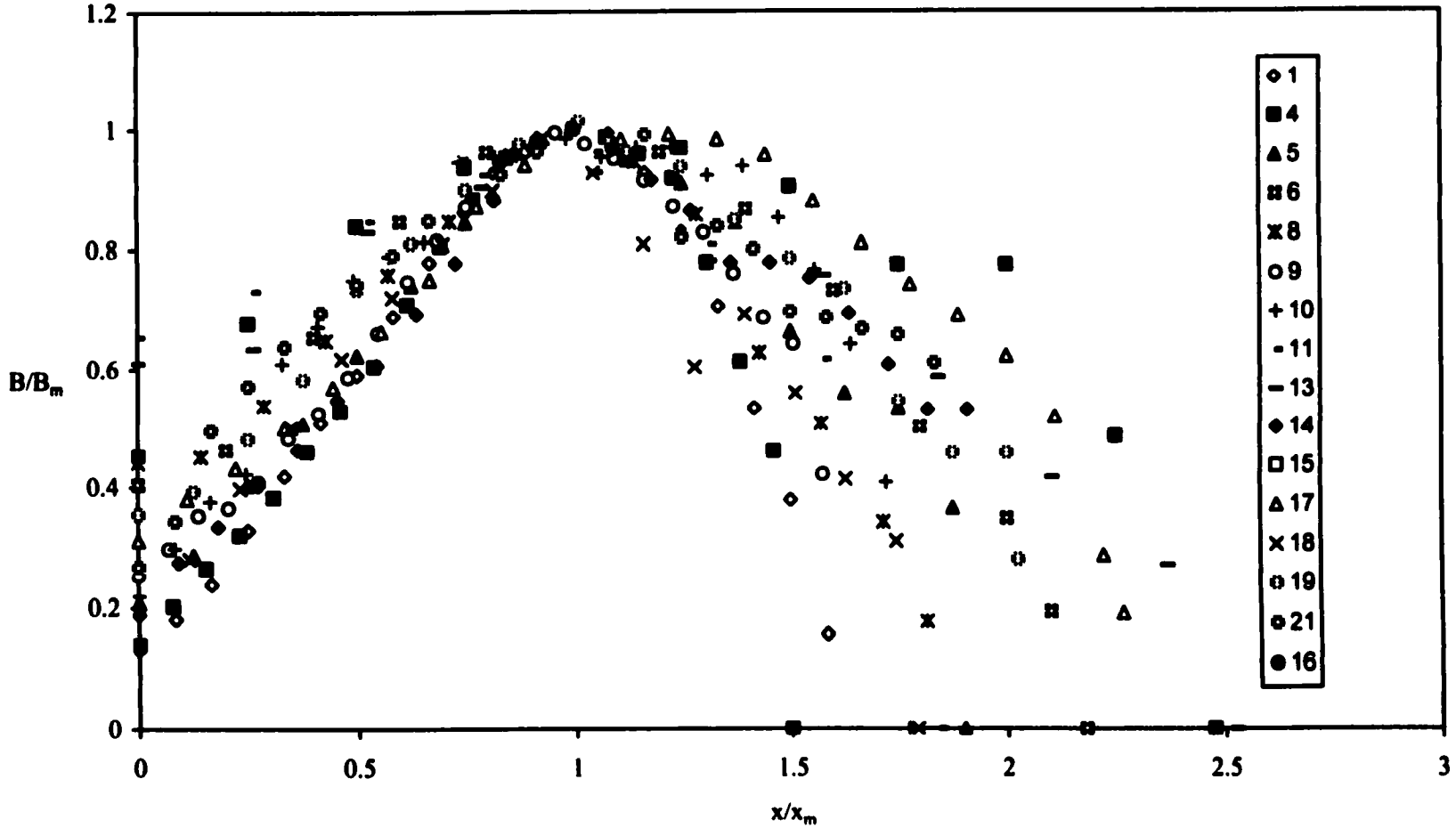

Fig. 4.19 Dimensionless growth profiles of half-width with x_w.

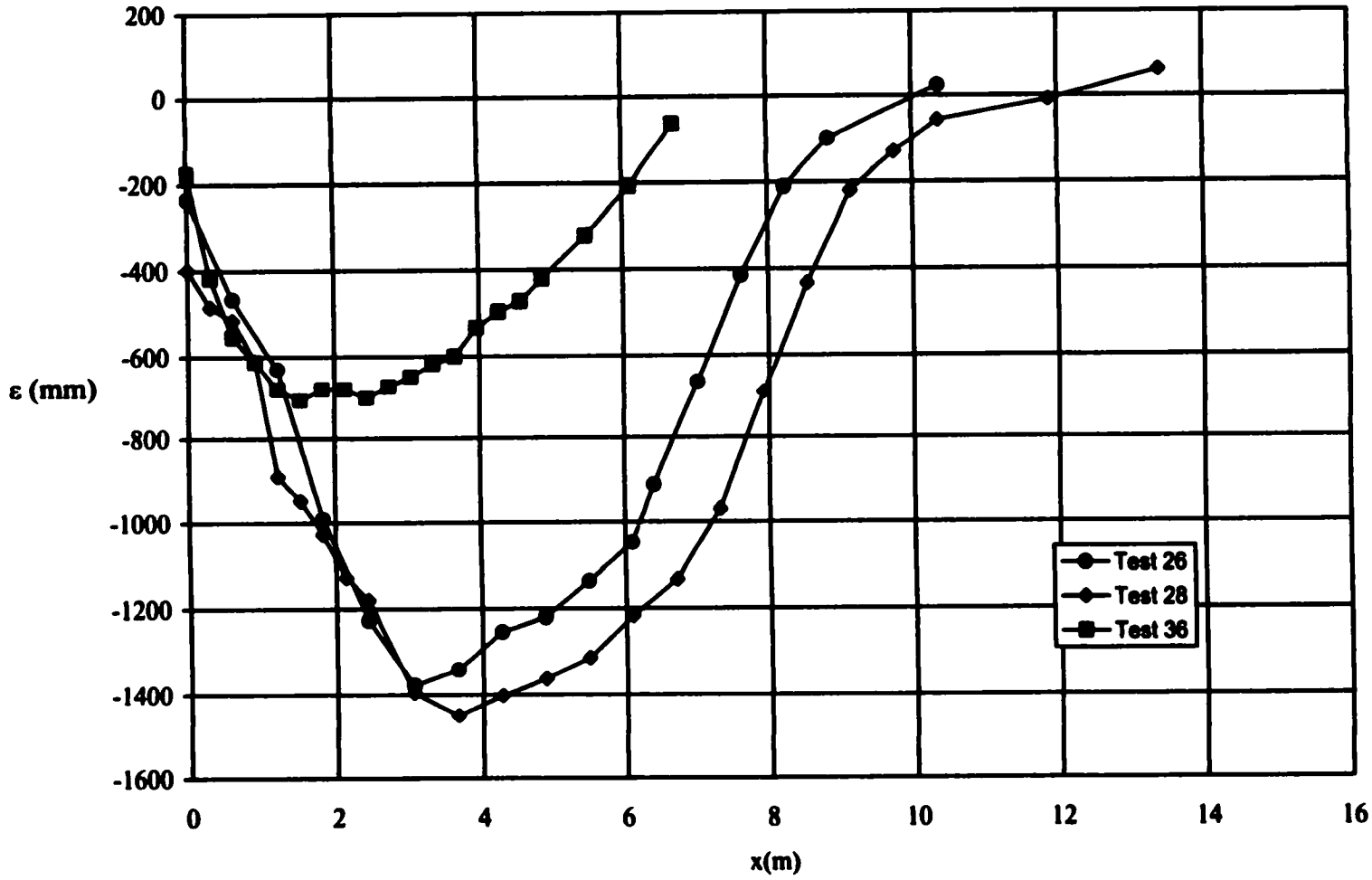

Fig. 4.20 Scour hole profiles along centreline-Abt's data at 1000 min.

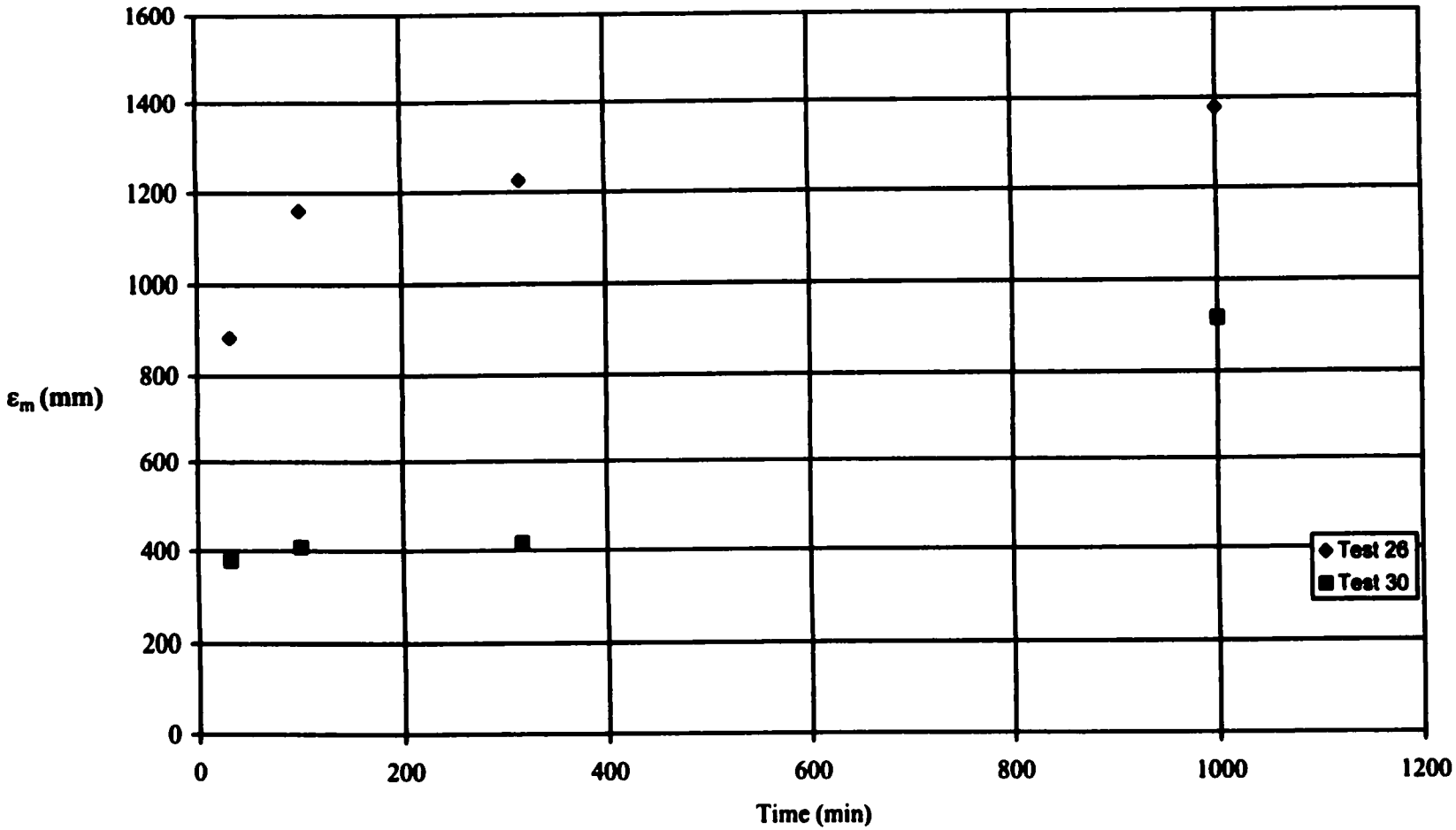

Fig. 4.21 Typical growth of maximum scour hole depth with time-Abt's data.

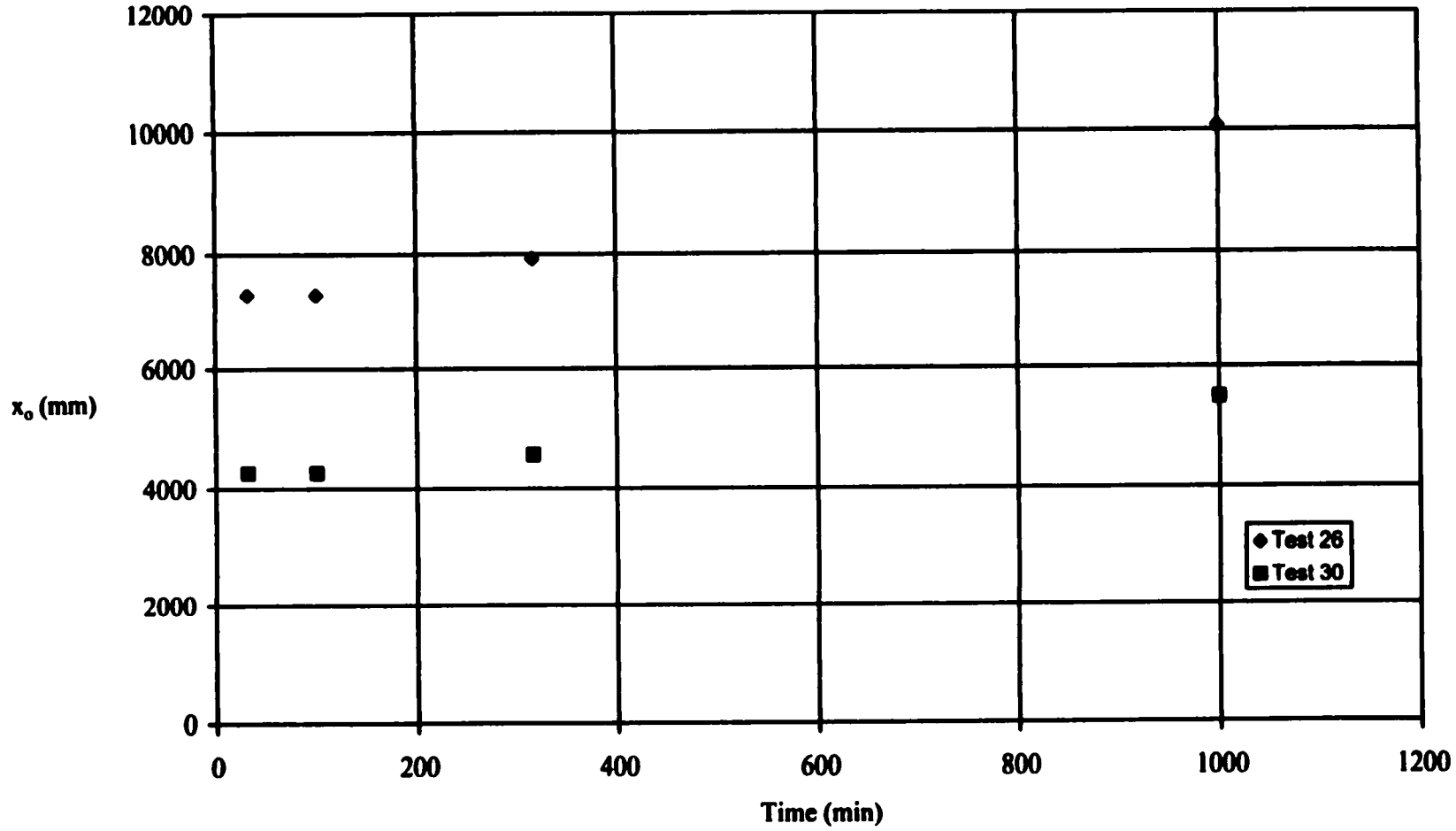

Fig. 4.22 Typical growth of scour hole length with time-Abt's data.

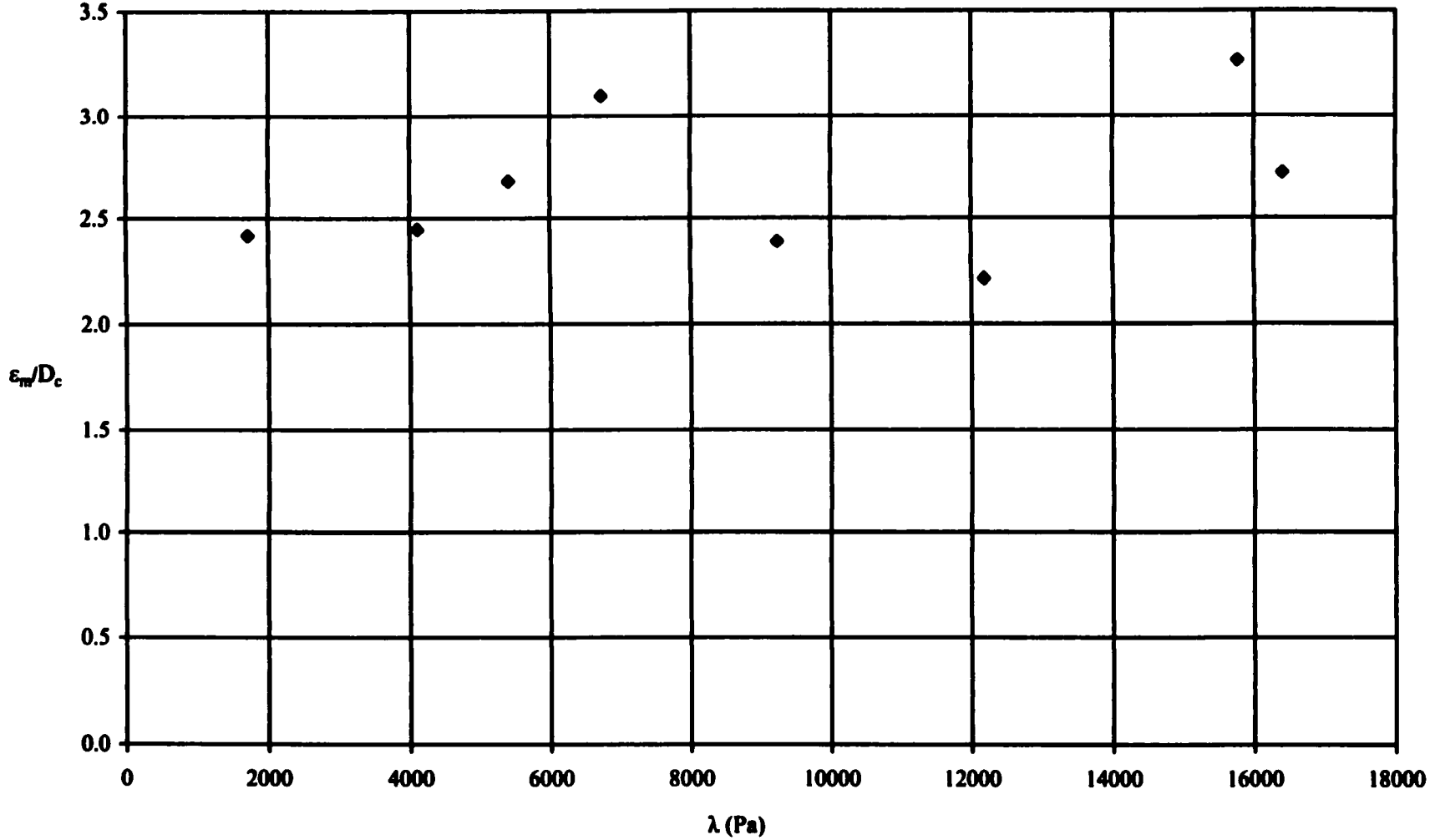

Fig. 4.23 Dimensionless maximum scour hole depth at 1000 min-Abt's data.

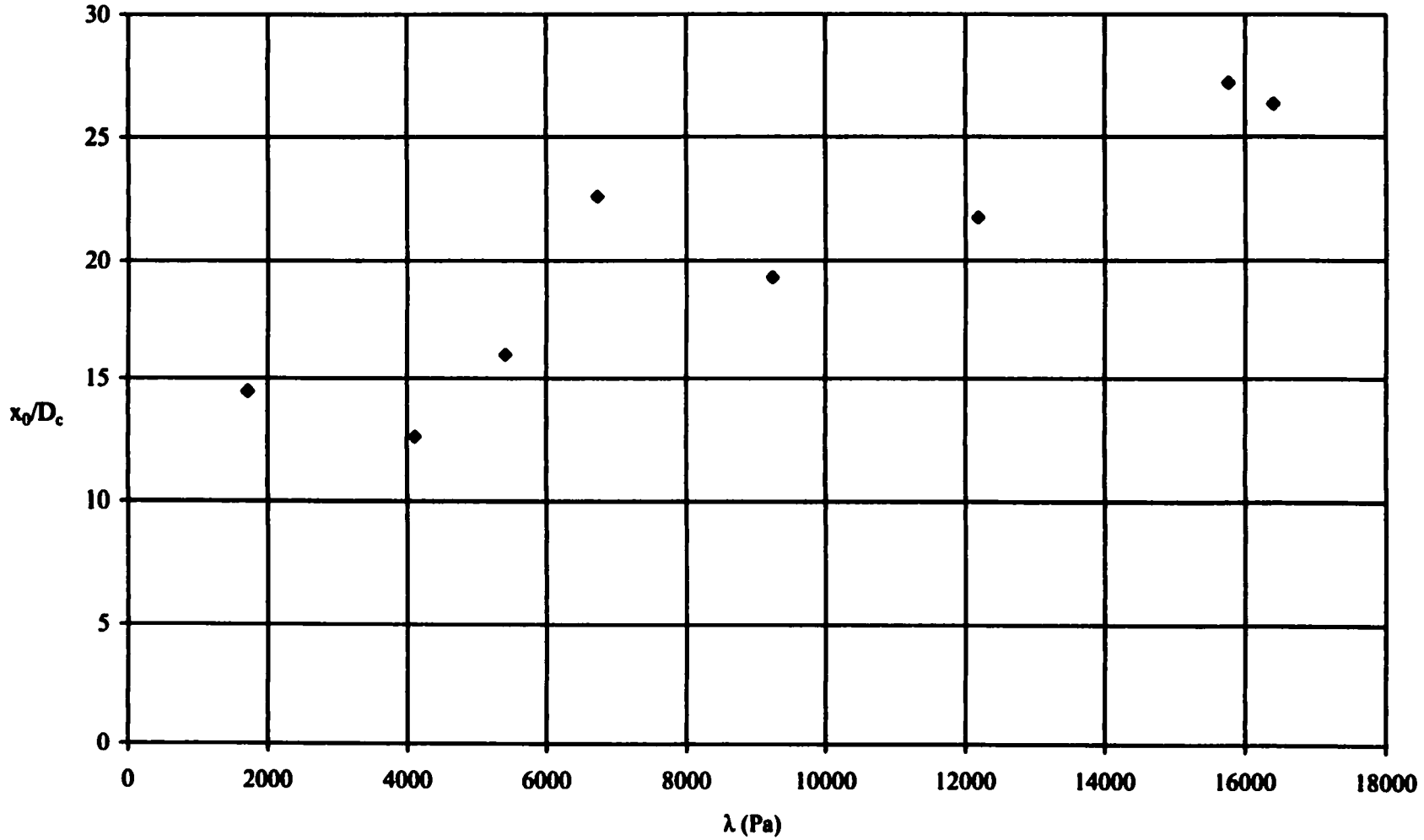

Fig. 4.24 Dimensionless maximum scour hole length at 1000 min.

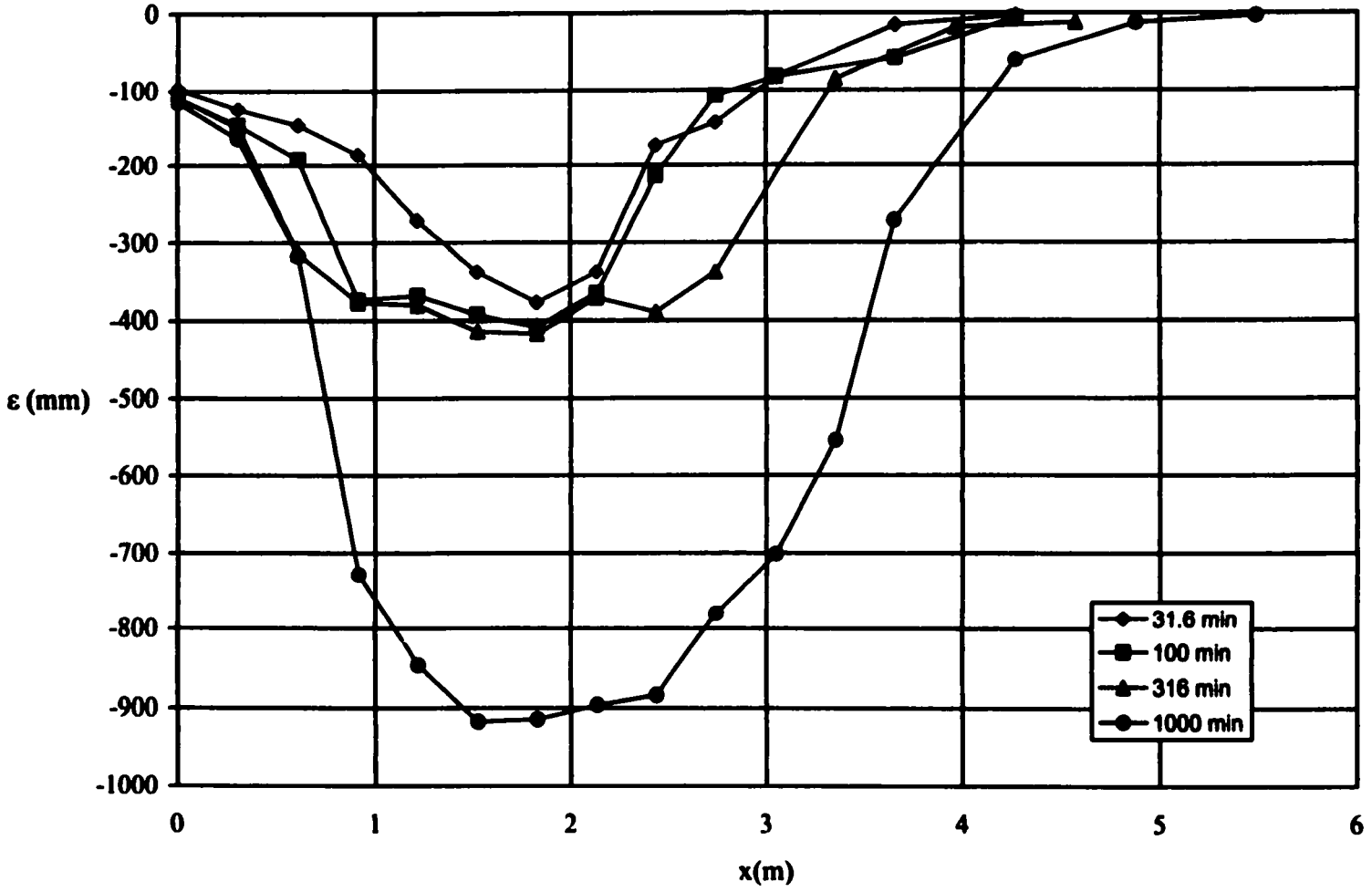

Fig. 4.25 Scour hole profiles along centreline-Abt's test 30.

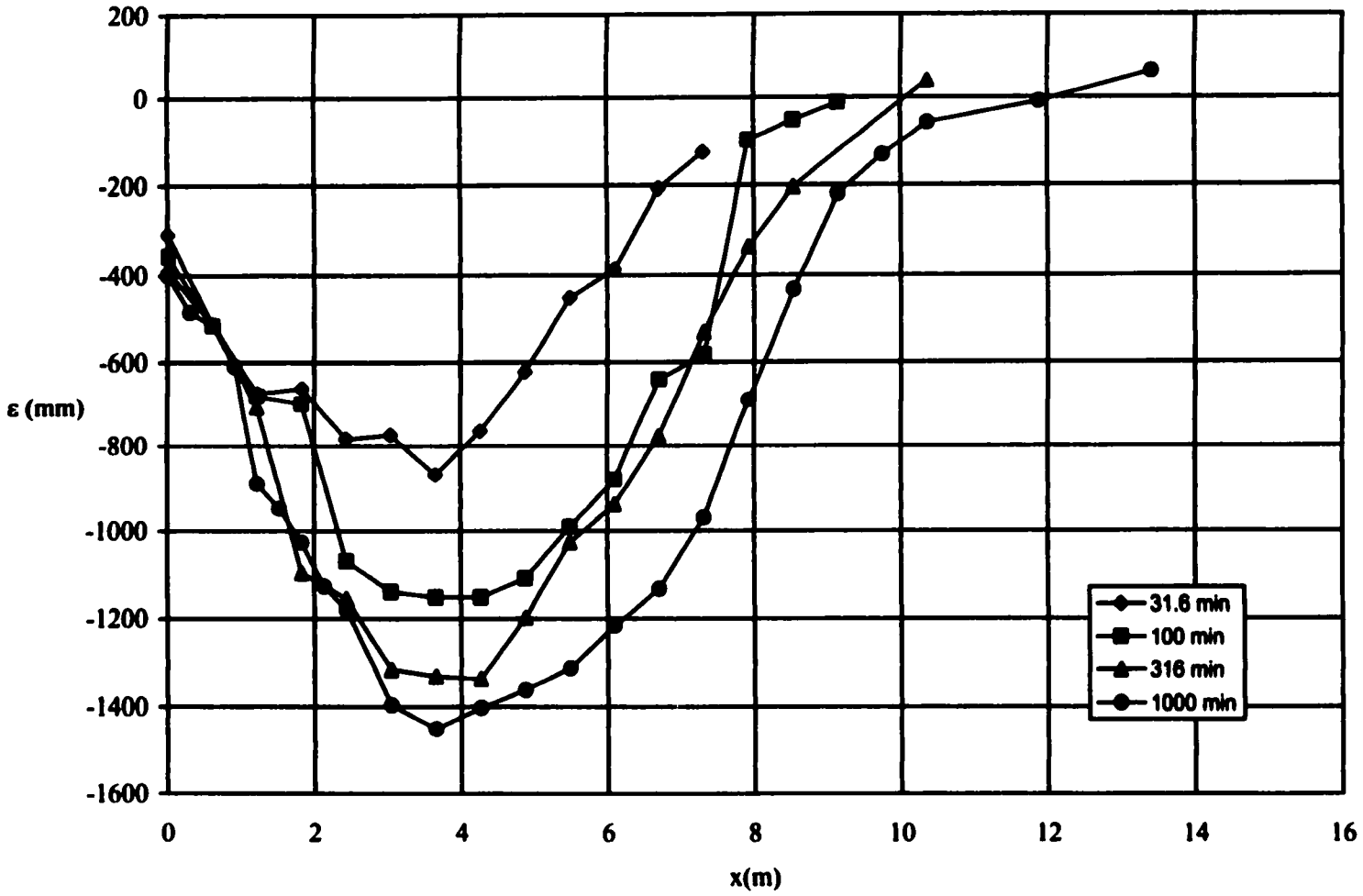

Fig.4.26 Scour hole profiles along centreline-Abt's test 28.

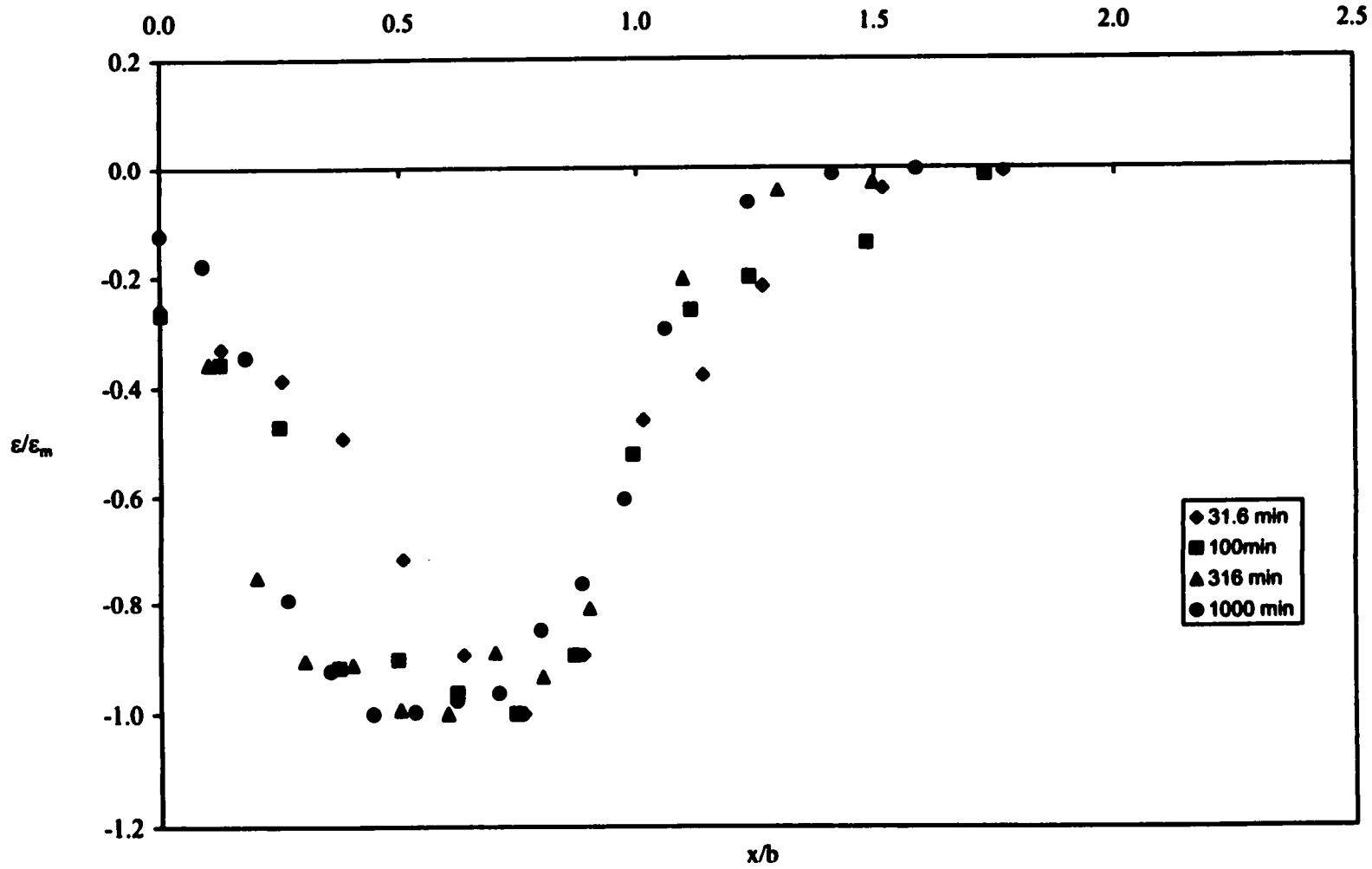

Fig. 4.27 Dimensionless scour profile-Abt's test 30.

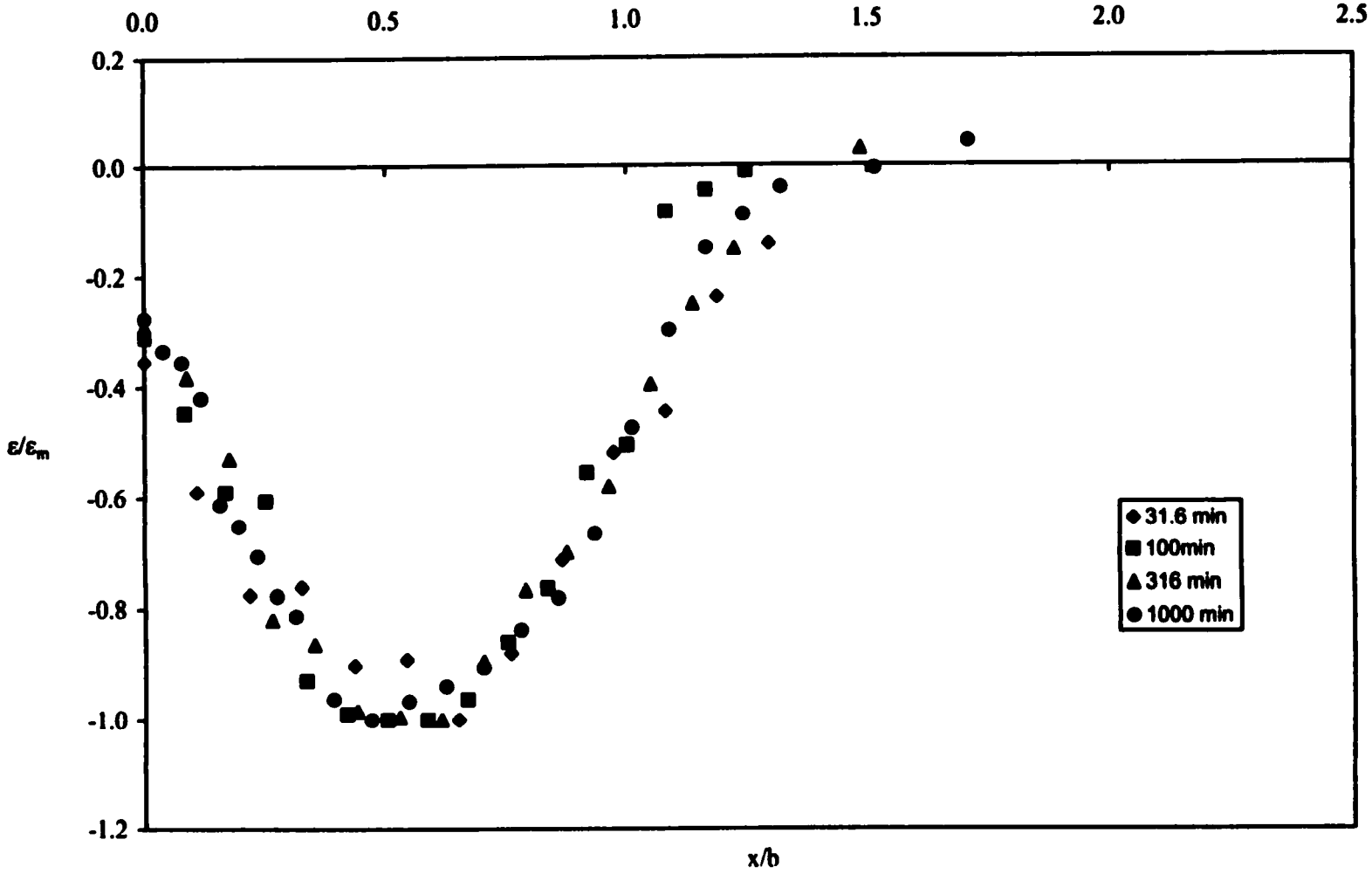

Fig. 4.28 Dimensionless scour profile-Abt's test 28.

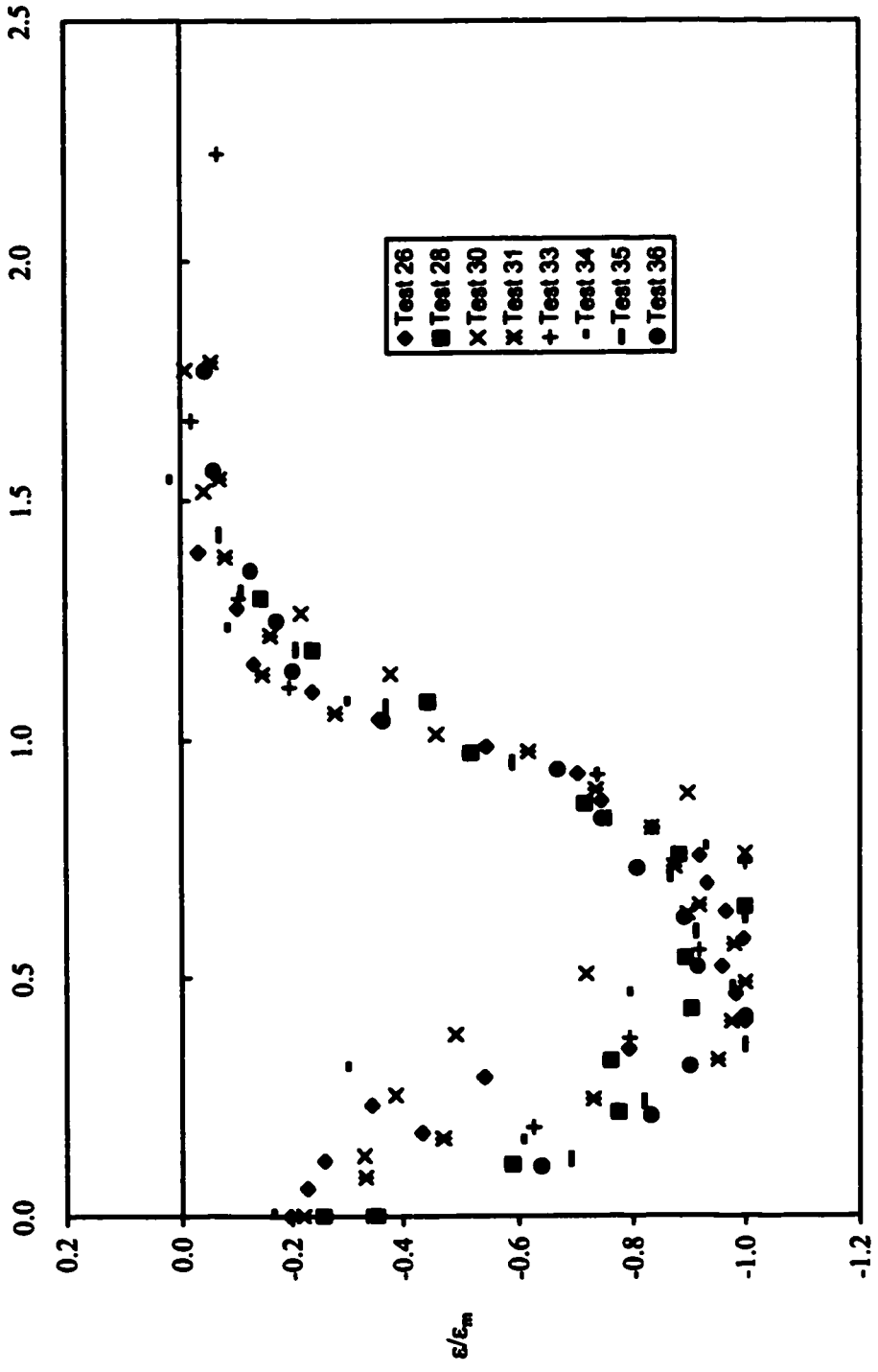

Fig. 4.29 Dimensionless scour hole profile: Abt's data at 31.6 min.

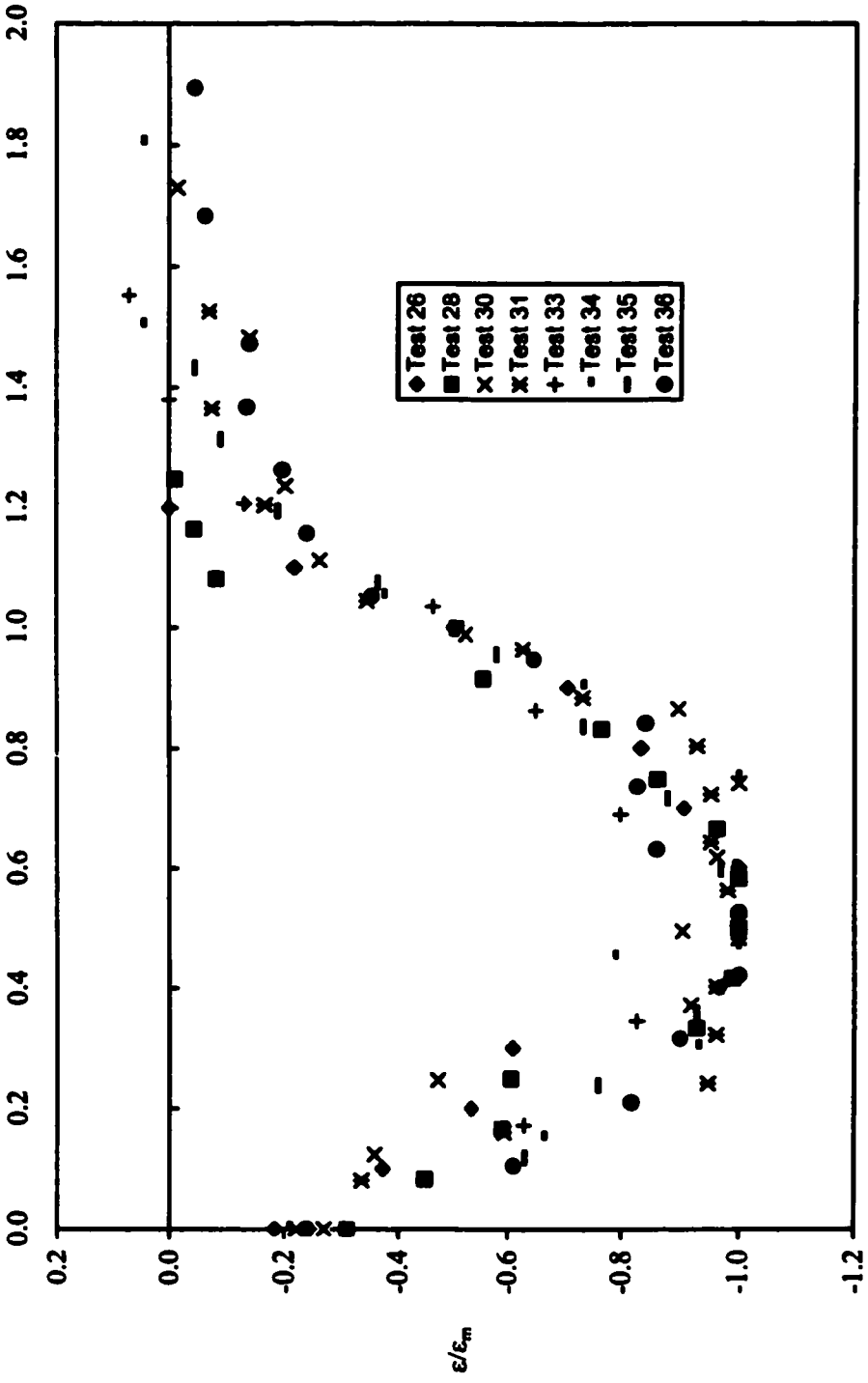

Fig. 4.30 Dimensionless scour hole profile: Abt's data at 100 min.

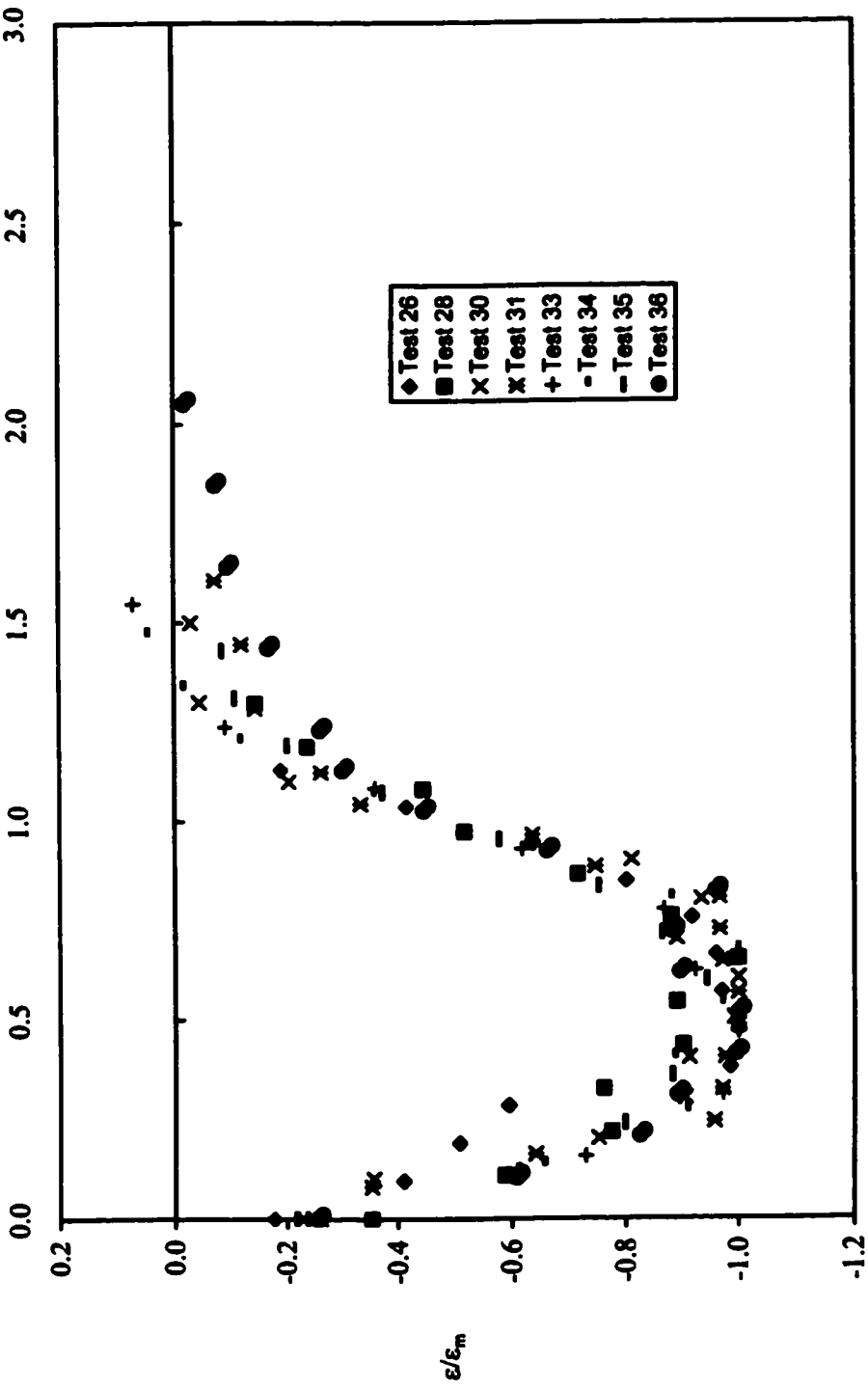

Fig. 4.31 Dimensionless scour hole profile: Abt's data at 316 min.

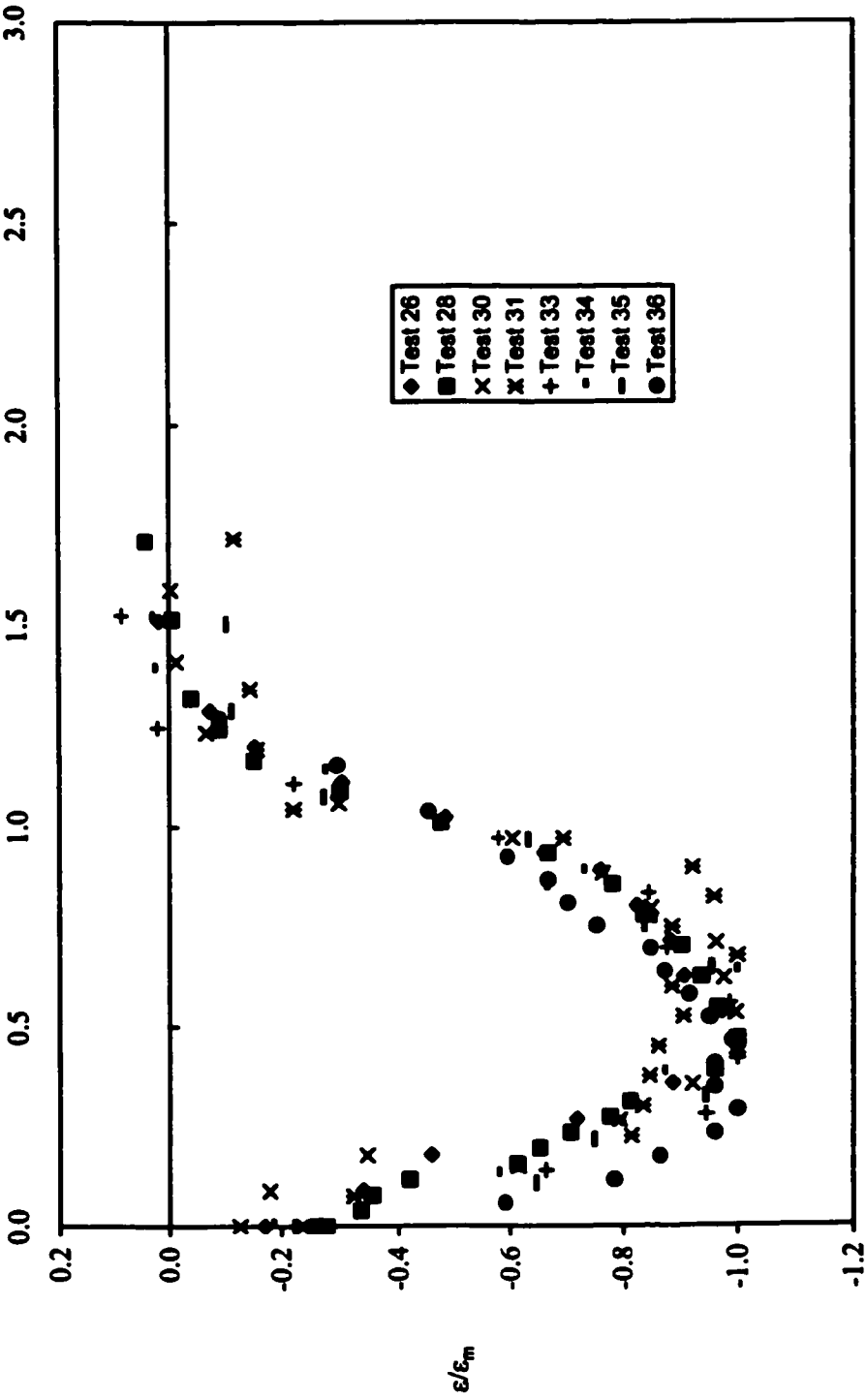

Fig.4.32 Dimensionless scour hole profile: Abt's data at 1000 min.

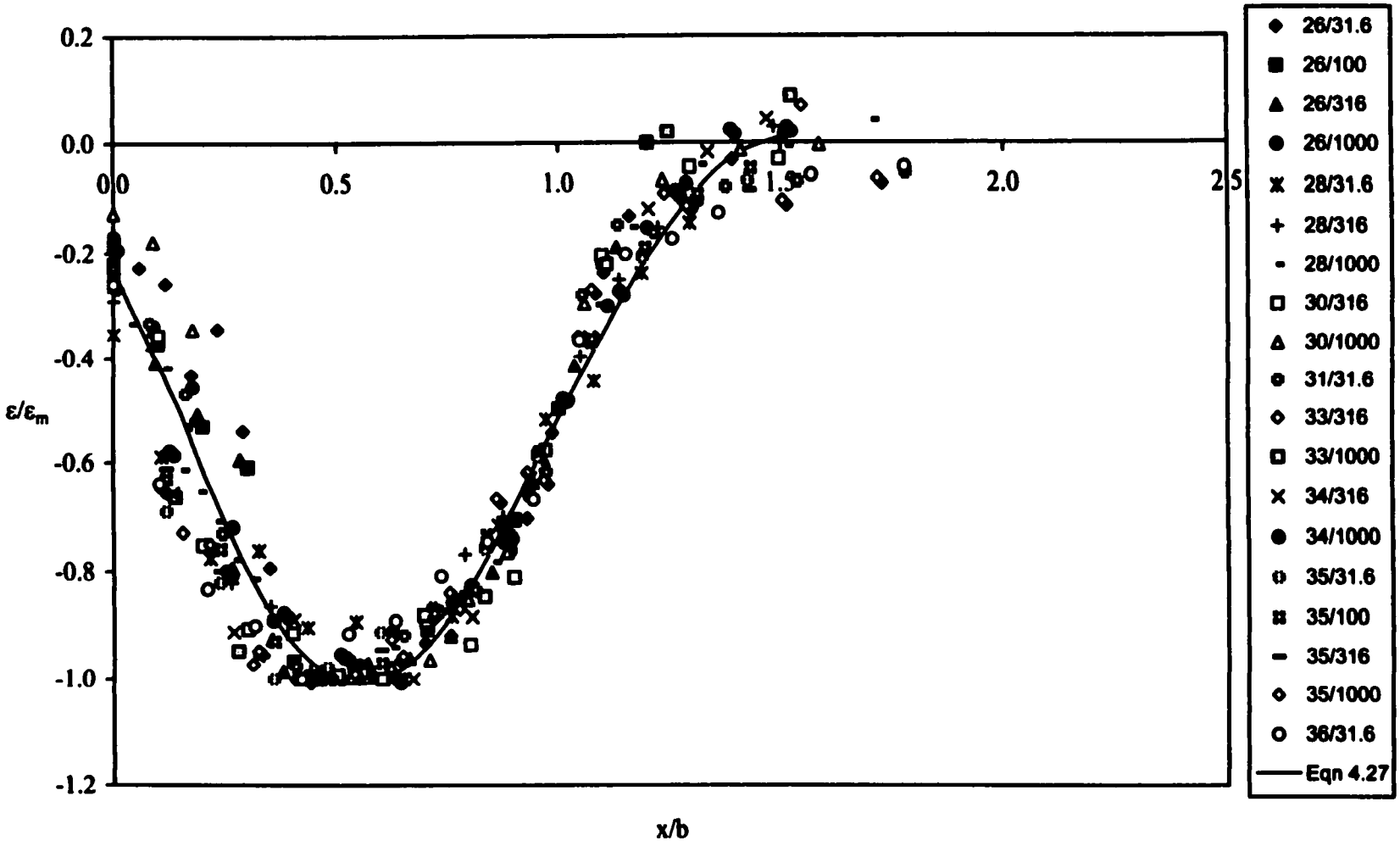

Fig. 4.33 Dimensionless scour profile-Abt's all tests.

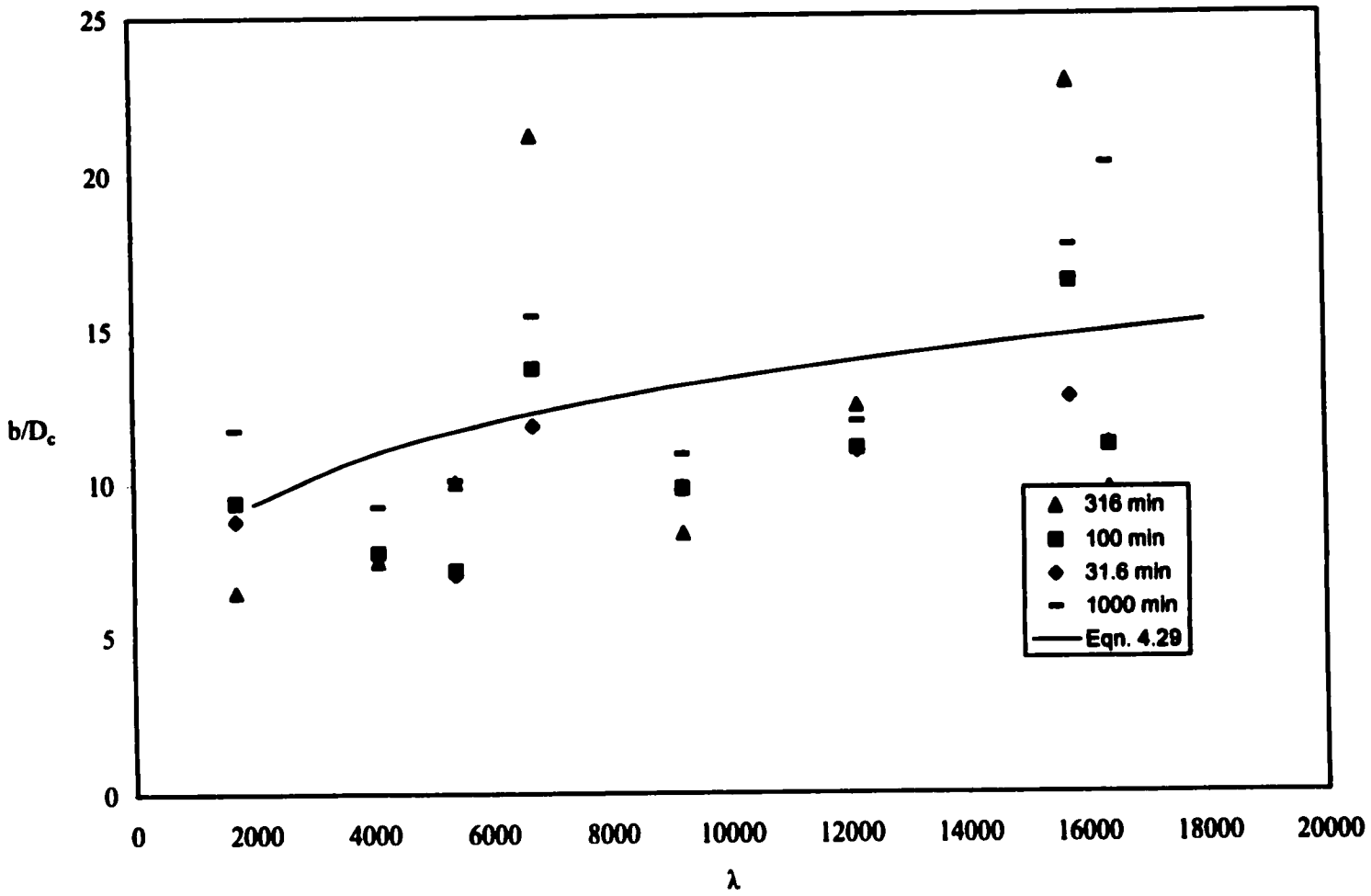

Fig. 4.34 Dimensionless profile of b as a function of λ.

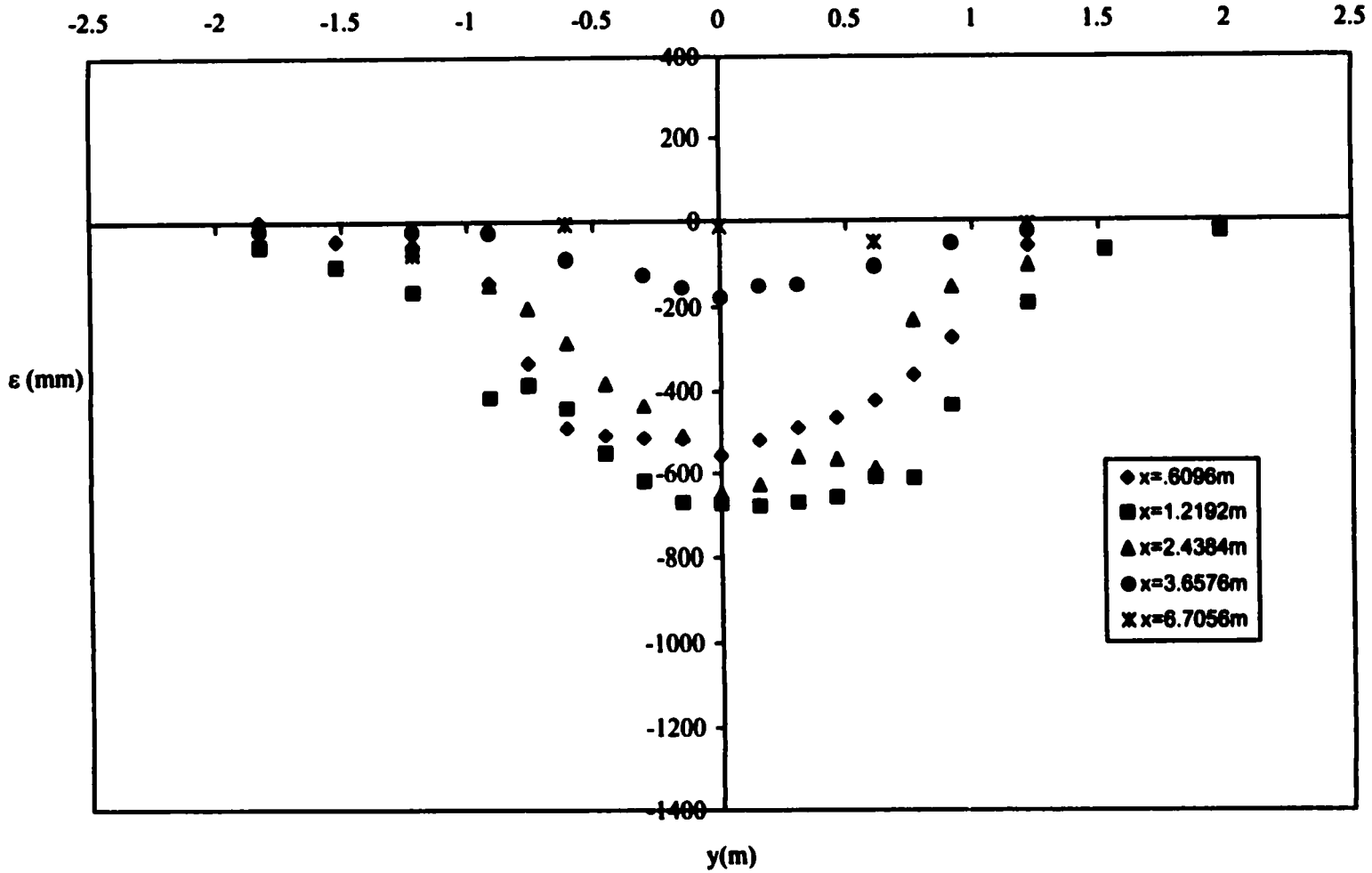

Fig 4.35 Cross section profile-Abt's test 36 at 316 min.

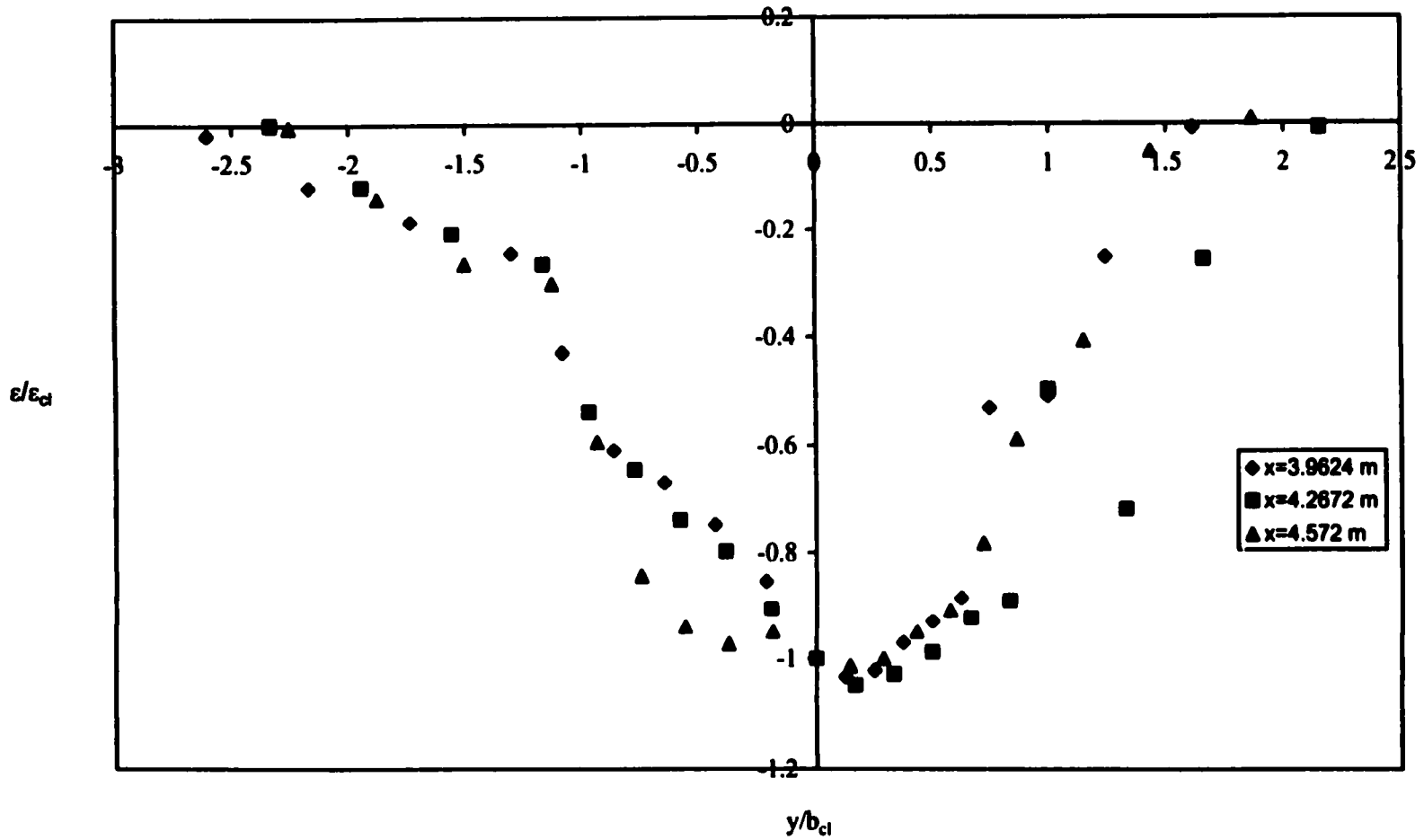

Fig. 4.36 Typical dimensionless cross section profile-Abt's data.

CHAPTER 5 CONCLUSION

5.1 Summary

As discussed in the chapter 1, local scour caused by water jets is a problem of considerable importance in hydraulic engineering. Nevertheless the scour of cohesive soils has received little attention. A review of the literature showed that the experimental studies on the flow at the outlets of the culverts by Abt (1980) and the laboratory work by Mazurek (unpublished) are the only studies available on scour of cohesive materials by circular wall jets. Abt did his own analysis of his experiments, with much scatter of the results. There is no previous analysis for the Mazurek data.

This thesis presents an analysis on the Abt and Mazurek data. A method was developed for predicting the scour hole dimensions from the properties of the jet and the clay. The results can be referred to determine the characteristics of scour in cohesive materials by circular wall jets. In this chapter, a brief discussion and general conclusions are presented on these two sets of data.

5.2 Conclusions

The first set of data is a series of experiments on scour downstream of culvert outlets in one cohesive material at prototype scale. The general findings of the Abt experiments include:

1. The scour holes were generally similar in geometric configuration and appearance.
2. The scour hole profiles were made dimensionless using the culvert diameter and the distance from the culvert outlet where the scour depth was half the maximum depth. For each test run, the scour hole profiles with time (31.6 min, 100 min, 316

min and 1000 min) all appear to have the same dimensionless shape. Dimensionless scour hole profiles at the same time scale are approximately the same in shape for different test runs.

3. Scour hole cross-section profiles appear to have a similar general shape.
4. Larger diameter materials were deposited at the downstream end of the scour hole. There was a mound formed downstream of the scour hole in some tests.

The second set of data is a laboratory study of the scour of clays by a submerged circular wall jet produced in two cohesive soils by a flow through a nozzle of three different diameters. The general findings of the experiments include:

1. The scour hole in plan grew linearly in the first part of the scour hole and then was more rounded at the end of the scour hole. There was no formation of mound at the end of the scour hole.
2. Mass erosion was the predominant erosion type by the removal of small chunks, usually 2-3 mm in size.
3. The scour hole generally reached the equilibrium state within 72 h.
4. The dimensions of the scour hole at equilibrium state (maximum depth, the location of the maximum depth of scour hole, the length of the scour hole, maximum width, the location of the maximum width and the distance from the nozzle to where the scour is half the maximum scour depth) can be related to the parameter $\lambda=\rho U_0^2$ and equations were developed to predict the scour hole dimensions.
5. There is a critical value of λ below which no significant erosion occurred. λ is estimated at 17000 Pa for clay M390 and 21000 Pa for clay M332. These critical

1. λ are equivalent to critical shear stress values of 42 Pa for clay M390 and 52 Pa for clay M332.
2. The scour hole profiles were made dimensionless in the same manner as mentioned in Abt's data. The dimensionless scour hole profiles are similar in shape and can be described quite well by the curve fitted to Abt's data in the range $x/b<1.5$.

The equations developed herein are limited to cohesive materials that are not dispersive (where there is no critical shear stress), fissured or otherwise disturbed, or where there are layers or lenses of sand or silt They also only apply to the range of shear stresses tested, for jet Reynolds number *R* greater than about 10,000, and only for jets that are not offset from or inclined to impinge on the bed.

5.3 Recommendations for Future Work

The equations developed in this work only give the prediction of the scour hole dimensions at the equilibrium state. The evolution of scour hole dimensions with time should also be considered. For the two sets of data discussed in this thesis, Abt's tests did not reach the equilibrium state while Mazurek tests did not record the evolution with time. The data should be expanded by performing experiments on the evolution of scour in future research to get more data for the prediction equations.

The current tests with the circular wall jet examine only the scour by submerged jet. Abt's tests focused on the scour with the tailwater maintained at $0.45D_c \pm 0.05D_c$ above the culvert invert and Mazurek's used a submerged circular wall jet. There is a need to examine the effects of submergence and the tailwater condition on scour. As well, there is a need to study the development of the scour hole if the jet is offset. Those future works can be performed by changing the location of the jet and the hydraulic conditions.

REFERENCES

Abida, H., and Townsend, R. (1991) "Local Scour Downstream of Box-culvert", Journal of Irrigation and Drainage, ASCE, **117**: 25-40.

Abramovich,G. (1963) The Theory of Turbulent Jets (English translation), MIT Press, Cambridge, Mass., US.

Abt, S.R. (1980) Scour at Culvert Outlets in Cohesive Bed Material, Ph.D. Thesis, Colorado State University, Fort Collins, Colorado, US.

Aderibigbe, O.O. (1996) Contribution to Erosion by Jets, Ph.D. Thesis, University of Alberta, Edmonton, Alberta, Canada.

Ali, K H.M. and Lim, S.Y. (1986) "Local Scour Caused by Submerged Wall Jets", Proceedings of the Institution of Civil Engineers, Water, Maritime and Energy, **81**(2): 607-645.

Bohan, J. (1970) "Erosion and Riprap Requirements at Culvert and Storm-Drain Outlets", US Army Engineer Waterways Experiment Station, Vicksburg, Mississippi, Report No. H-70-2.

Day, R.A., Liriano, S L. and White, W.R. (2001) "Effect of Tailwater Depth and Model Scale on Scour at Culvert Outlets", Proceedings of the Institution of Civil Engineers, Water and Maritime Engineering, **148**(3): 189-199.

Dunn, I. (1959) "Tractive Resistance of Cohesive Channels." Journal of the Soil Mechanics and Foundations Division, **85**(SM3): 1-24.

Fletcher, B. and Grace, J. (1972) "Practical Guidance for Estimating and Controlling

Erosion at Culvert Outlets", US Army Engineer Waterways Experiment Station, Vicksburg, Mississippi, Report No. H-72-5.

Hedges, J. (1990) The Scour of Conhesive Soils by an Inclined Submerged Water Jet, M.Sc. Thesis, Texas A & M University, College Station, Texas, US.

Laushey, L.M., Kappus, U. and Ofwona, M.P. (1967) "Magnitude and Rate of Erosion at Culvert Outlets", Proceedings of the 12th International Association for Hydraulic Research Congress, Fort Collins, US, 338-345.

Lim, S.Y. (1995) "Scour below Unsubmerged Full-flowing Culvert Outlets", Proceedings of the Institution of Civil Engineers, Water, Maritime and Energy, **112**: 136-149.

Lim, S.Y. and Chin, C.O. (1992), "Scour by Circular Wall Jets with Non-uniform Sediments", Advances in Hydro-Science and Engineering, **1**:1989-1994.

Mazurek, K.A. (2001), Scour of Clay by Jets, PhD. Thesis, University of Alberta, Edmonton, Alberta, Canada.

Mazurek, K A., Rajaratnam, N. and Sego, D.C. (1999) "The Characteristics of Erosion of a Consolidated Clay", Proceedings of the 14th Hydrotechnical Conference of the CSCE, Regina, Saskatchewan, Canada, June 2-5, 1999, **2**:207-216.

Moore, W. and Masch, F. (1962) "Experiments on the Scour Resistance of Cohesive Sediments", Journal of Geophysical Research, **67**(4): 1437-1449.

Opie, T. (1967) Scour at Culvert Outlets, MSc. Thesis, Colorado State University, Fort Collins, Colorado, US.

Paaswell, R. (1973) "Causes and Mechanism of Cohesive Soil Erosion: The State of the Art" Soil Erosion: Causes and Mechanism, Prevention and Control, Special Report No. 135, Highway Research Board, Washington, D.C., US, 52-74.

Pani, B.S. (1972) Three-Dimensional Turbulent Wall Jets, Ph.D. Thesis, University of Alberta, Edmonton, Alberta, Canada.

Partheniades, E. (1965) "Erosion and Deposition of Cohesive Soils", Journal of the Hydraulics Division, **91**(HY1): 105-139.

Rajaratnam, N. and Pani, B. S. (1974) " Three-Dimensional Turbulent Wall Jets", Journal of the Hydraulic Division, **100**(HY1): 69-83.

Rajaratnam, N. (1976) Turbulent Jets, Development in Water Science 5, Elseiver Science Publishing Co., Amsterdam, Netherlands.

Rajaratnam, N. and Berry, B. (1977) "Erosion by Circular Turbulent Wall Jets", Journal of Hydraulic Research, **15**(3): 277-289.

Rajaratnam, N. (1981) "Erosion by Plane Turbulent Jets", Journal of Hydraulic Research, **19**(4): 339-358.

Rajaratnam, N. and Diebel, M. (1981) "Erosion below Culvert-like Structures", Proceedings of the 5th Canadian Hydro-technical Conference, May 1981, Fredericton, New Brunswick, Canada.

Raudkivi, A.J. (1998) "Loose Boundary Hydraulics", 4th edition, A.A. Balkema: The Netherlands.

Sforza, P. and Herbst, G. (1967), "A Study of Three Dimensional Incompressible Turbulent Wall Jets", PIBAL Report 1022, Polytechnic Institute of Brooklyn, Brooklyn, New York, US, Oct., 1967.

Stevens, M. (1969) Scour in Riprap at Culvert Outlets, Ph.D. Dissertation, Colorado State University, Fort Collins, Colorado.

Appendix A Scour Hole Dimensions (Mazurek's Data)

Appendix A
Test 1

Clay	U_0 (m/s)	d (mm)	Q (L/min)	ε (mm)	x_m (mm)	b (mm)
M390	13.67	4.9	15.50	9.41	55	92

x (mm)	ε (mm)	x (mm)	B (mm)
0	-1.50	0	8.0
5	-1.99	10	11.0
10	-2.78	20	14.5
15	-3.98	30	20.0
20	-5.67	40	25.5
25	-6.76	50	31.0
30	-7.45	60	36.0
35	-8.04	70	42.0
40	-8.74	80	47.5
45	-8.93	90	52.5
50	-9.32	100	57.5
52	-9.32	110	60.0
55	-9.41	120	61.0
60	-8.81	130	60.5
65	-8.20	140	56.5
70	-7.49	150	50.5
80	-6.47	160	43.0
90	-4.96	170	32.5
100	-3.24	180	23.0
110	-2.33	190	9.5
120	-2.01		
130	-1.49		
140	-1.08		
150	-1.06		
160	-0.55		
170	-0.43		
180	-0.22		
190	0.00		

Test 4

Clay	U_0 (m/s)	d (mm)	Q (L/min)	ε (mm)	x_m (mm)	b (mm)
M390	15.67	4.9	17.70	14.30	67	101.97

x (mm)	ε (mm)	x (mm)	B (mm)
0	-2.61	0	10.0
5	-3.88	10	14.5
10	-5.08	20	19.0
15	-6.96	30	23.0
20	-8.35	40	27.5
25	-9.87	50	33.0
30	-11.56	60	38.0
35	-11.88	70	43.5
40	-12.36	80	51.0
45	-12.85	90	58.0
50	-13.32	100	63.5
55	-13.61	110	68.5
60	-14.16	120	70.5
65	-14.22	130	72.0
67	-14.30	140	71.0
70	-14.22	150	69.0
75	-13.77	160	66.0
80	-12.46	170	56.0
85	-11.76	180	44.0
90	-10.30	190	33.0
95	-8.93	195	0.0
100	-7.57		
110	-5.44		
120	-3.89		
130	-2.72		
140	-2.04		
150	-1.53		
160	-0.98		
170	-0.72		
180	-0.21		
190	0.00		

Cross-section profile				
y (mm)	x=20 mm	x=40 mm	x=67 mm	x=100 mm
0	0.0	0.0	0.0	0.0
2	-6.1	-14.2	-21.1	-7.6
4	-24.9	-42.8	-36.4	-16.2
6	-52.0	-72.1	-54.3	-18.8
8	-60.8	-93.3	-75.4	-24.3
10	-69.6	-106.9	-93.6	-29.0
12	-80.5	-116.5	-106.6	-38.3
13	-83.4	-130.3		
14	-79.5	-126.4	-123.2	-42.3
15	0.0	-130.9	0.0	0.0
16	-72.5	-126.4	-136.5	-48.8
18	-51.3	-122.5	-144.5	-57.9
20	-2.9	-111.0	-152.1	-64.9
21	-0.3			
22		-97.9	-141.5	-76.7
24		-73.7	-132.1	-94.5
26		-42.8	-120.9	-91.8
28		-9.0	-106.1	-85.1
30		0.0	-91.5	-81.0
32			-66.2	-77.0
34			-46.8	-76.0
36			-28.0	-72.5
38			-11.9	-68.2
40			-2.6	-64.6
42				-57.8
44				-53.1
46				0.0
48				-44.7
50				
52				-37.9
54				
56				-25.5
58				
60				-13.2

Test 5

Clay	U_0 (m/s)	d (mm)	Q (L/min)	ε (mm)	x_m (mm)	b (mm)
M390	11.64	4.9	11.60	6.80	38	73

x (mm)	ε (mm)	x (mm)	B (mm)	Cross-section profile	
0	-1.35	0	8.0	y (mm)	x=38 mm
5	-2.08	10	11.0	-12	-1.9
10	-2.90	20	15.5	-10	-14.7
15	-3.77	30	19.5	-8	-31.4
20	-4.96	40	24.0	-6	-48.2
25	-5.55	50	28.5	-4	-62.0
30	-6.26	60	32.5	-2	-65.2
35	-6.69	70	37.0	0	-69.3
38	-6.80	80	38.5	2	-61.9
40	-6.68	90	36.5	4	-53.5
45	-6.12	100	35.0	6	-43.5
50	-5.32	110	32.5	8	-25.0
55	-4.74	120	25.5	10	-8.4
60	-4.74	130	21.5	11	-1.0
70	-3.75	140	20.5		
80	-2.59	150	14.0		
90	-1.75	152	0.0		
100	-0.92				
110	-0.49				
120	-0.12				
130	-0.06				
140	-0.01				
150	0.00				

Test 6

Clay	U_0 (m/s)	d (mm)	Q (L/min)	ε (mm)	x_m (mm)	b (mm)
M390	8.35	4.9	9.40	4.99	14	51

x (mm)	ε (mm)	x (mm)	B (mm)
0	-3.95	0	10.5
5	-4.33	10	12.0
10	-4.51	20	17.0
14	-4.99	30	22.0
15	-4.97	40	25.0
20	-4.66	50	26.0
25	-4.18	60	25.0
30	-3.69	70	22.5
35	-3.73	80	19.0
40	-3.13	90	13.0
45	-2.80	100	9.0
50	-2.58	105	5.0
60	-1.93	109	0.0
70	-1.74		
80	-1.07		
90	-0.76		
100	-0.27		
107	0.00		

Test 7

Clay	U_0 (m/s)	d (mm)	Q (L/min)	ε (mm)	x_m (mm)	b (mm)
M390	12.18	4.9	13.80	7.30	36	63.16

x (mm)	ε (mm)
0	-2.19
5	-2.83
10	-3.67
15	-5.79
20	-6.62
25	-7.04
30	-7.09
35	-7.31
36	-7.31
40	-7.25
45	-6.69
50	-5.89
55	-4.84
60	-3.99
70	-2.93
80	-2.62
90	-2.87
100	-2.68
110	-2.32
125	-1.82
140	-1.55
150	-0.94
160	-0.53
170	-0.46
180	-0.21
184	0.00

Test 8

Clay	U_0 (m/s)	d (mm)	Q (L/min)	ε (mm)	x_m (mm)	b (mm)
M390	9.58	5.97	16.10	8.36	0	48.28

x (mm)	ε (mm)	x (mm)	B (mm)
0	-8.36	0	20.0
5	-6.24	10	20.5
10	-6.10	20	24.5
15	-5.66	30	29.5
20	-5.65	40	34.5
25	-5.62	50	38.5
30	-5.43	60	43.5
35	-5.10	70	45.5
40	-4.98	80	43.0
45	-4.60	90	39.0
50	-3.96	100	28.5
55	-3.14	110	23.0
60	-2.43	120	15.5
65	-2.05	127	8.0
70	-1.54		
75	-1.17		
80	-0.92		
90	-0.65		
95	-0.47		
100	-0.32		
110	-0.17		
120	-0.07		
127	0.00		

Test 9

Clay	U_0 (m/s)	d (mm)	Q (L/min)	ε (mm)	x_m (mm)	b (mm)
M390	8.35	5.97	24.20	14.12	63	99.80

x (mm)	ε (mm)	x (mm)	B (mm)
0	-7.29	0	20.5
5	-7.66	10	24.0
10	-8.99	20	28.5
15	-10.08	30	29.5
20	-10.86	40	33.0
25	-11.88	50	39.0
30	-12.01	60	42.5
35	-12.57	70	47.5
39	-12.48	80	53.5
40	-12.36	90	60.5
50	-13.91	100	66.0
55	-13.84	110	70.5
60	-13.97	120	75.0
63	-14.12	130	78.0
65	-14.03	140	80.5
70	-13.93	146	81.0
75	-13.82	150	79.0
80	-12.25	160	77.0
90	-10.05	170	74.0
100	-7.00	180	70.5
110	-4.81	190	67.0
120	-2.93	200	61.5
130	-2.04	210	55.5
140	-1.91	220	52.0
150	-2.02	-18	34.0
160	-1.83		
170	-1.31		
180	-1.15		
190	-0.85		
200	-0.71		
210	-0.45		
220	-0.23		
230	0.00		

Test 10

Clay	U_0 (m/s)	d (mm)	Q (L/min)	ε (mm)	x_m (mm)	b (mm)
M332	14.31	5.97	24.00	13.94	42	99.20

x (mm)	ε (mm)	x (mm)	B (mm)	Cross-sectional Profiles		
				y (mm)	x=20 mm	x=40 mm
0	-4.16	0	14.0	-220		-3.5
5	-4.91	10	19.0	-200		-58.8
10	-6.77	20	24.0	-180		-68.3
15	-8.11	30	27.0	-160		-83.4
20	-9.46	40	39.0	-140		-88.3
25	-11.39	50	43.0	-120		-98.4
30	-12.52	60	48.0	-110	-2.2	0.0
35	-13.69	70	50.5	-100	-5.9	-107.5
40	-13.92	80	52.0	-80	-25.0	-115.5
42	-13.94	90	60.5	-60	-51.1	-140.1
45	-13.56	100	61.0	-50	0.0	-149.4
50	-13.65	110	62.0	-40	-68.4	-148.5
55	-13.36	120	63.0	-20	-81.5	-140.2
60	-13.22	122	64.0	0	-103.1	-137.2
70	-12.32	130	61.0	20	-105.4	-132.6
80	-10.39	140	62.0	30	-107.2	0.0
90	-8.59	150	62.0	40	-106.5	-120.7
100	-6.83	160	59.0	60	-103.1	-108.2
110	-5.29	170	60.0	80	-80.1	-97.9
120	-3.85	180	54.5	100	-52.5	-79.8
130	-2.87	190	49.0	120	-26.9	-57.3
140	-1.54	200	41.0	140	-7.2	-24.6
150	-1.28	210	26.0	150	-2.0	0.0
160	-1.08	216	0.0	160		-7.7
170	-0.98			170		0.3
180	-1.00					
190	-0.83					
200	-0.54					
210	-0.05					
214	0.00					

Test 11

Clay	U_0 (m/s)	d (mm)	Q (L/min)	ε (mm)	x_m (mm)	b (mm)
M390	4.41	5.97	7.40	2.79	0	17.18

x (mm)	ε (mm)	x (mm)	B (mm)
0	-2.79	0	8.5
5	-2.17	5	9.5
8	-2.41	10	11.0
10	-2.31	15	12.0
15	-1.69	19	13.0
20	-1.16	20	12.5
25	-0.51	25	10.5
30	-0.14	30	8.0
0	0.00	35	0.0

Test 12

Clay	U_0 (m/s)	d (mm)	Q (L/min)	ε (mm)	x_m (mm)	b (mm)
M390	2.98	5.97	5.00	1.47	0	18.14

x (mm)	ε (mm)
0	-1.47
5	-1.09
15	-1.12
20	-0.18
21	-1.75

Test 13

Clay	U_0 (m/s)	d (mm)	Q (L/min)	ε (mm)	x_m (mm)	b (mm)
M332	5.74	5.97	9.60	4.03	5	21.92

x (mm)	ε (mm)	x (mm)	B (mm)
0	-3.25	0	12.5
5	-4.03	10	13.0
10	-2.84	20	17.0
15	-2.16	30	18.5
20	-2.10	38	20.5
25	-1.84	40	19.0
30	-1.79	50	16.0
40	-1.54	60	15.5
50	-1.36	70	12.0
60	-1.17	80	8.5
70	-0.77	90	5.5
80	-0.41	96	0.0
90	-0.18		
96	-0.03		
100	0.00		

Test 14

Clay	U_0 (m/s)	d (mm)	Q (L/min)	ε (mm)	x_m (mm)	b (mm)
M332	13.10	5.97	22.00	10.70	63	108.10

x (mm)	ε (mm)	x (mm)	B (mm)
0	-0.98	0	11.0
5	-2.81	10	16.0
10	-4.79	20	19.5
15	-5.76	30	23.5
20	-6.36	40	27.0
25	-6.90	50	32.0
30	-7.25	60	35.5
35	-7.72	70	40.5
40	-8.27	80	45.5
45	-8.98	90	51.5
50	-9.89	100	56.5
55	-10.57	110	58.5
60	-10.64	120	56.5
62.5	-10.70	130	53.5
65	-10.61	140	50.5
70	-9.99	150	45.5
75	-9.43	160	45.5
80	-8.40	170	44.0
85	-7.24	180	40.5
95	-5.81	190	35.5
105	-5.48	200	31.0
115	-5.06	210	31.0
125	-3.49		
135	-3.15		
145	-3.11		
155	-3.08		
165	-1.74		
175	-1.06		
185	-0.51		
195	-0.03		
205	-0.10		
214	0.00		

Test 15

Clay	U_0 (m/s)	d (mm)	Q (L/min)	ε (mm)	x_m (mm)	b (mm)
M332	3.74	5.97	6.30	1.37	0	14.27

x (mm)	ε (mm)
0	-1.37
5	-0.60
10	-0.56
13	-1.13
15	-0.43

Test 16

Clay	U_0 (m/s)	d (mm)	Q (L/min)	ε (mm)	x_m (mm)	b (mm)
M332	7.94	5.97	13.30	8.96	44	68.24

x (mm)	ε (mm)	x (mm)	B (mm)
0	-6.09	0	7.0
5	-6.10	10	10.5
10	-5.95	20	13.0
15	-6.17	30	14.5
20	-6.84	40	15.5
25	-7.59	50	15.0
30	-7.83	60	14.0
35	-7.91	70	12.0
40	-7.93	80	12.0
44	-8.96	90	7.5
45	-8.46	99	0.0
50	-8.13		
55	-8.20		
60	-7.09		
65	-5.58		
70	-3.88		
75	-2.60		
80	-1.72		
85	-0.71		
90	-0.12		
95	-0.03		
99	0.00		

Test 17

Clay	U_0 (m/s)	d (mm)	Q (L/min)	ε (mm)	x_m (mm)	b (mm)
M332	13.66	5.97	22.90	10.20	27	78.57

x (mm)	ε (mm)	x (mm)	B (mm)	Cross-sectional Profiles			
0	-7.93	0	18.0	y (mm)	x=20 mm	x=40 mm	x=60 mm
5	-7.98	10	22.0	-230			-8.9
10	-8.09	20	25.0	-220			-13.4
15	-9.14	30	29.0	-200			-21.5
20	-9.75	40	33.0	-180			-30.4
25	-10.04	50	38.5	-170		-5.0	
27	-10.20	60	43.5	-160		-13.3	-38.5
30	-9.90	70	50.5	-140	0.5	-42.2	-48.2
35	-9.56	80	54.5	-120	-23.4	-64.7	-58.2
40	-9.10	90	58.0	-100	-61.5	-78.5	-65.7
45	-8.61	100	57.0	-80	-78.6	-84.6	-75.0
50	-8.17	110	57.5	-60	-96.8	-90.3	-76.0
60	-7.33	120	57.0	-40	-98.7	-93.5	-77.0
70	-6.24	130	55.5	-20	-99.6	-93.1	-77.9
80	-4.91	140	51.0	0	-98.1	-94.5	-76.6
90	-3.89	150	47.0	20	-97.4	-91.9	-74.7
100	-3.00	160	43.0	40	-91.2	-90.6	-71.8
110	-2.89	170	40.0	60	-81.6	-82.8	-62.1
120	-1.71	180	36.0	80	-64.4	-77.1	-54.5
130	-1.36	190	30.0	100	-39.4	-60.5	-46.1
140	-0.65	200	16.5	120	-5.4	-37.5	-36.0
150	-0.39	204	11.0	130	2.2		
160	-0.45			140	1.0	-20.7	-30.3
170	-0.35			150		-6.1	
180	-0.02			160			-23.8
190	-0.12			180			-17.2
200	-0.17			210			-9.4
204	0.00						

Test 18

Clay	U_0 (m/s)	d (mm)	Q (L/min)	ε (mm)	x_m (mm)	b (mm)
M332	8.43	5.97	14.20	3.53	45	94.51

x (mm)	ε (mm)	x (mm)	B (mm)
0	-0.86	10	9.5
5	-1.62	20	13.5
10	-2.41	30	17.0
15	-3.04	40	21.0
18	-3.11	50	24.5
20	-2.98	60	27.5
24	-3.26	70	30.5
25	-3.26	80	33.5
30	-3.09	86	34.0
35	-3.27	90	31.5
40	-3.08	100	27.5
45	-3.53	110	20.5
50	-3.44	120	23.5
55	-3.40	130	19.0
60	-3.33	140	14.0
65	-3.10	150	10.5
70	-2.75	154	0.0
75	-2.37		
80	-2.11		
90	-1.95		
100	-1.54		
110	-1.67		
120	-1.73		
130	-1.18		
140	-0.64		
150	-0.11		
154	0.00		

Test 19

Clay	U_0 (m/s)	d (mm)	Q (L/min)	ε (mm)	x_m (mm)	b (mm)
M332	10.45	5.97	17.60	6.78	31	65.00

x (mm)	ε (mm)	x (mm)	B (mm)
0	-3.49	0	14.0
5	-4.27	10	15.5
10	-5.53	20	19.0
15	-6.30	30	23.0
20	-6.71	40	29.0
25	-6.67	50	32.0
30	-6.73	60	35.5
31	-6.78	70	38.5
35	-6.64	80	39.5
40	-6.35	81	40.0
45	-6.04	90	38.0
50	-5.63	100	37.0
60	-4.15	110	33.5
70	-2.63	120	31.0
80	-1.64	130	29.0
90	-0.92	140	21.5
100	-0.67	150	18.0
110	-0.69	160	18.0
120	-0.50	162	11.0
130	-0.42		
140	-0.28		
150	-0.27		
160	0.00		

Test 20

Clay	U_0 (m/s)	d (mm)	Q (L/min)	ε (mm)	x_m (mm)	b (mm)
M390	5.06	12.18	35.40	3.11	30	63.95

x (mm)	ε (mm)	x (mm)	B (mm)
0	-1.62	0	10.0
5	-1.78	10	16.5
10	-1.97	20	22.5
15	-2.01	30	27.0
20	-2.14	40	33.0
25	-3.08	47	33.0
30	-3.11	50	34.0
35	-3.03	60	28.0
40	-2.72	70	23.0
45	-2.37	80	27.0
50	-2.16	90	20.3
55	-1.75	100	21.0
60	-1.63	110	20.0
70	-1.44	120	19.0
80	-1.39	130	16.0
90	-1.11	140	14.0
100	-0.80	150	11.0
110	-0.66		
120	-0.46		
124	-0.36		
130	-0.29		
140	-0.16		
150	0.00		

Test 21

Clay	U_0 (m/s)	d (mm)	Q (L/min)	ε (mm)	x_m (mm)	b (mm)
M390	7.59	12.18	53.10	1.90	40	-

x (mm)	ε (mm)	x (mm)	B (mm)
0	-1.47	0	14.0
5	-1.45	10	18.0
10	-1.69	20	26.0
15	-1.60	30	30.0
20	-1.56	40	33.5
25	-1.72	50	36.5
30	-1.82	60	39.0
35	-1.58	70	41.5
40	-1.90	80	44.5
45	-1.63	90	49.5
50	-1.59	100	48.5
55	-1.53	110	50.5
60	-1.55	120	52.5
70	-1.74	130	51.5
80	-1.49	140	52.0
90	-1.55	150	43.0
100	-1.62	160	44.0
110	-1.58	170	42.0
120	-1.59	180	36.5
130	-1.32	190	36.0
140	-1.39	200	35.0
150	-1.47	210	34.5
160	-1.42	220	32.0
170	-1.23		
180	-1.44		
190	-1.47		
200	-1.35		
210	-1.51		
220	-1.14		

Test 22

Clay	U_0 (m/s)	d (mm)	Q (L/min)	ε (mm)	x_m (mm)	b (mm)
M390	11.23	12.18	78.60	20.45	125	-

x (mm)	ε (mm)	x (mm)	B (mm)
0	-4.41	0	23.0
5	-4.82	10	29.0
10	-5.38	20	32.0
15	-6.42	30	33.0
20	-7.06	40	38.0
30	-8.54	50	42.5
40	-10.03	60	45.0
50	-12.14	70	49.0
60	-14.09	80	53.5
70	-15.42	90	57.5
80	-16.56	100	62.5
90	-17.40	110	66.5
100	-18.43	120	71.0
110	-19.64	130	76.5
120	-20.23	140	81.0
125	-20.45	150	85.5
130	-20.15	160	89.0
140	-19.66		
150	-19.14		
160	-17.86		
170	-16.56		
180	-15.10		

Test 23

Clay	U_0 (m/s)	d (mm)	Q (L/min)	ε (mm)	x_m (mm)	b (mm)
M390	9.78	12.18	68.40	20.64	120	-

x (mm)	ε (mm)	x (mm)	B (mm)	Cross-sectional Profiles (mm)			
				y (mm)	x=30 mm	x=60 mm	x=125 mm
0	-3.01	0	20.0	-39			-13.9
5	-3.42	10	23.0	-38			-18.6
10	-4.37	20	28.0	-36			-30.5
20	-5.37	30	31.0	-34			-38.2
30	-6.71	40	38.0	-32			-48.2
40	-8.52	50	40.0	-30			-62.8
50	-10.39	60	42.0	-28			-77.7
60	-12.96	70	50.0	-26			-91.6
70	-15.12	80	52.0	-24		-11.3	-113.0
80	-16.56	90	57.0	-22		-16.7	-120.9
90	-18.73	100	60.5	-20		-37.6	-143.2
100	-19.74	110	63.0	-18	-8.3	-56.2	-154.0
110	-20.30	120	70.0	-16	-12.8	-78.4	-168.8
120	-20.64	130	74.0	-14	-24.1	-91.8	-184.9
130	-19.98	140	78.0	-12	-48.0	-107.7	-206.8
140	-19.31	150	81.0	-10	-70.4	-124.9	-204.1
150	-17.98	160	83.0	-8	-84.2	-142.1	-212.5
160	-17.39	170	87.0	-6	-96.2	-147.0	-210.1
		180	89.0	-4	-91.4	-142.4	-208.0
		190	92.0	-2	-88.1	-142.8	-205.7
		200	93.5	0	-87.6	-144.3	-206.8
		210	93.5	2	-89.7	-146.5	-199.4
		220	95.0	4	-86.2	-148.9	-195.7
				6	-80.2	-148.1	-191.0
				8	-66.9	-143.9	-185.6
				10	-44.7	-132.0	-176.8
				12	-22.5	-119.0	-168.5
				14	-8.3	-102.2	-158.7
				16	-5.4	-76.7	-145.9
				18		-40.4	-130.0
				20		-20.5	-121.4
				22		-7.1	-93.8
				24			-72.5
				26			-51.4
				28			-34.6
				30			-22.6
				32			-13.4
				34			-6.0

Appendix B Scour Hole Profiles along the Plane of Symmetry (Mazurek's Data)

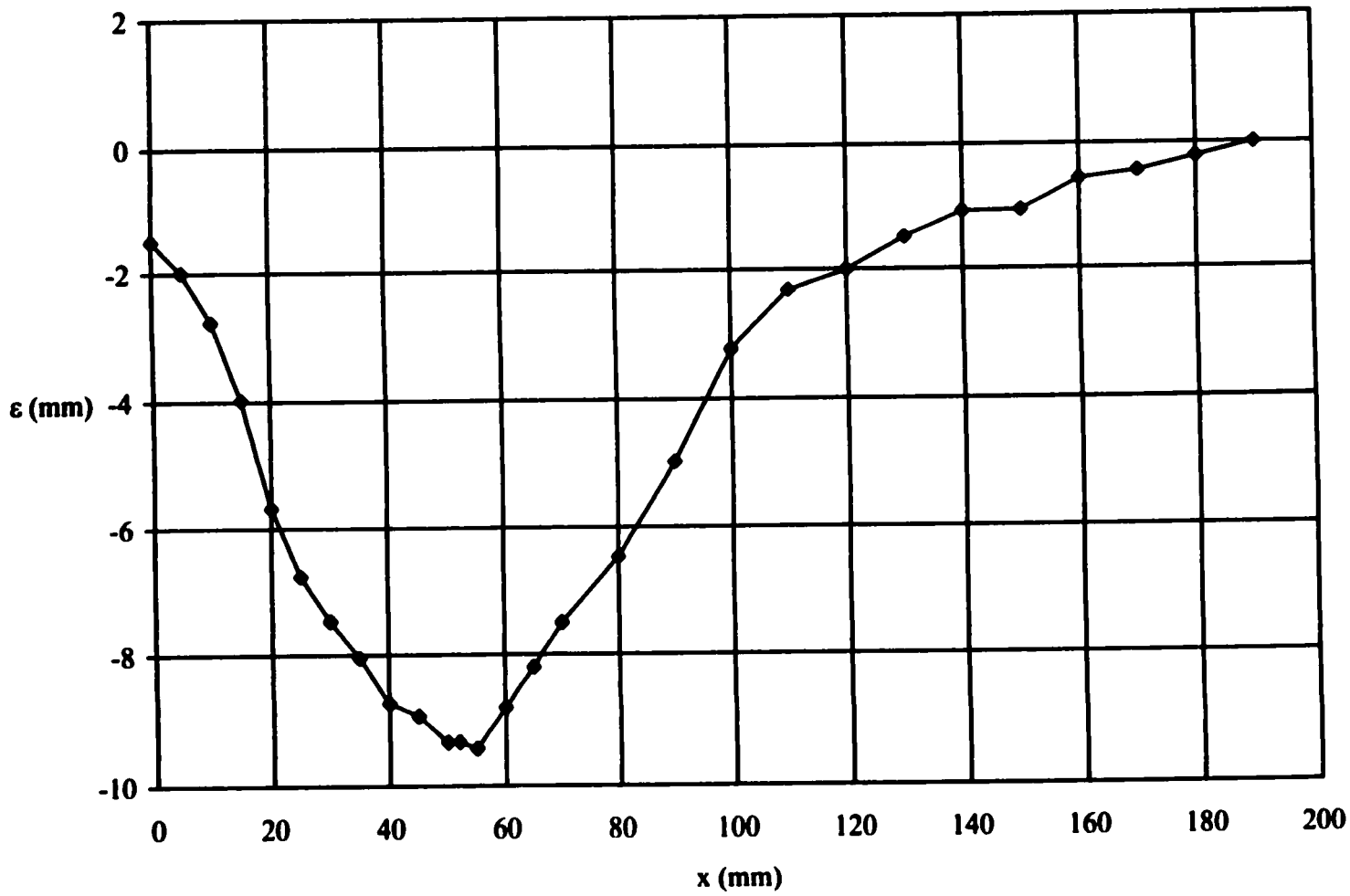

Fig. B-1 Scour hole profiles-Mazurek's test 1.

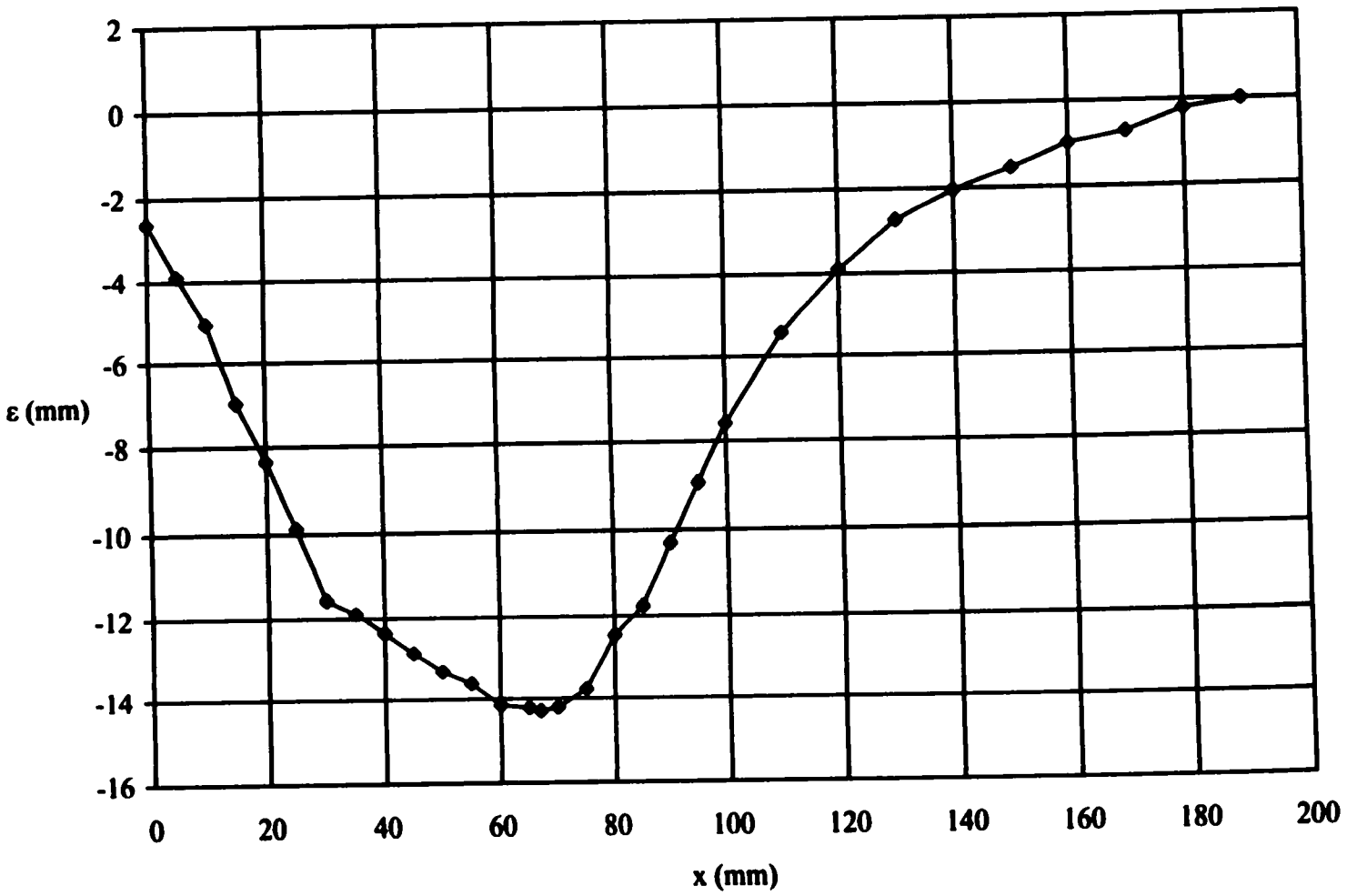

Fig. B-2 Scour hole profiles-Mazurek's test 4.

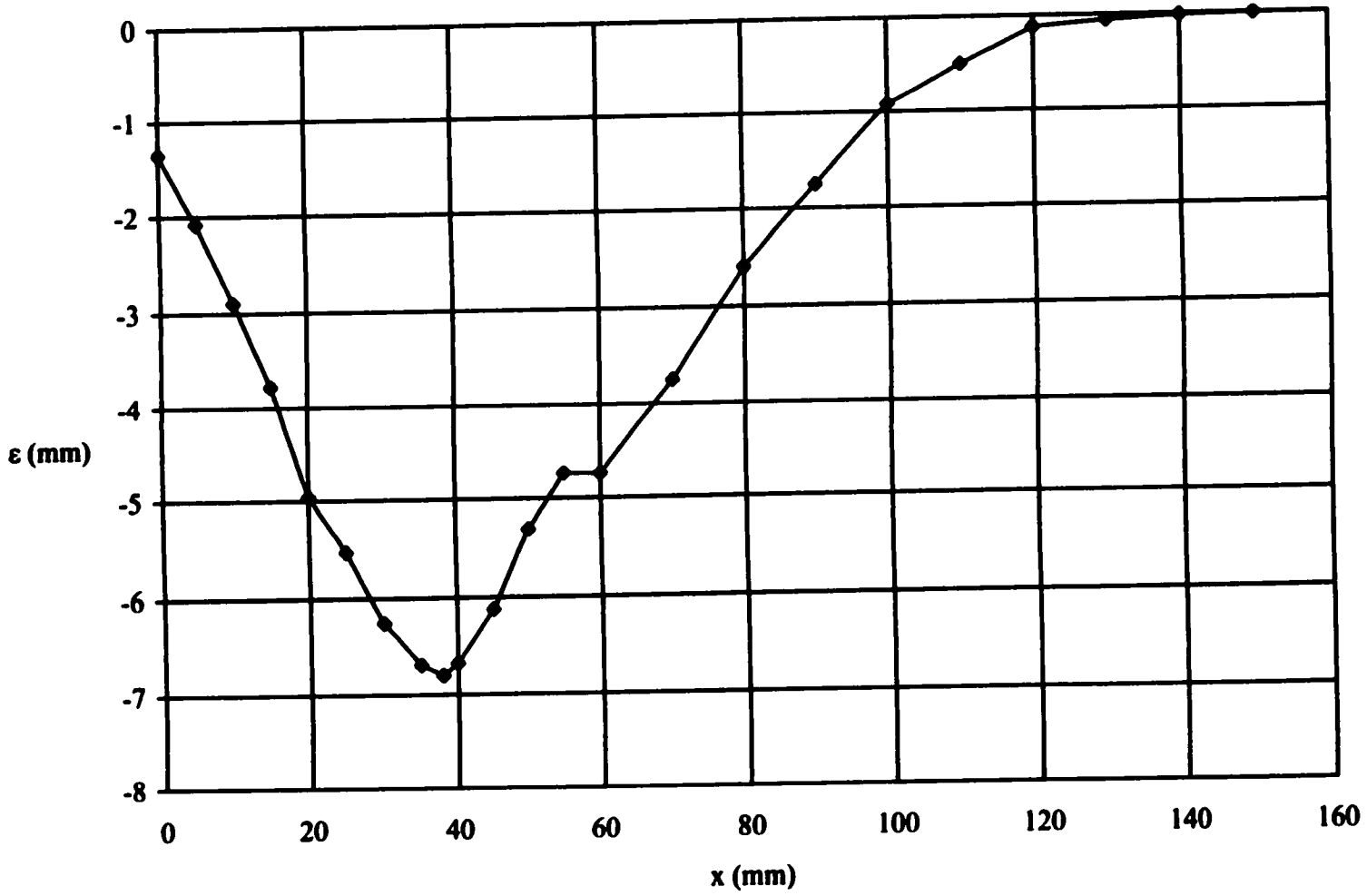

Fig. B-3 Scour hole profiles-Mazurek's test 5.

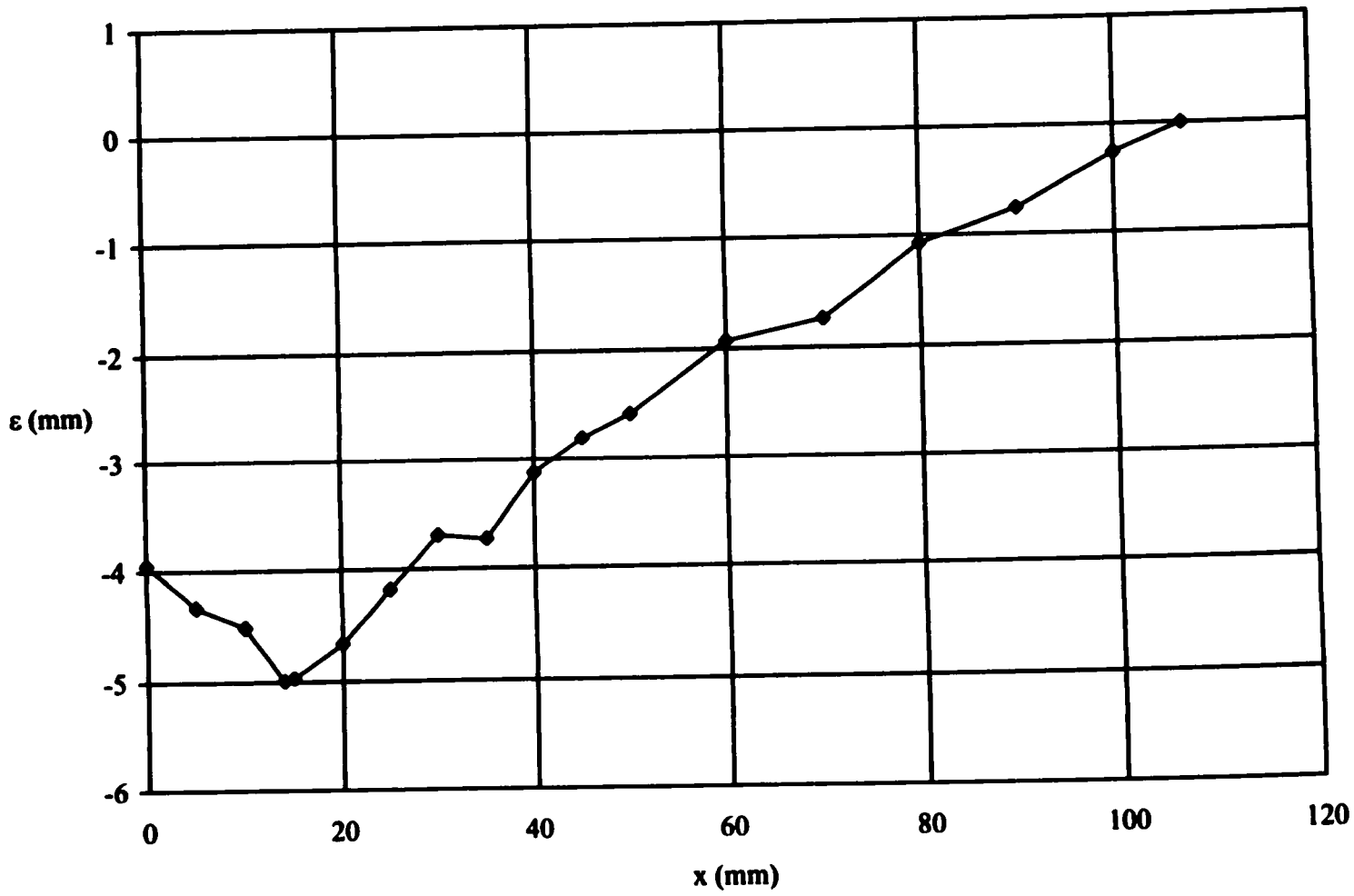

Fig. B-4 Scour hole profiles-Mazurek's test 6.

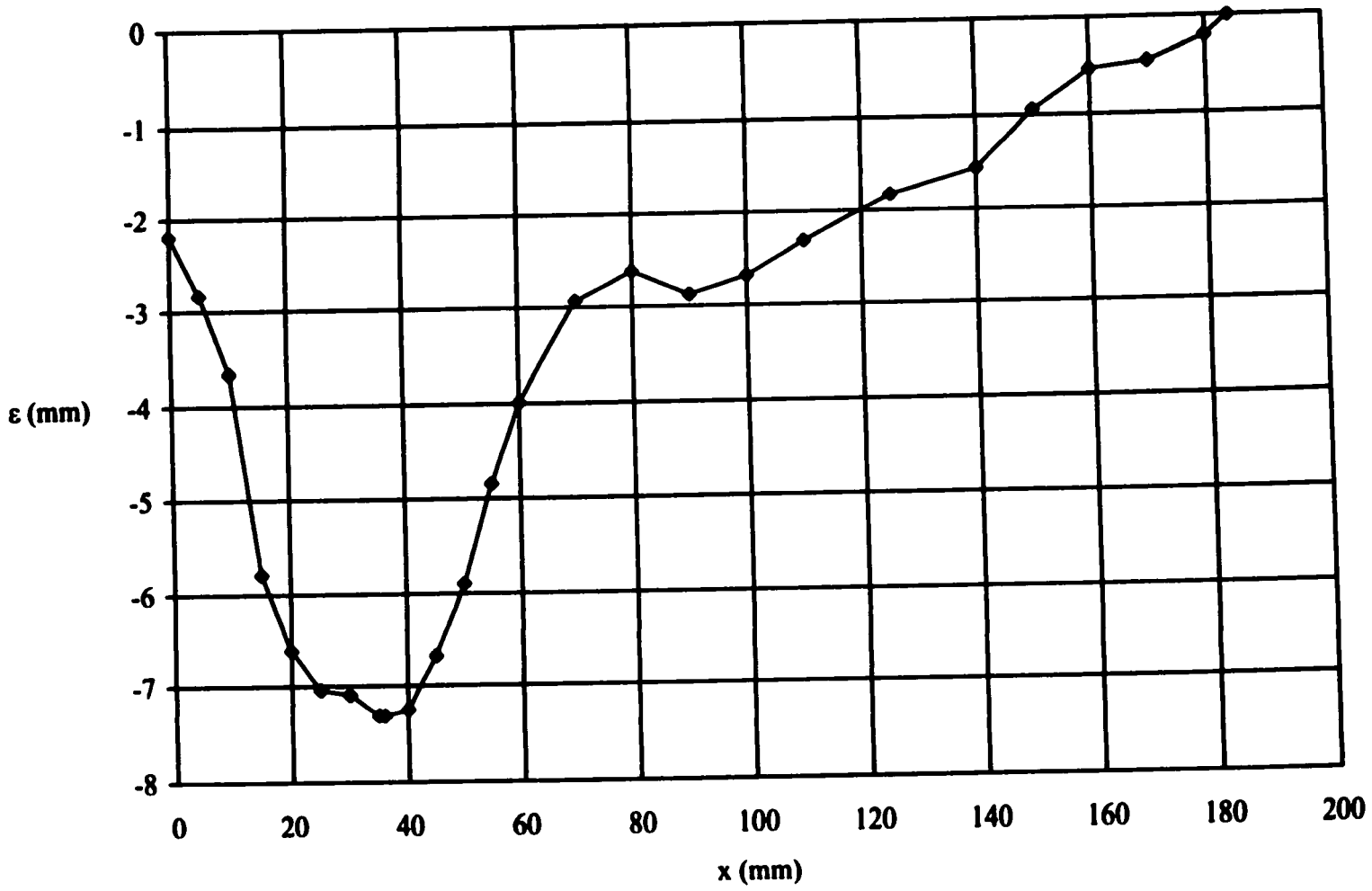

Fig. B-5 Scour hole profiles-Mazurek's test 7.

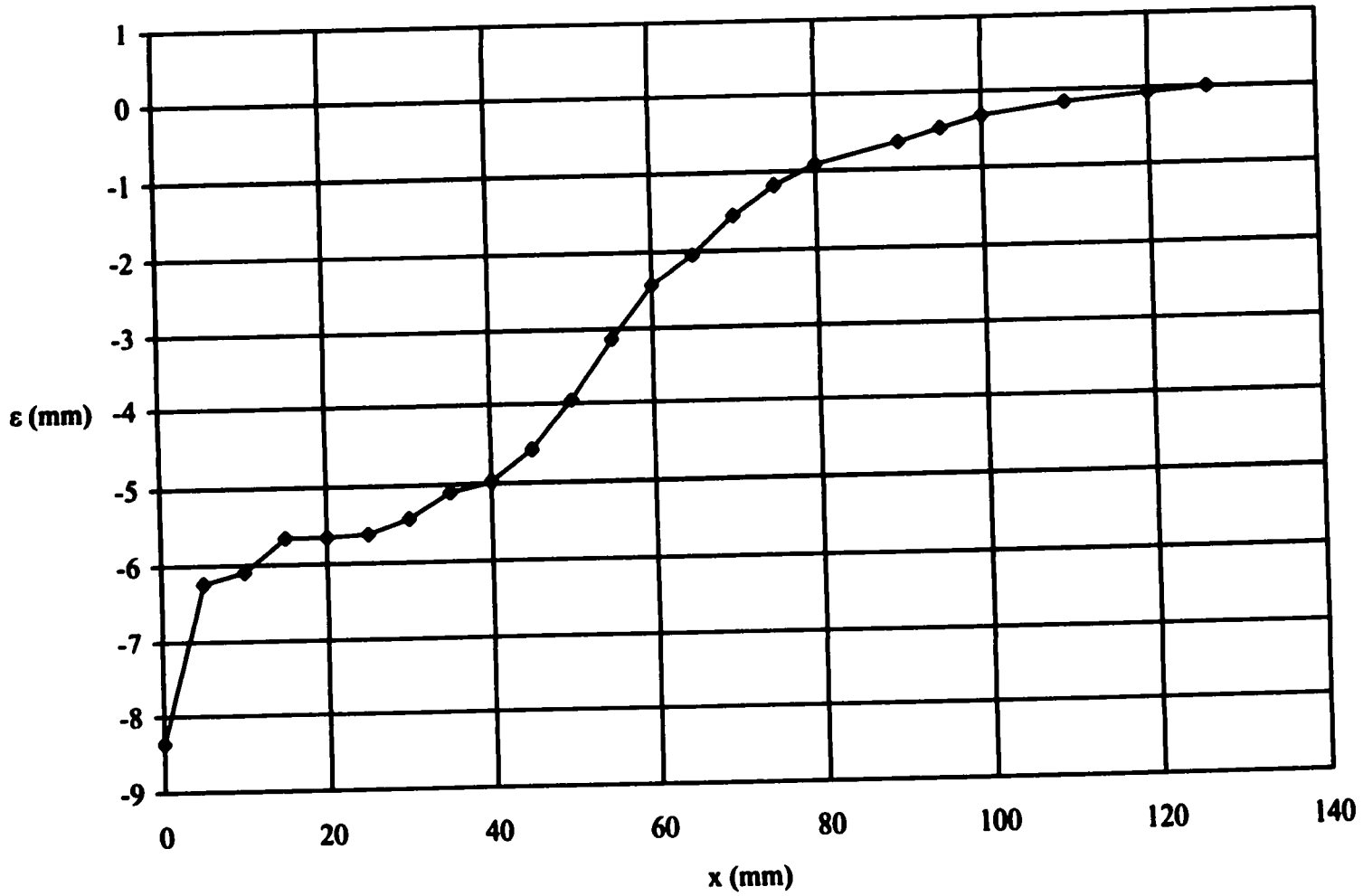

Fig. B-6 Scour hole profiles-Mazurek's test 8.

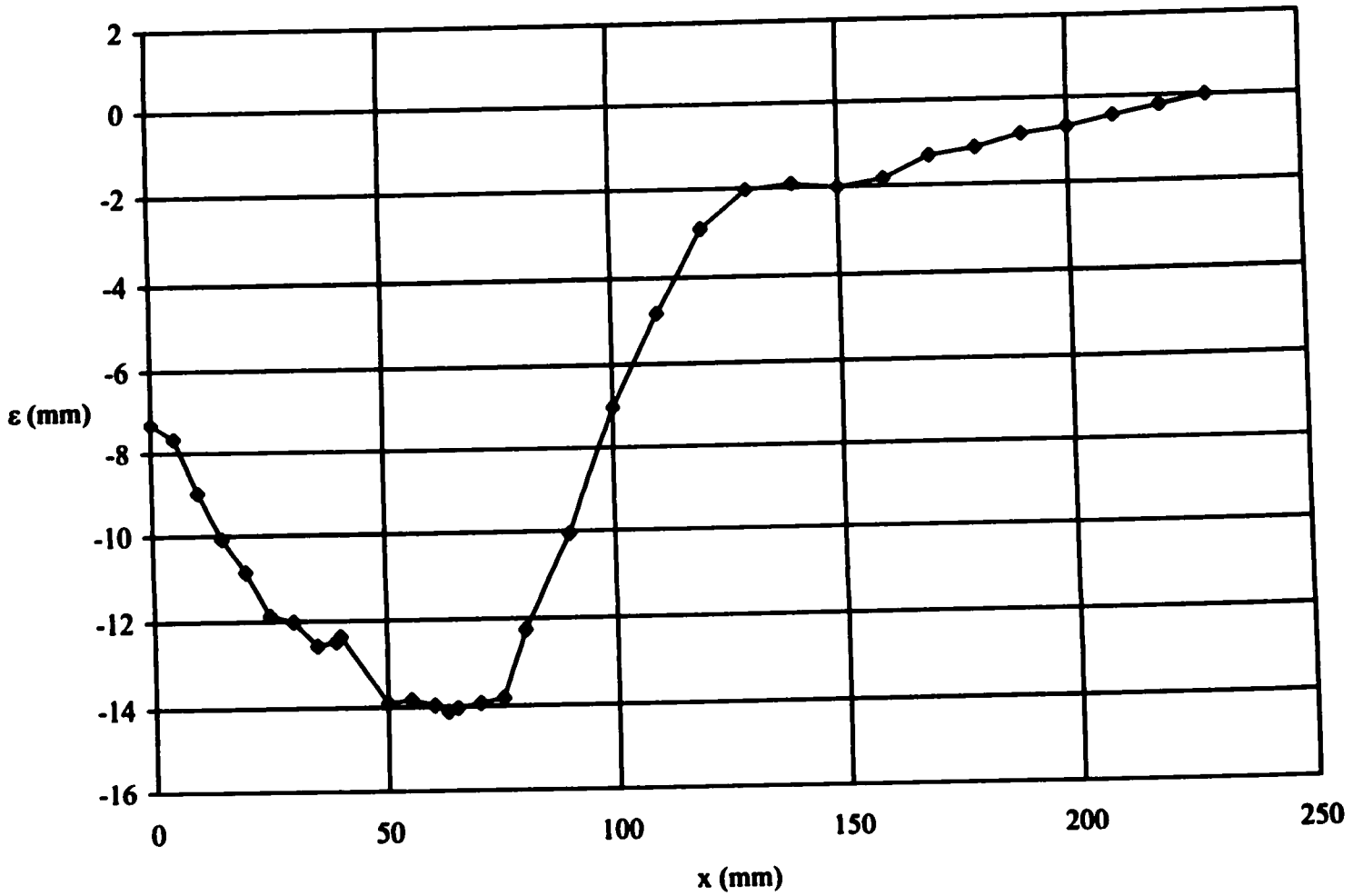

Fig. B-7 Scour hole profiles-Mazurek's test 9.

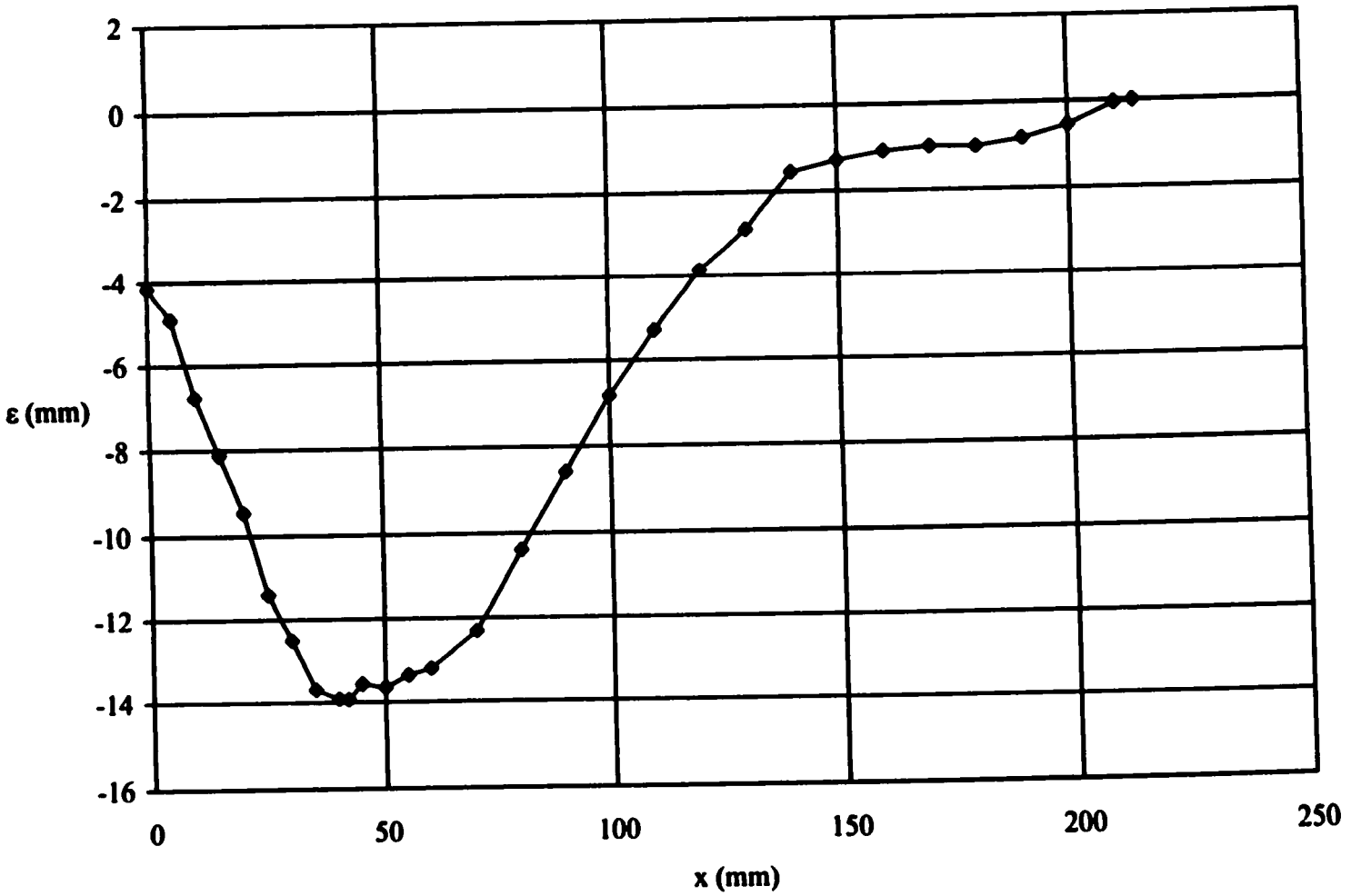

Fig. B-8 Scour hole profiles-Mazurek's test 10.

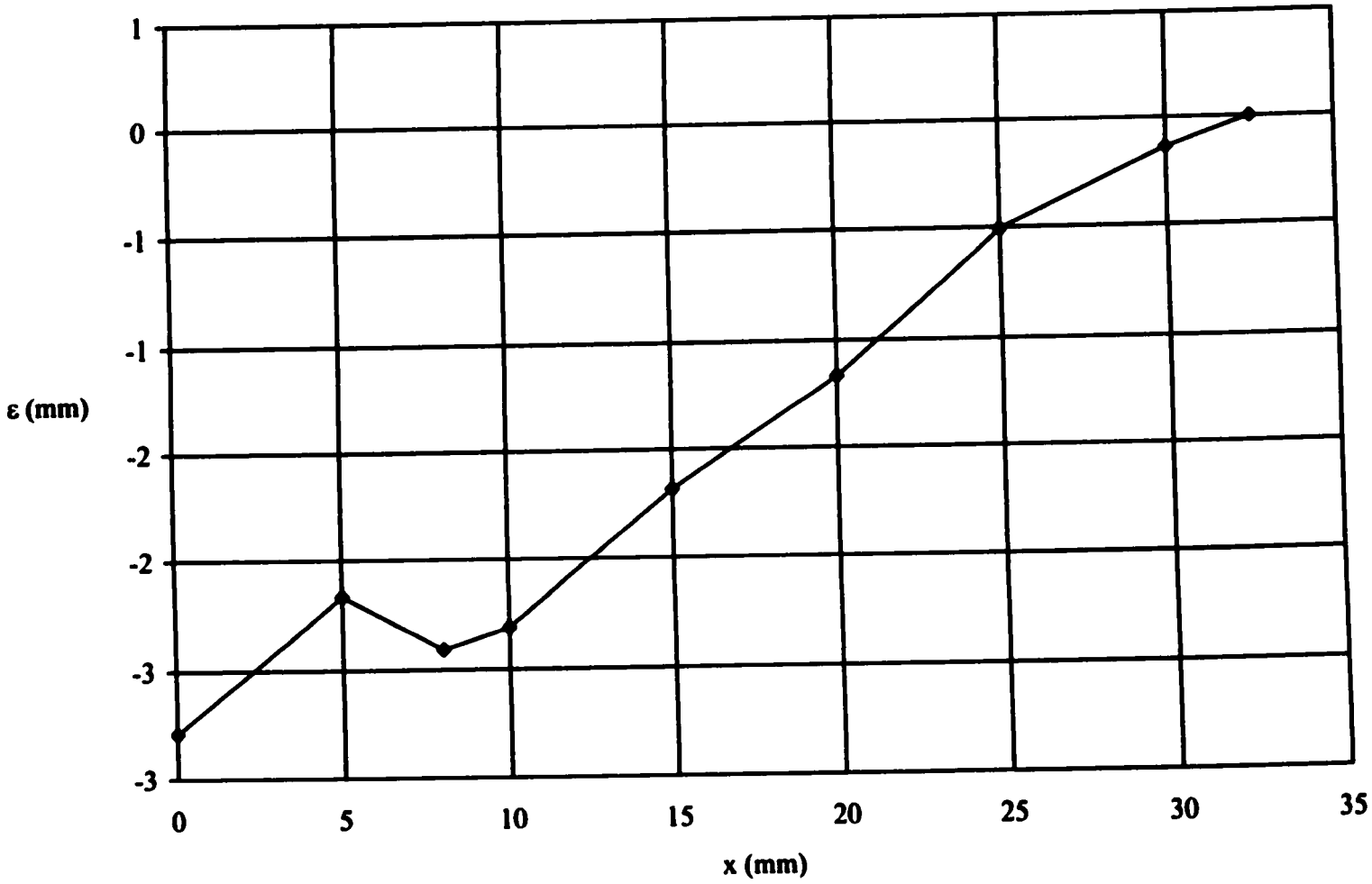

Fig. B-9 Scour hole profiles-Mazurek's test 11.

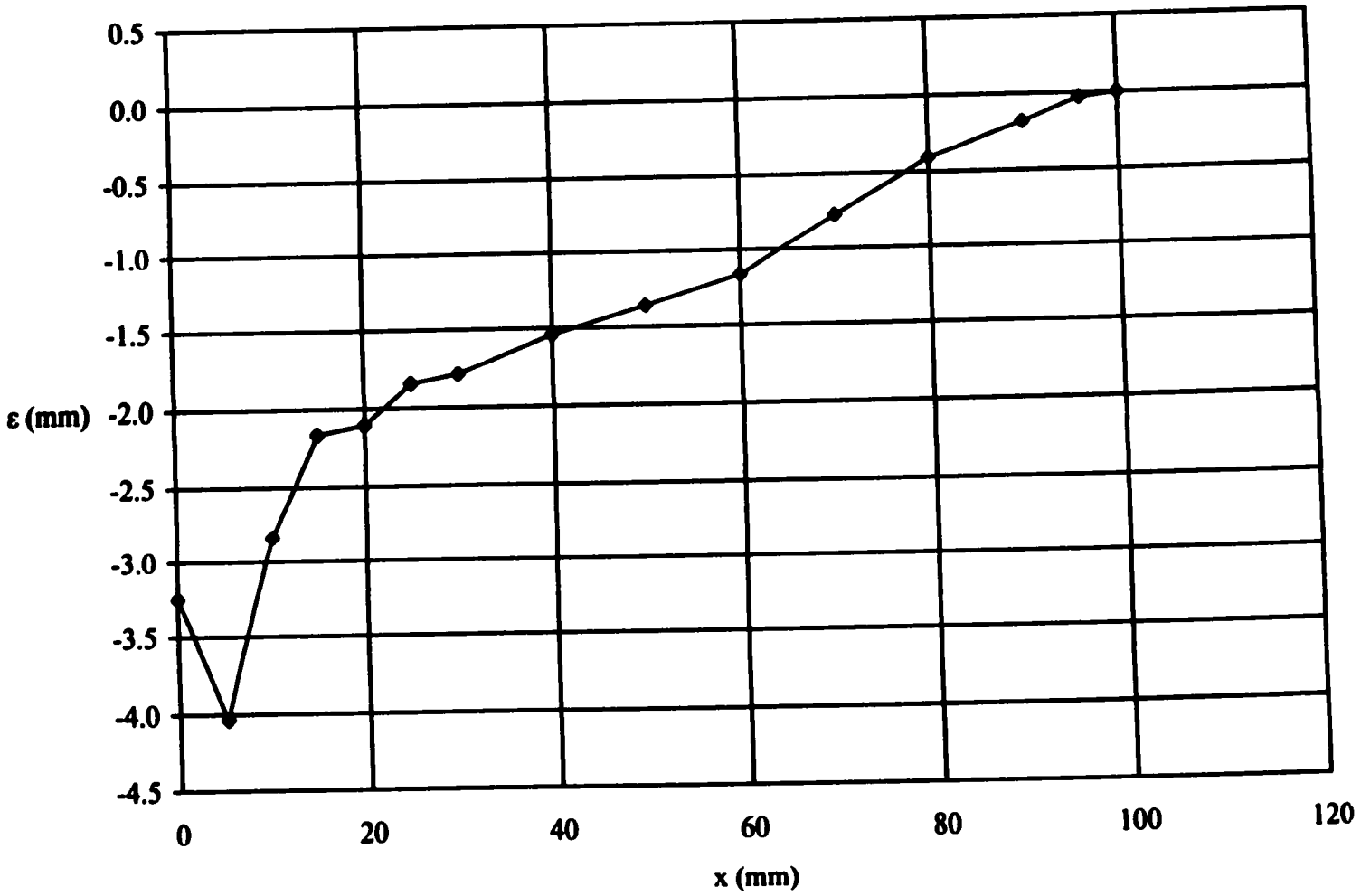

Fig. B-10 Scour hole profiles-Mazurek's test 13.

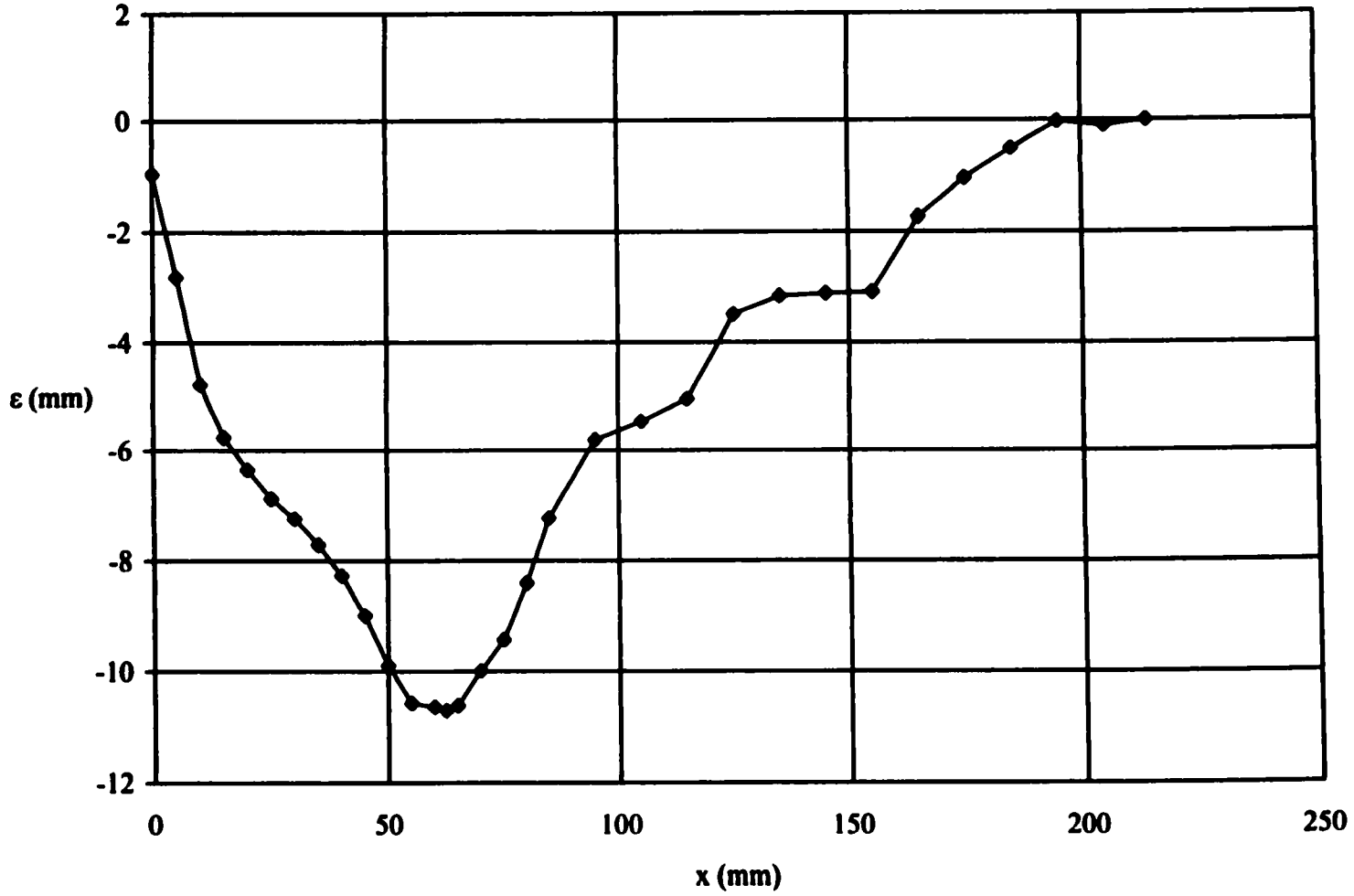

Fig. B-11 Scour hole profiles-Mazurek's test 14.

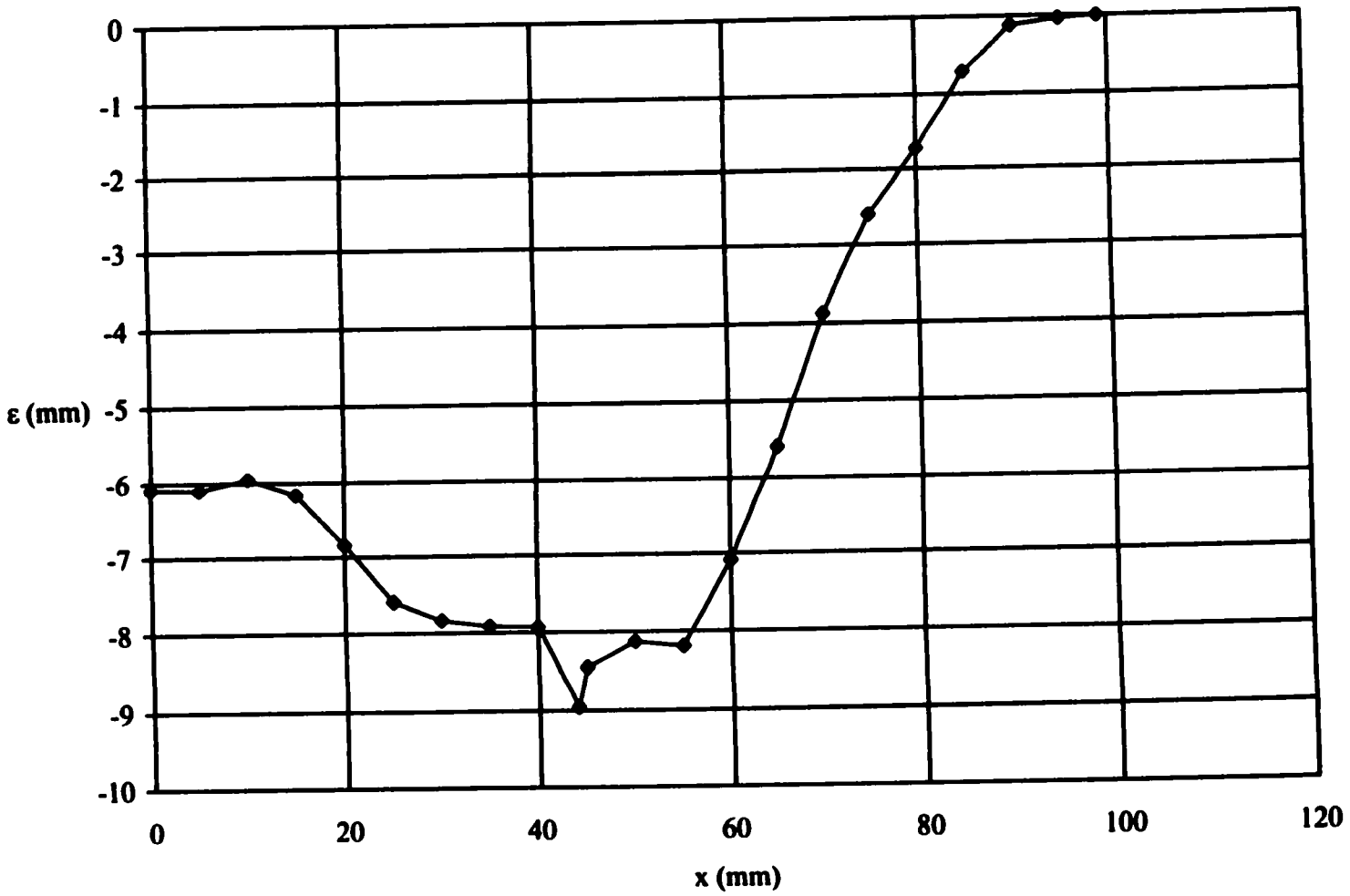

Fig. B-12 Scour hole profiles-Mazurek's test 16.

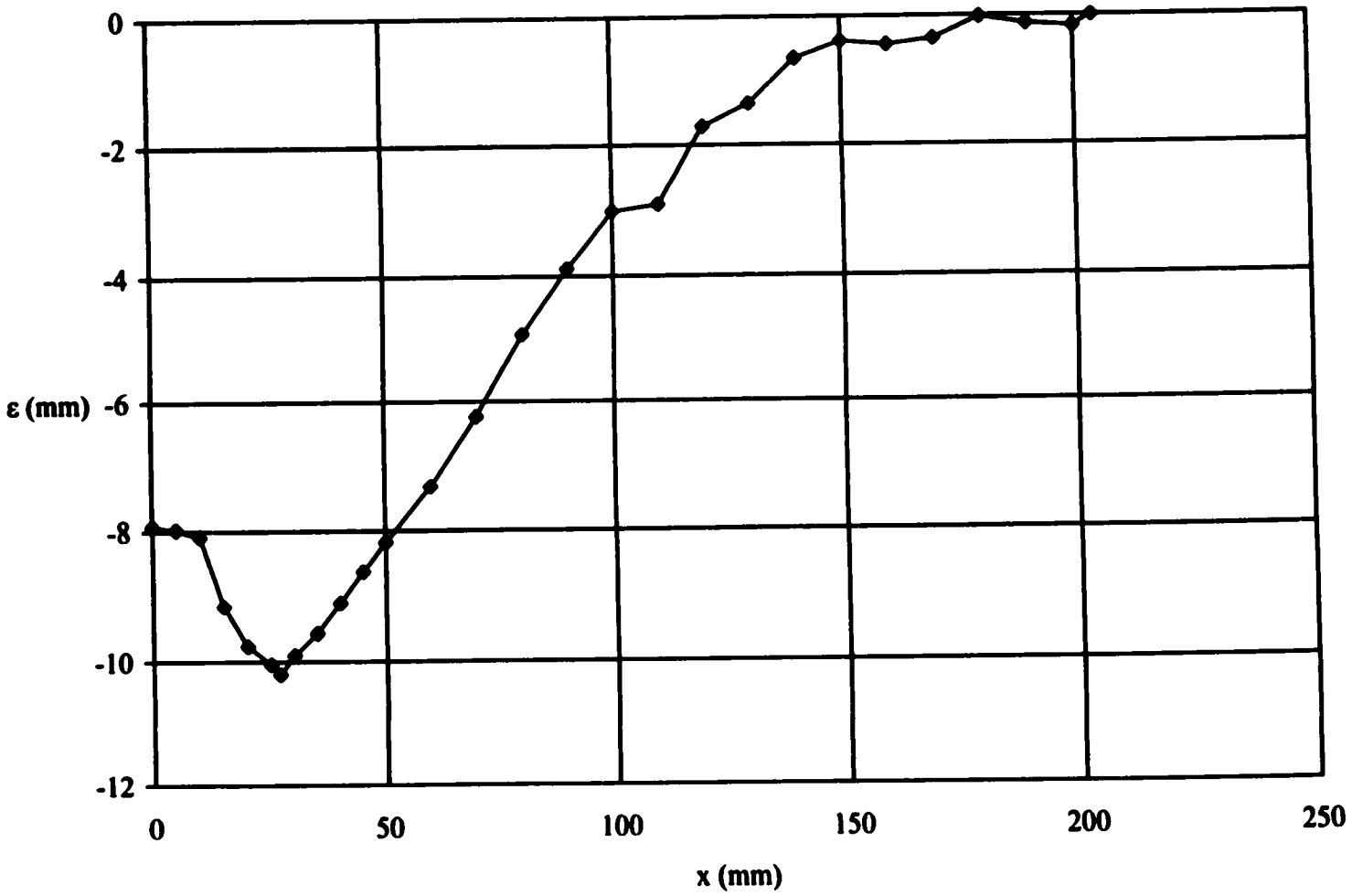

Fig. B-13 Scour hole profiles-Mazurek's test 17.

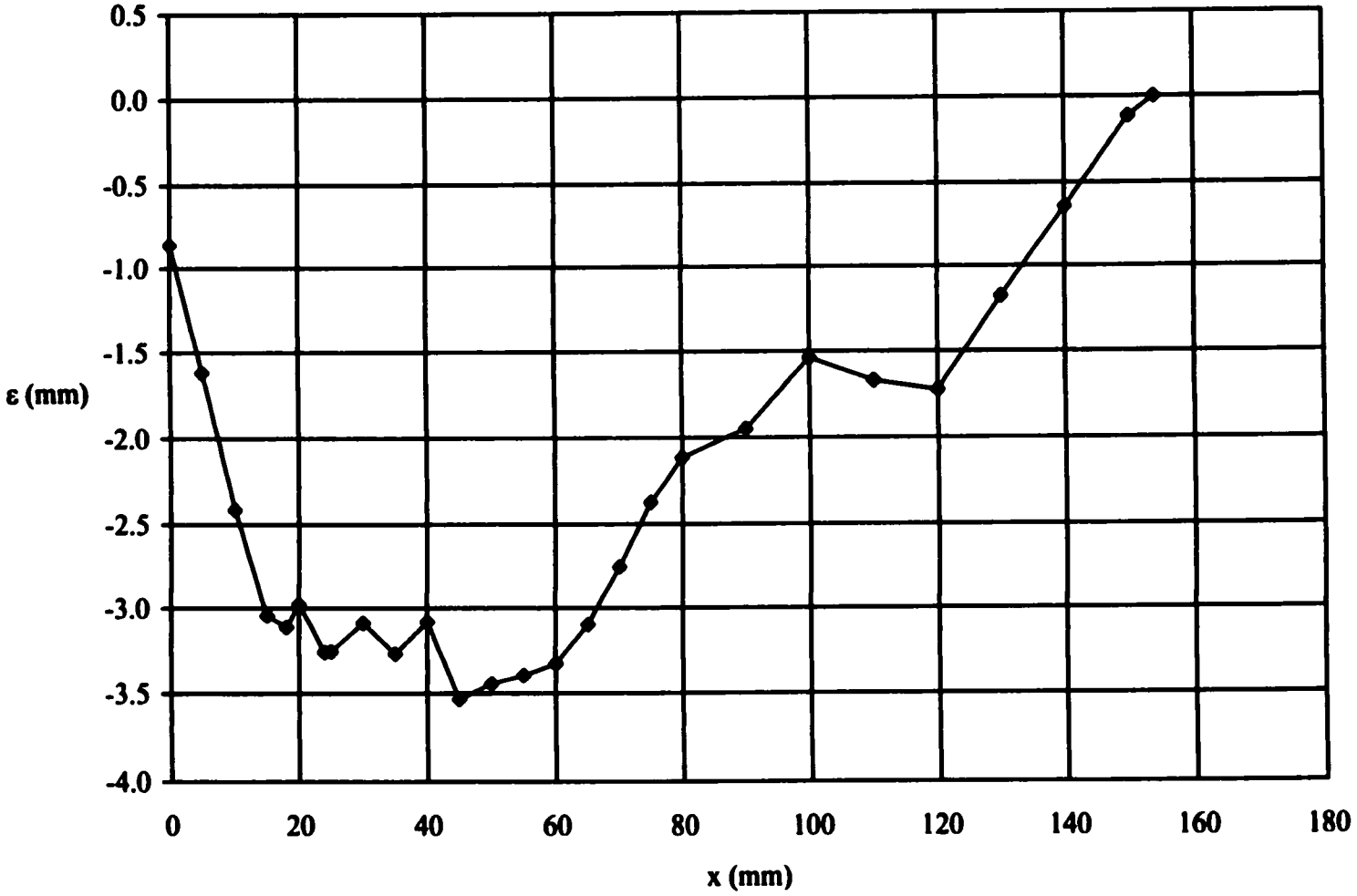

Fig. B-14 Scour hole profiles-Mazurek's test 18.

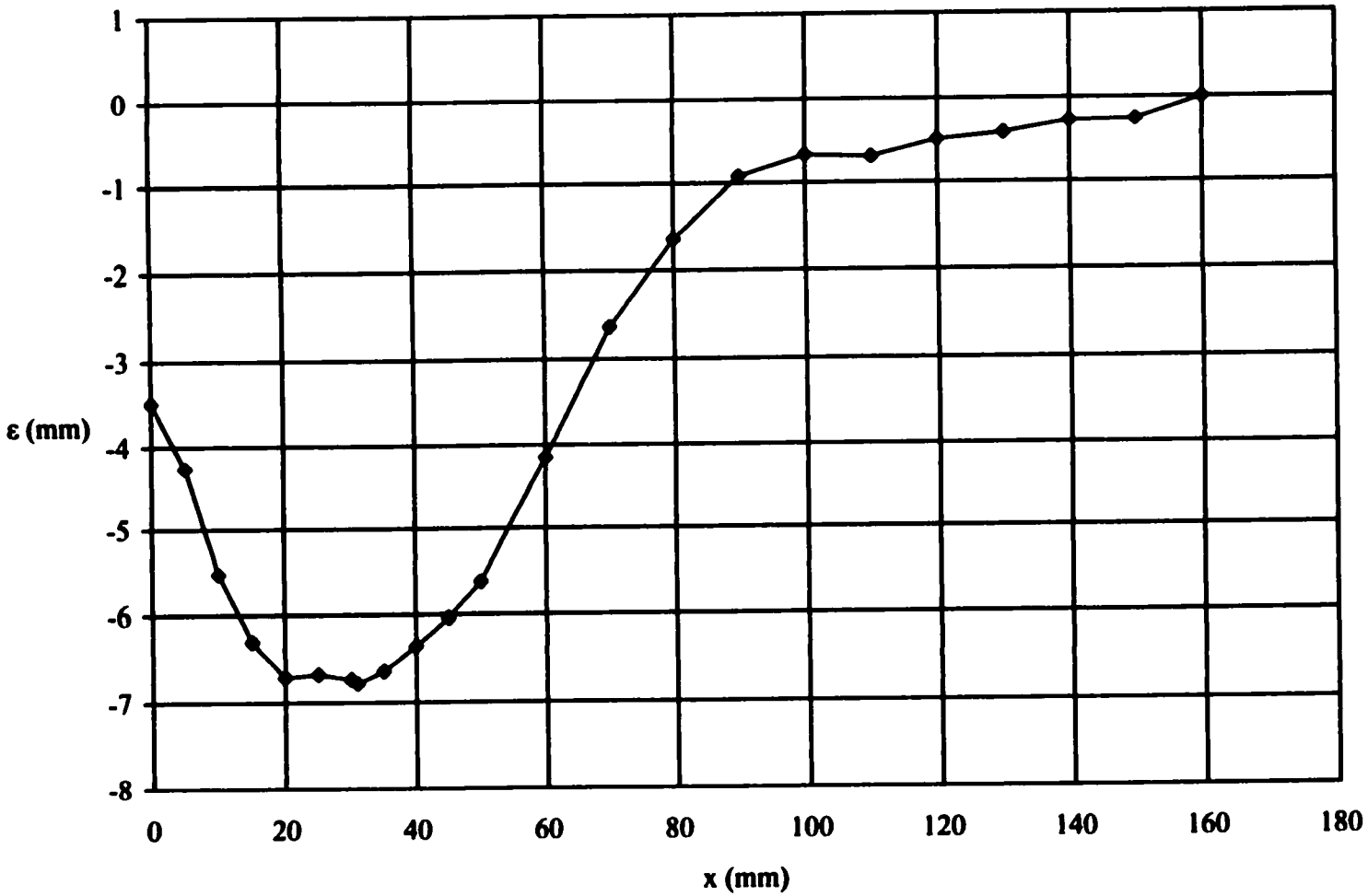

Fig. B-15 Scour hole profiles-Mazurek's test 19.

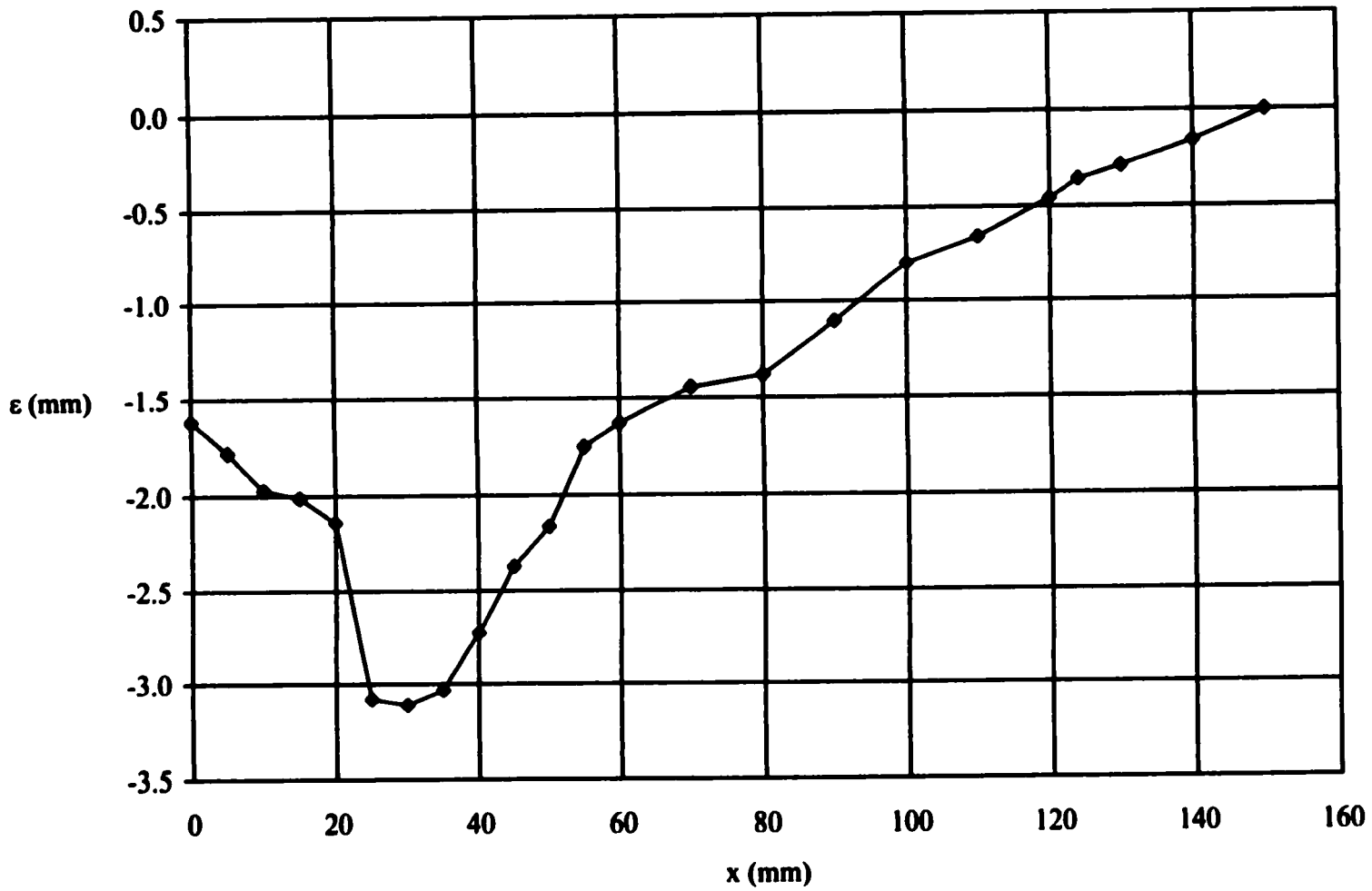

Fig. B-16 Scour hole profiles-Mazurek's test 20.

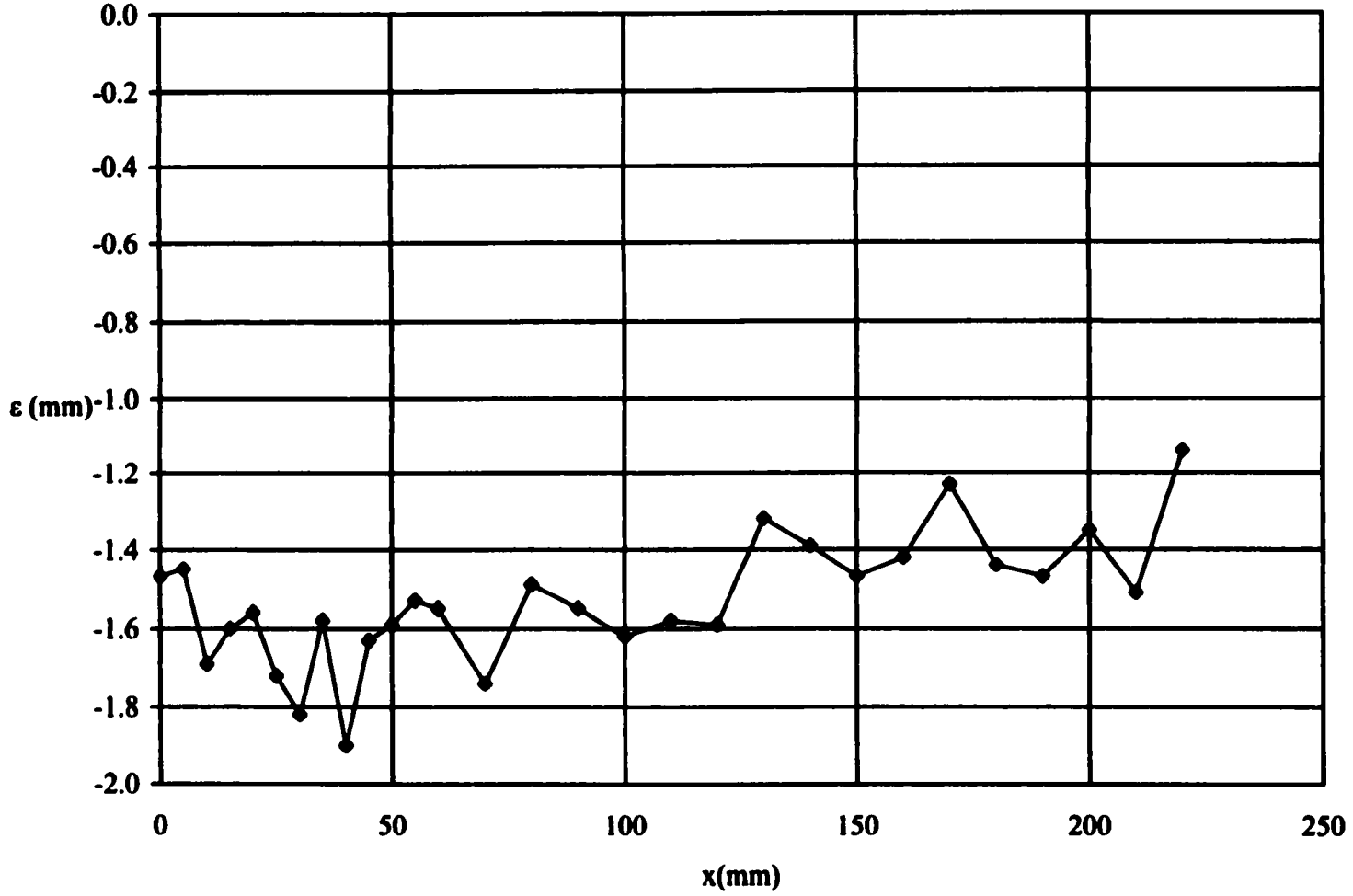

Fig. B-17 Scour hole profiles-Mazurek's test 21.

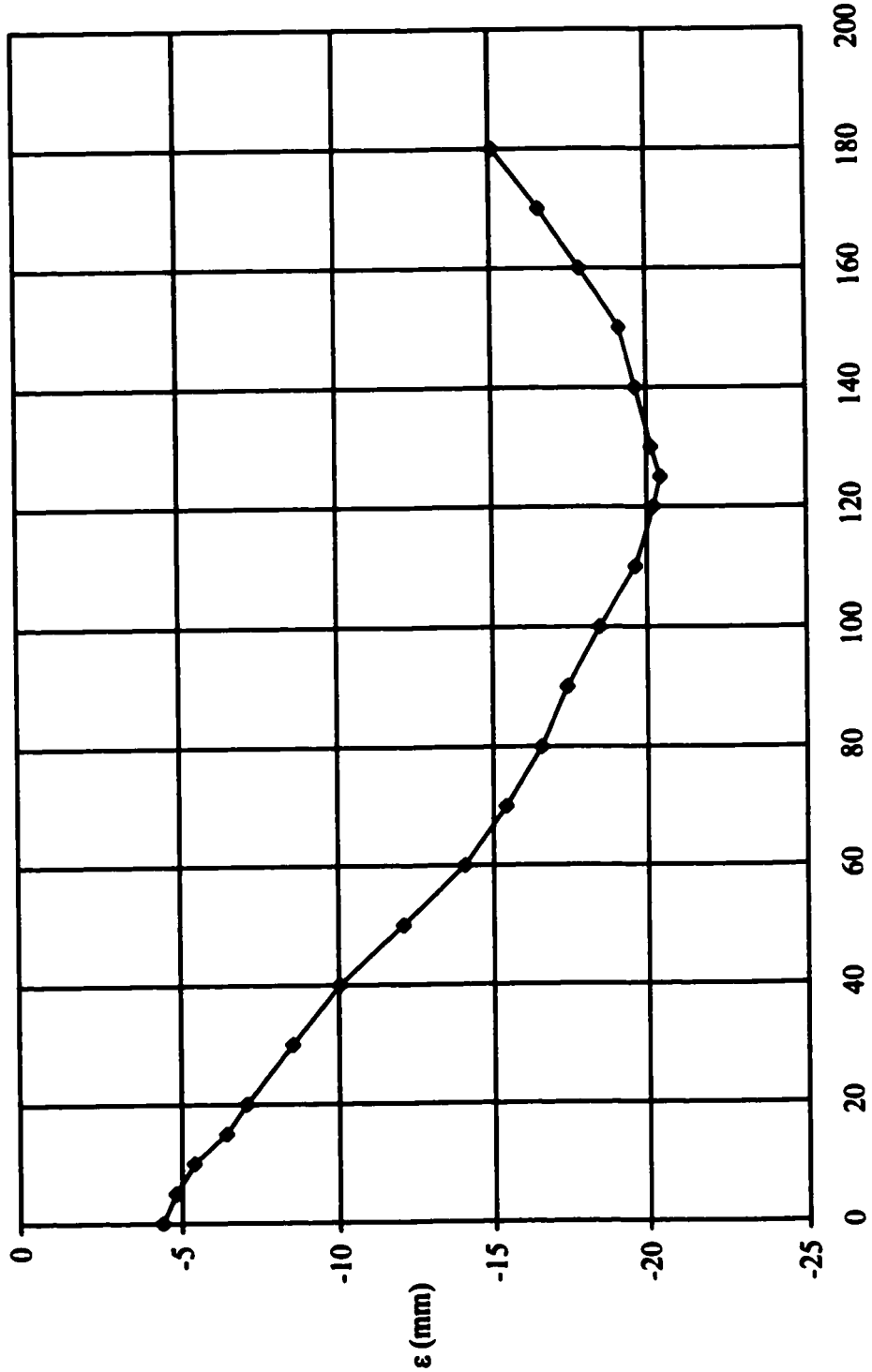

Fig. B-18 Scour hole profiles-Mazurek's test 22.

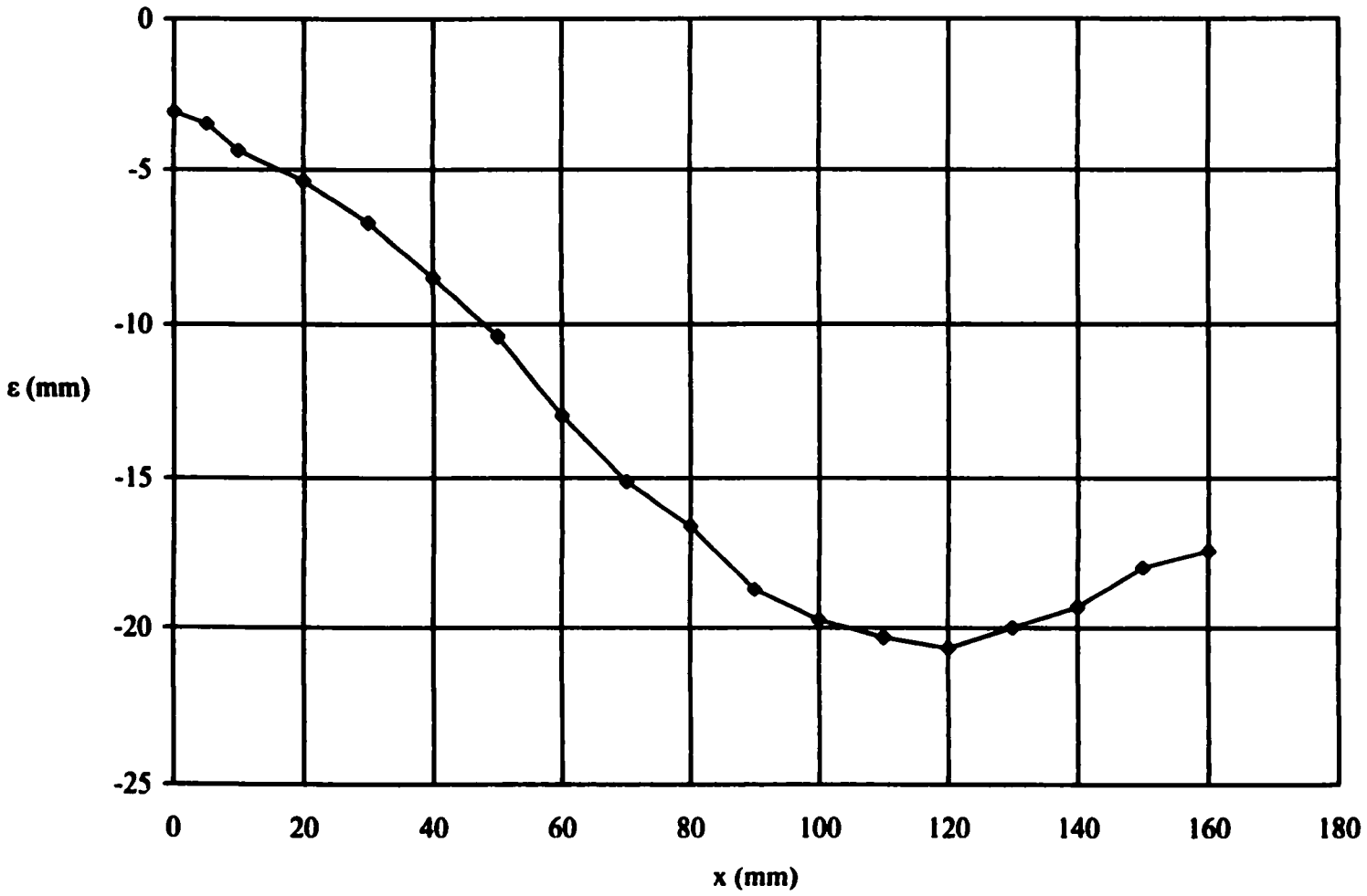

Fig. B-19 Scour hole profiles-Mazurek's test 23.

Appendix C Scour Hole Profiles at Four Different Time Scales (Abt's Data)

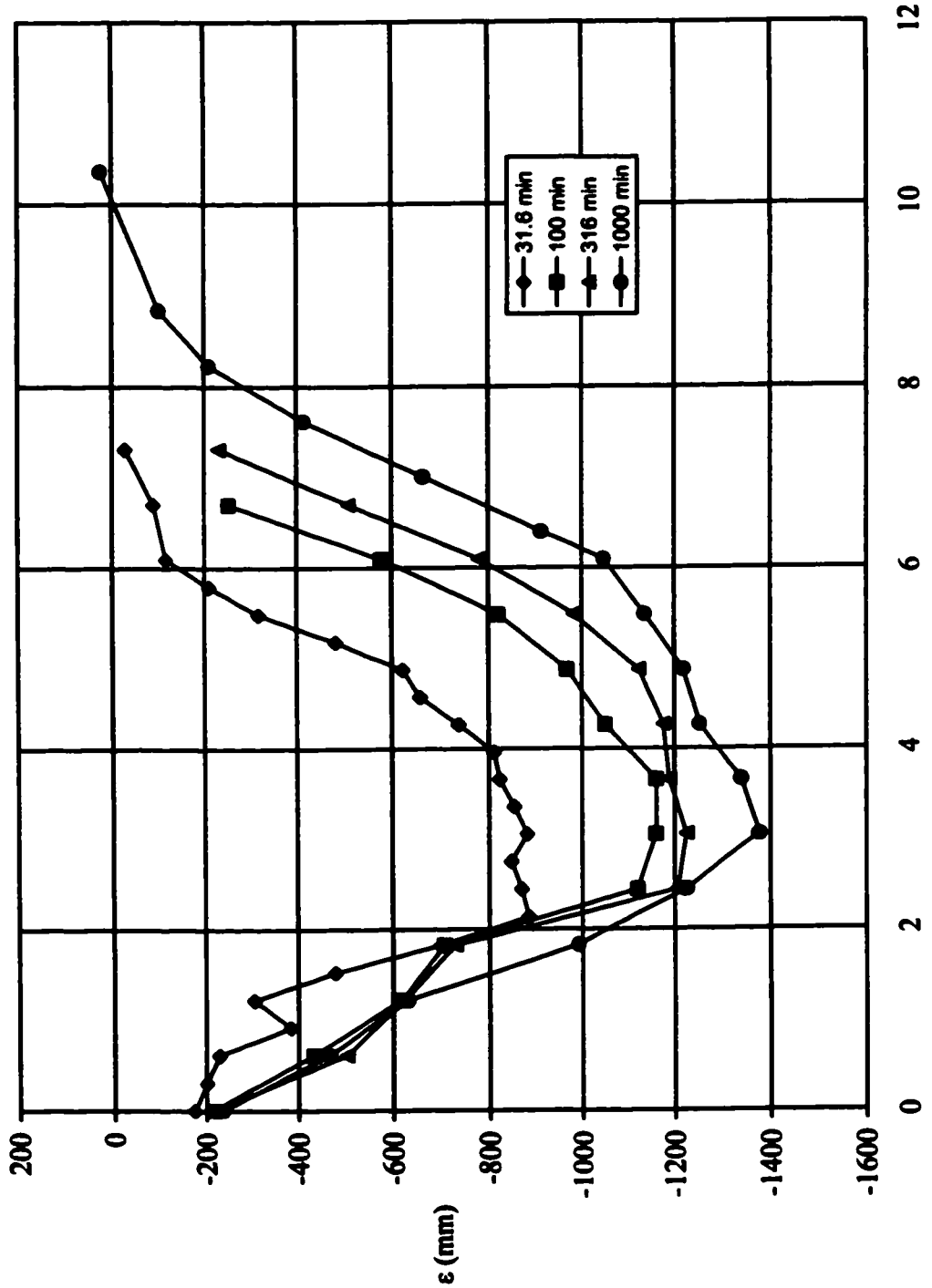

Fig. C-1 Scour hole profiles along centreline-Abt's test 26.

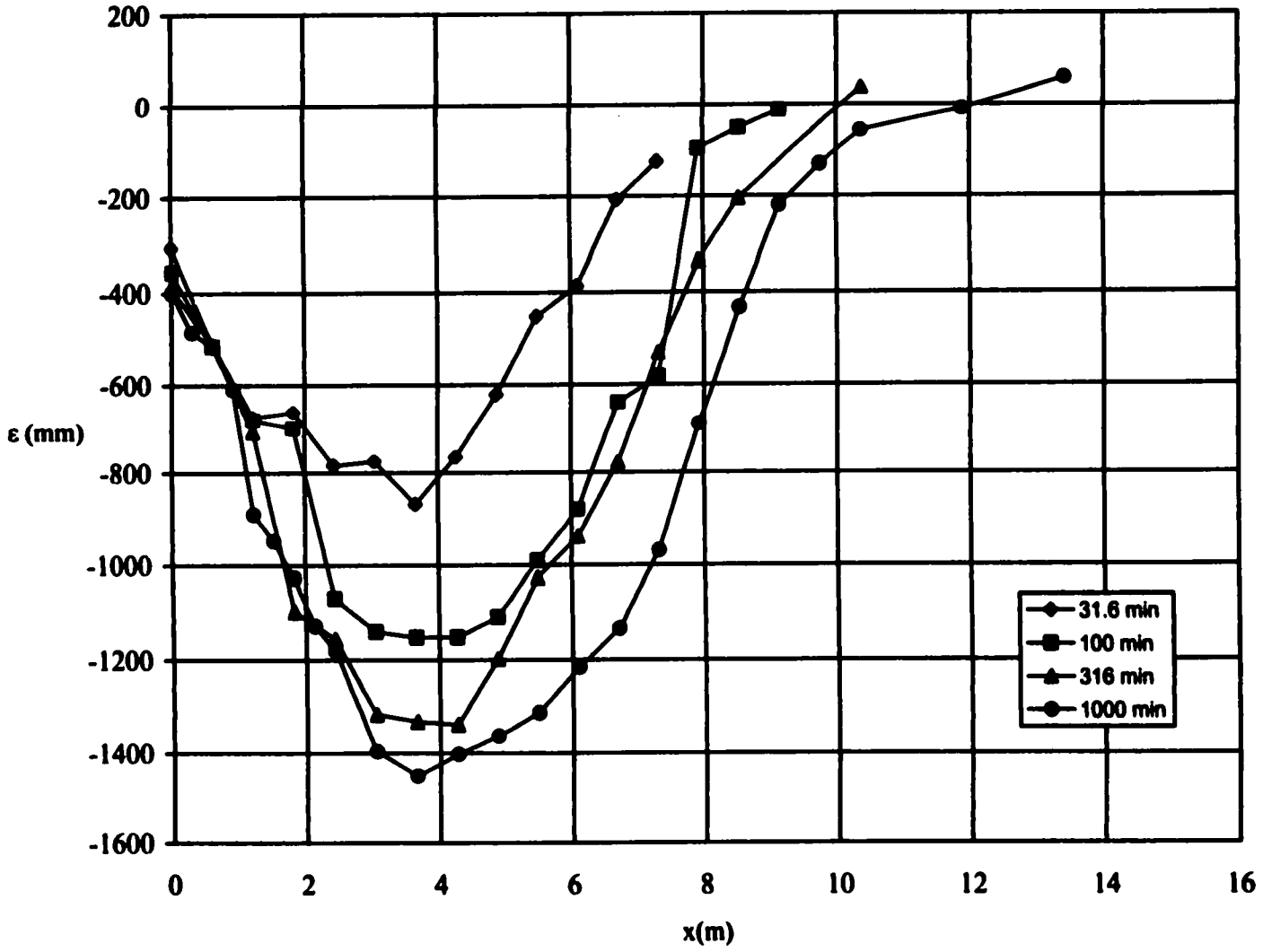

Fig. C-2 Scour hole profiles along centreline-Abt's test 28.

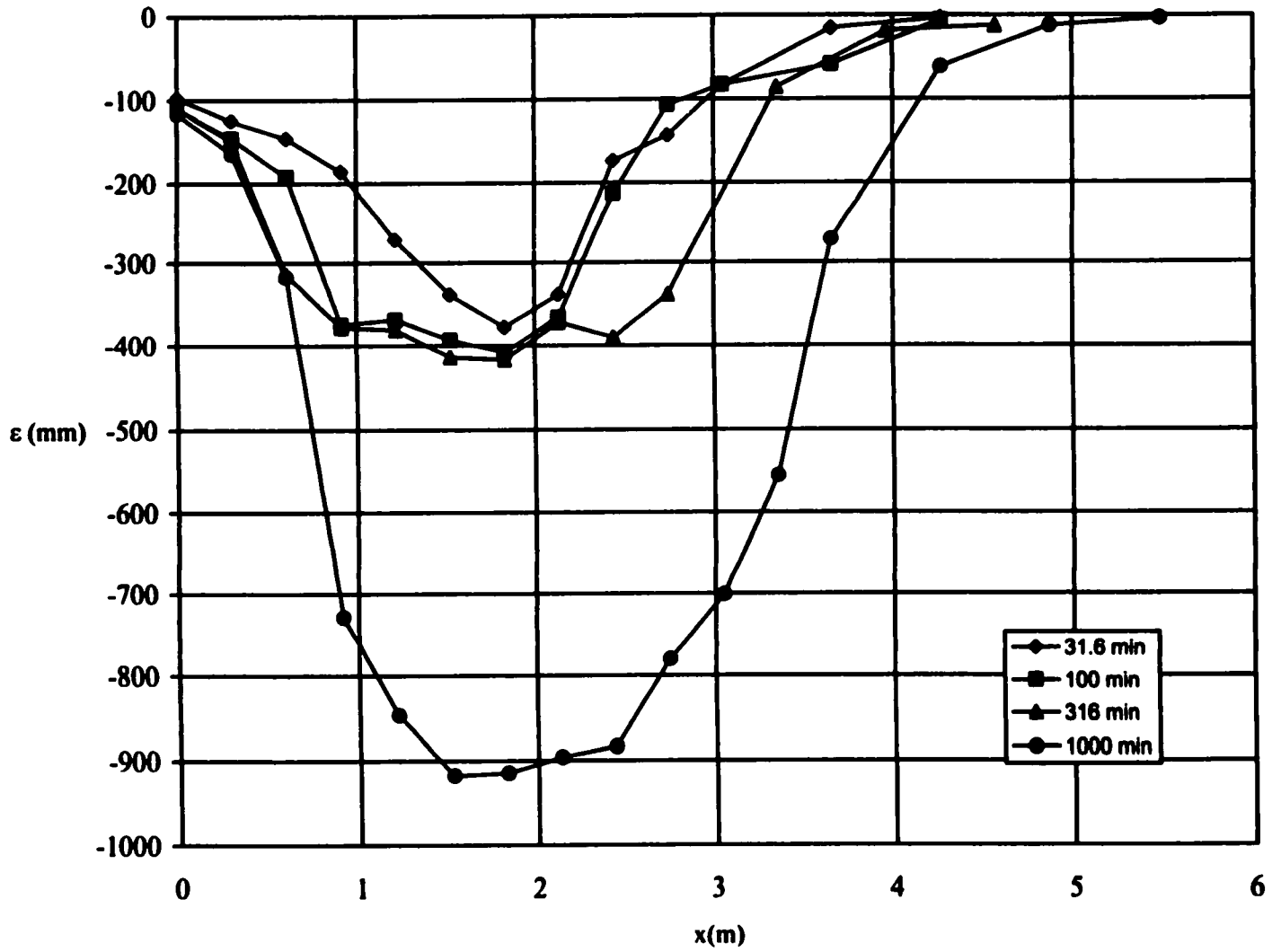

Fig. C-3 Scour hole profiles along centreline-Abt's test 30.

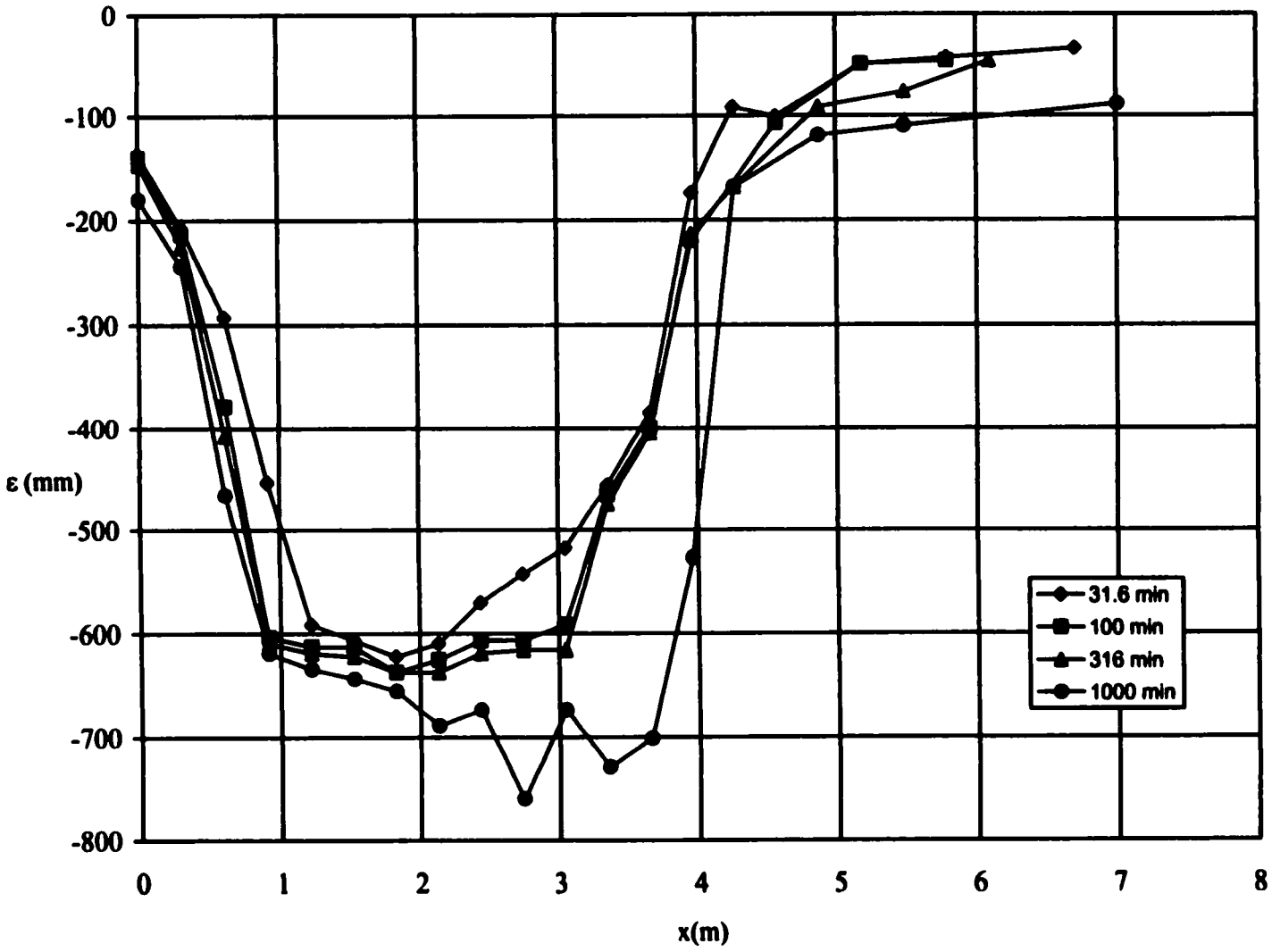

Fig. C-4 Scour hole profiles along centreline-Abt's test 31.

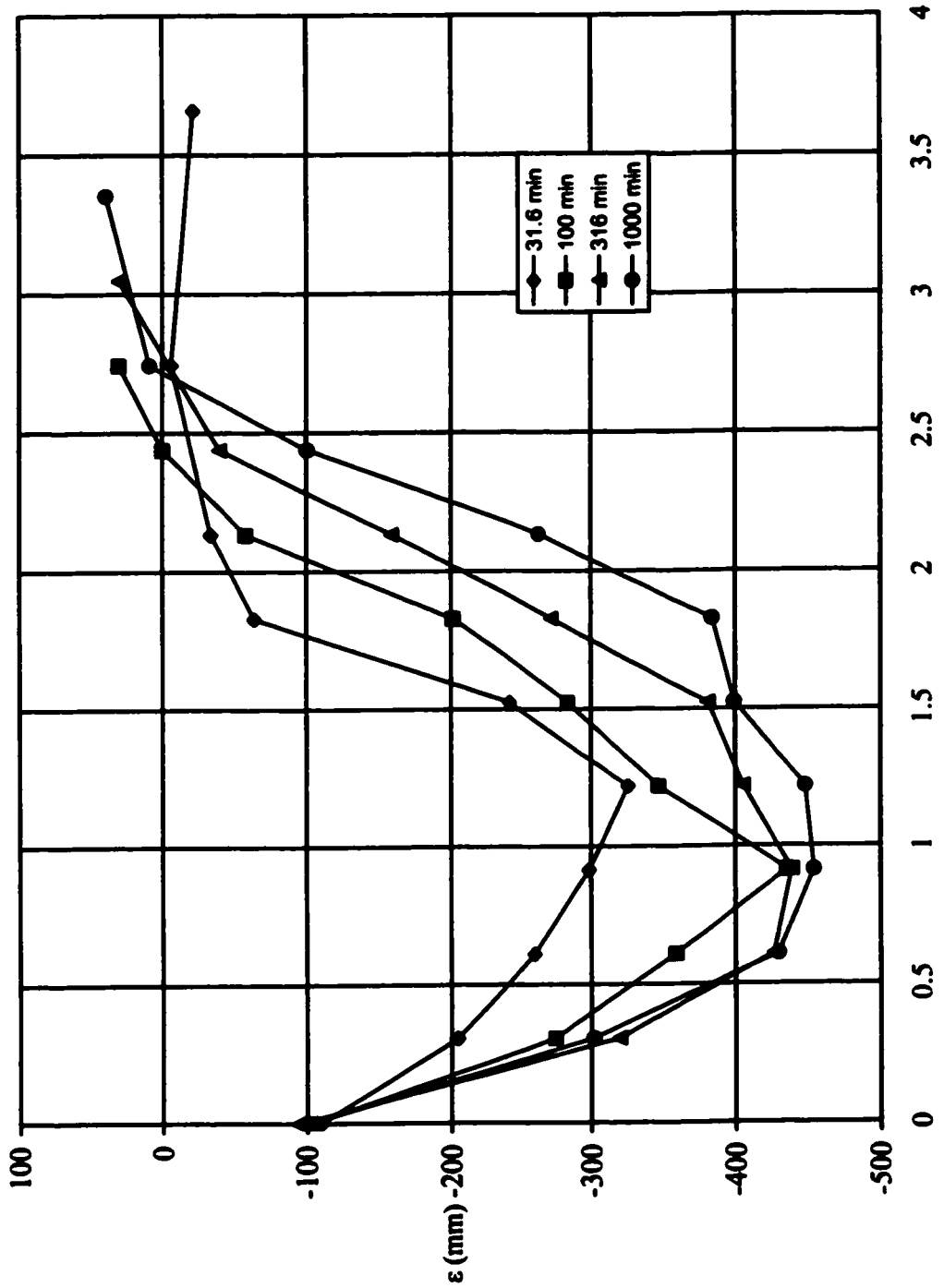

Fig. C-5 Scour hole profiles along centreline-Abt's test 33.

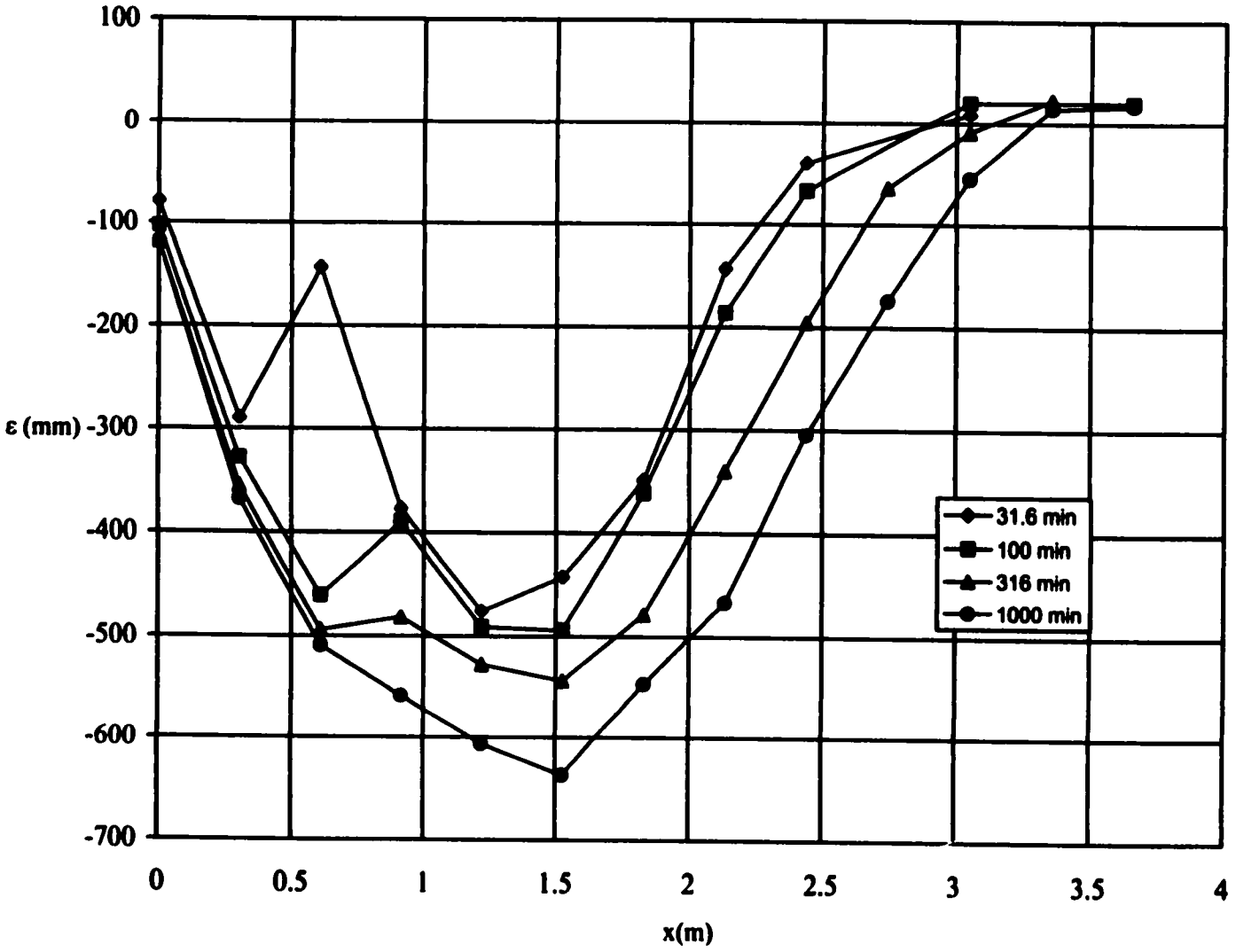

Fig. C-6 Scour hole profiles along centreline-Abt's test 34.

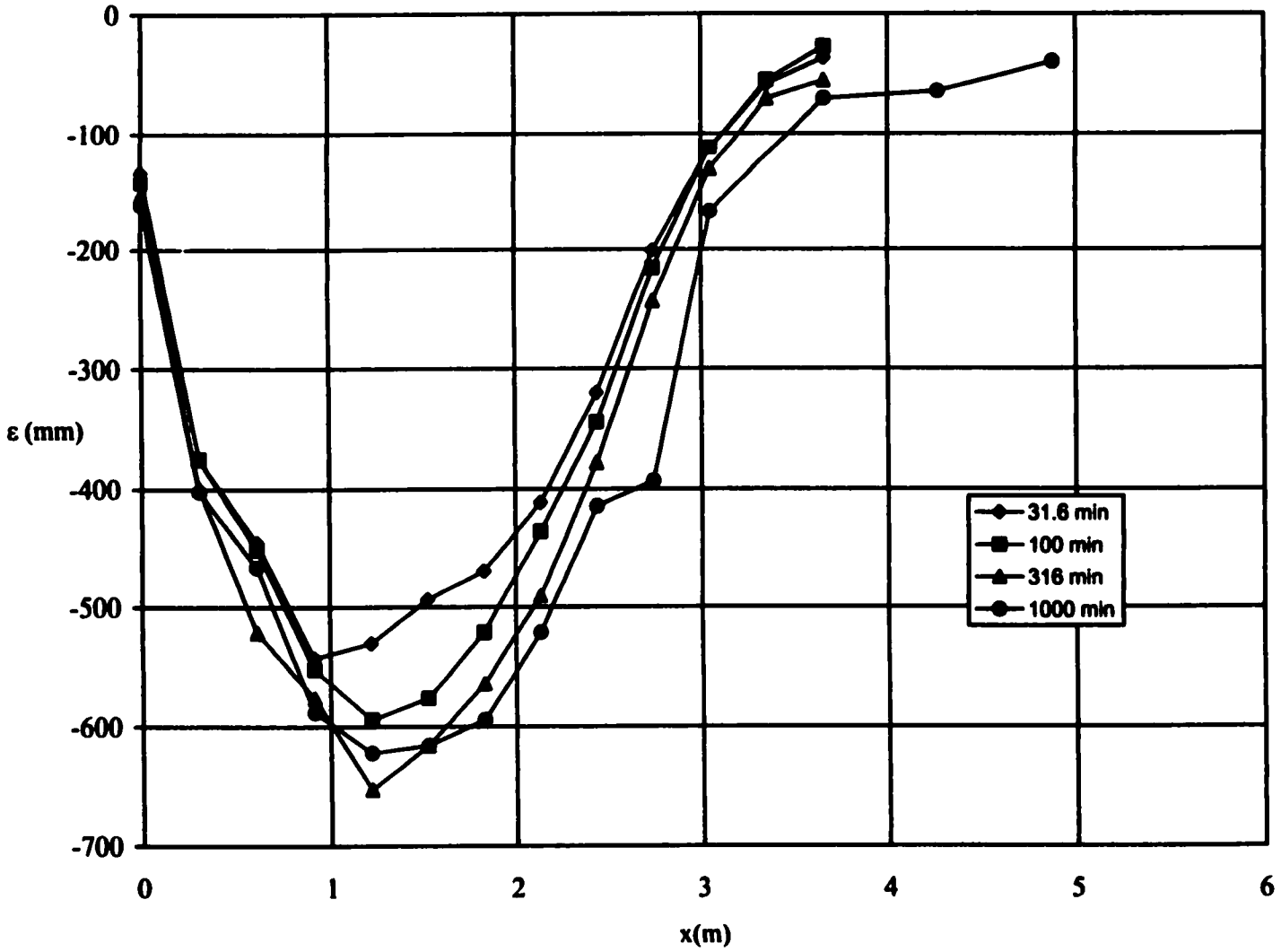

Fig. C-7 Scour hole profiles along centreline-Abt's test 35.

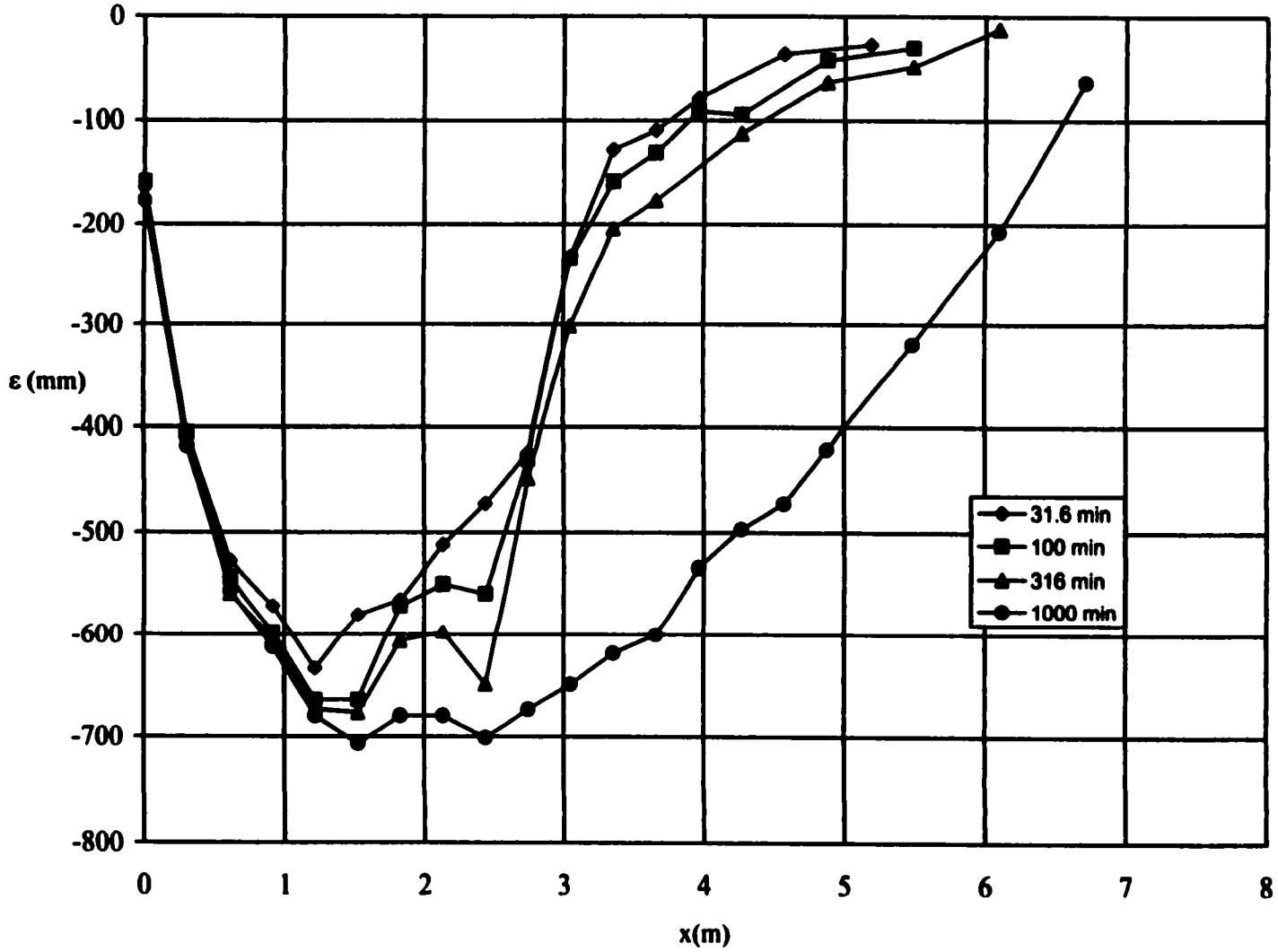

Fig.C-8 Scour hole profiles along centreline-Abt's test 36.

Appendix D Dimensional Scour Hole Profiles at Four Different Times (Abt's Data)

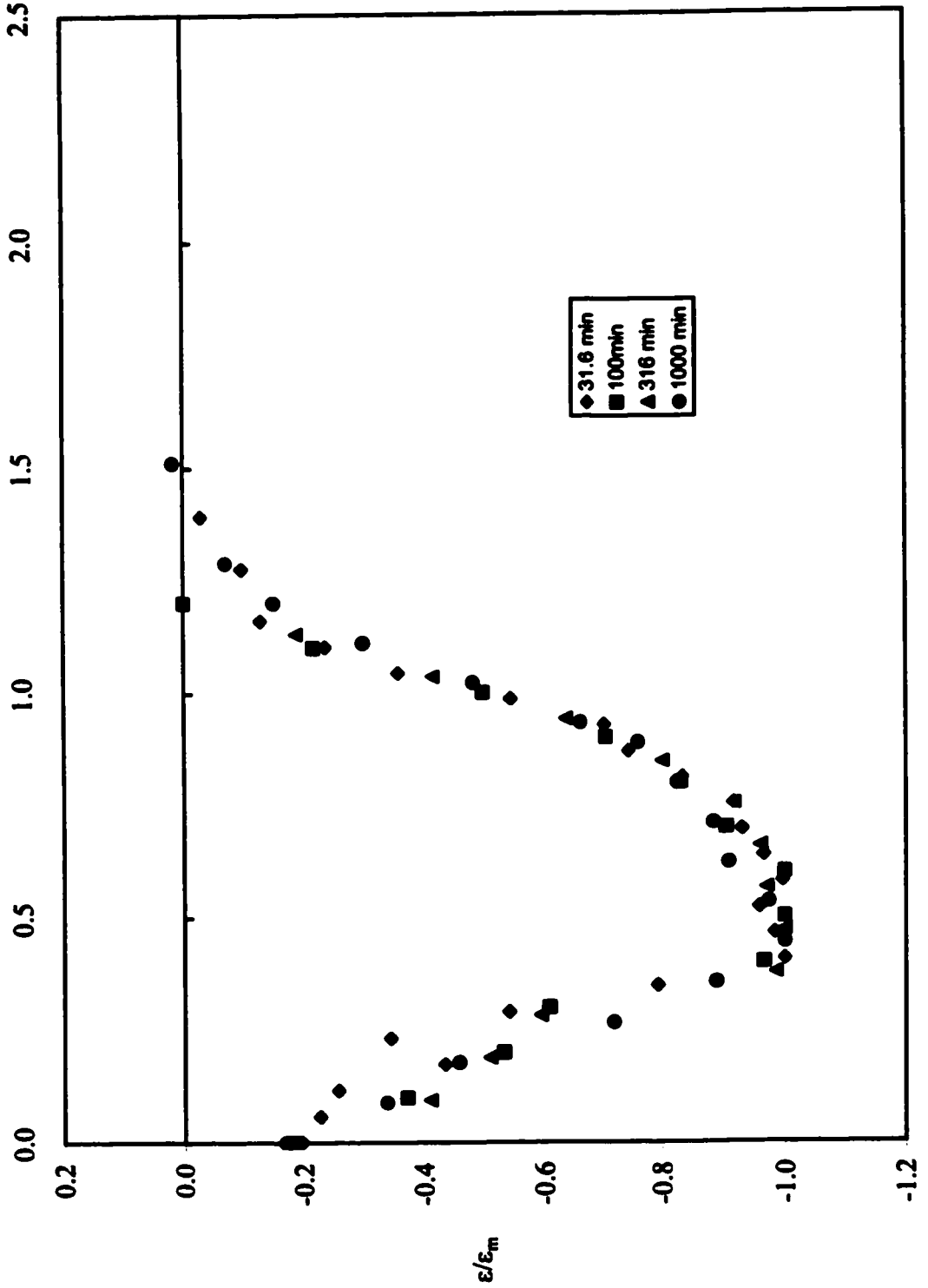

Fig. D-1: Dimensionless Scour Profile-Abt's test 26.

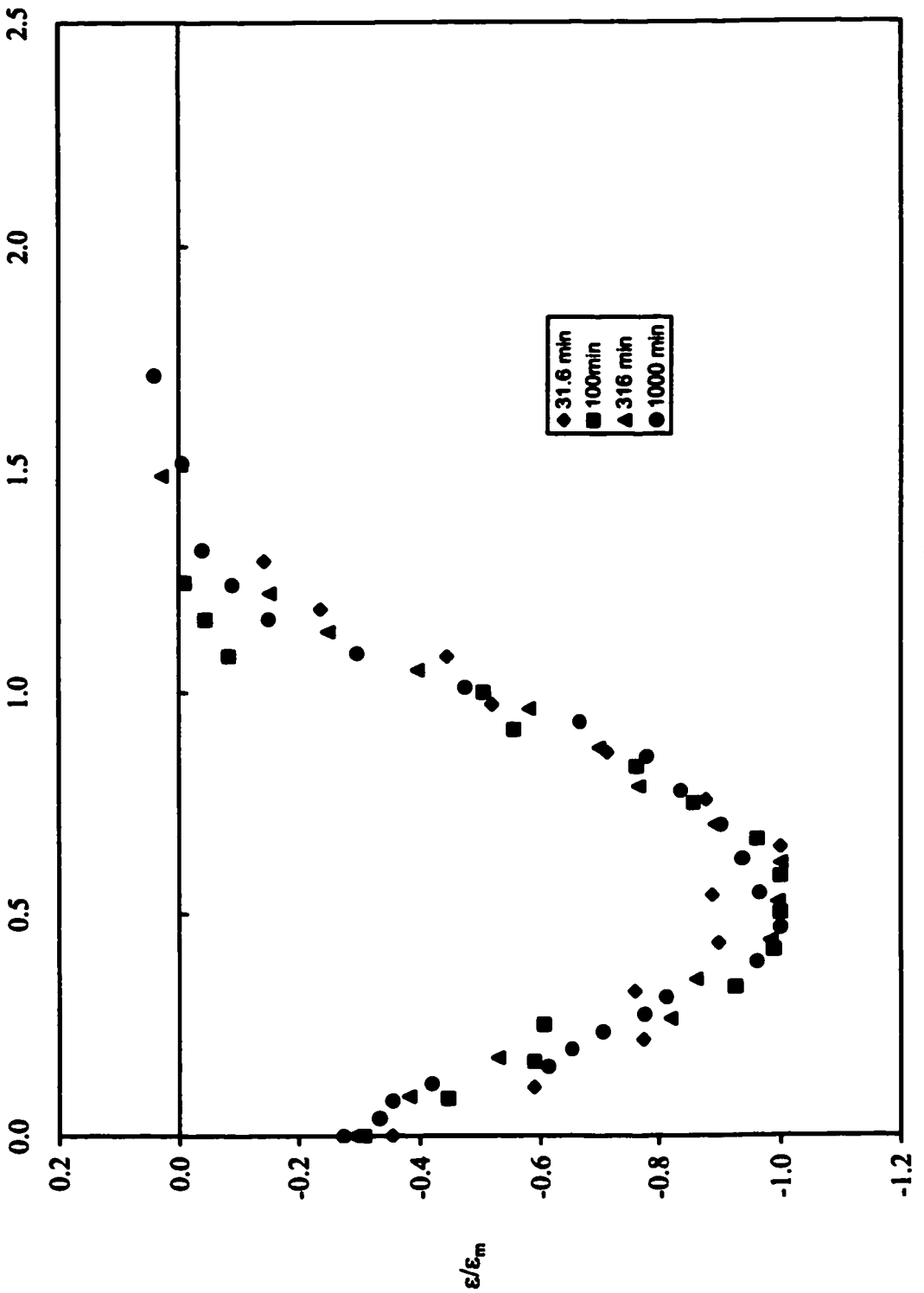

Fig. D-2 Dimensionless Scour Profile-Abt's test 28.

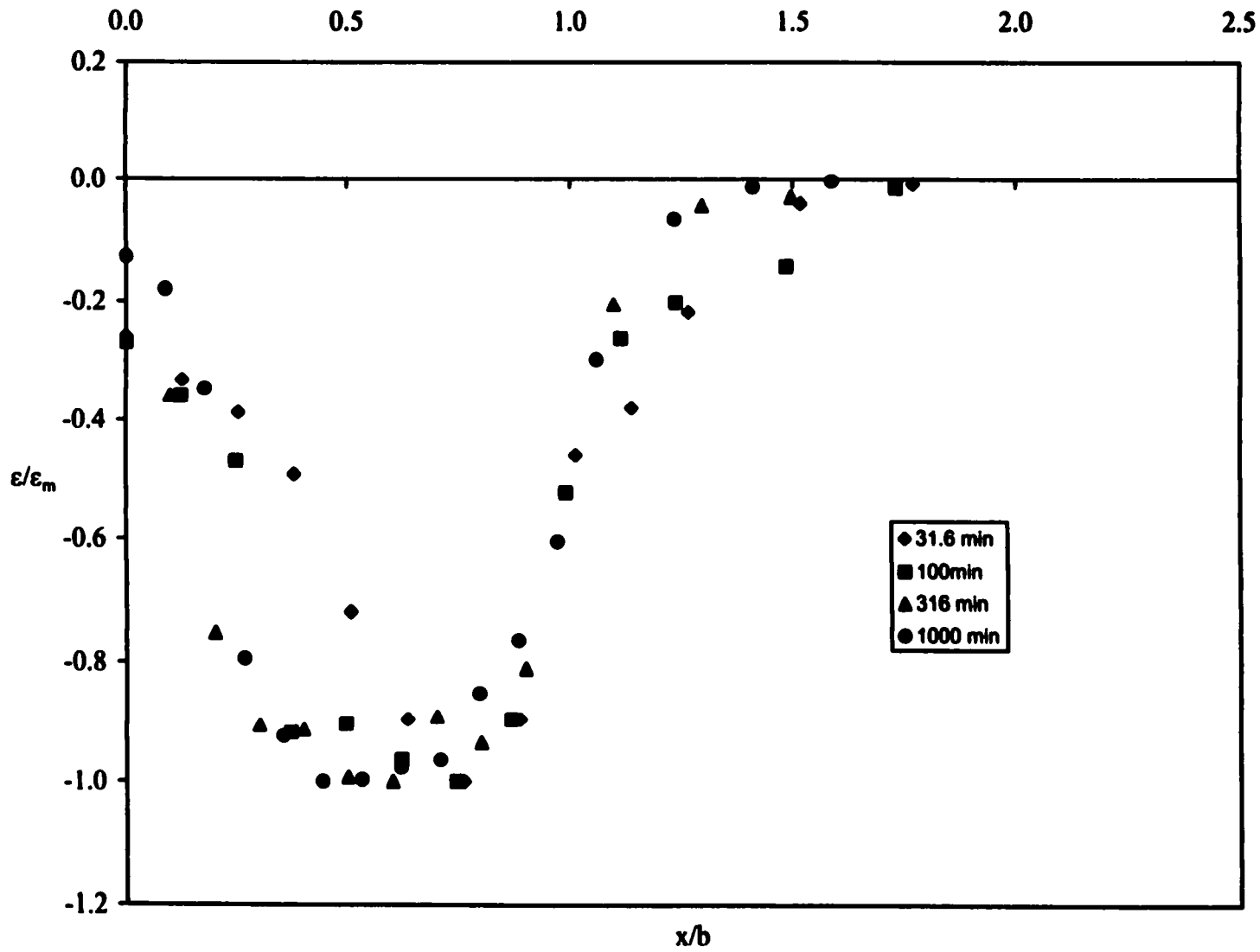

Fig. D-3 Dimensionless Scour Profile-Abt's test 30.

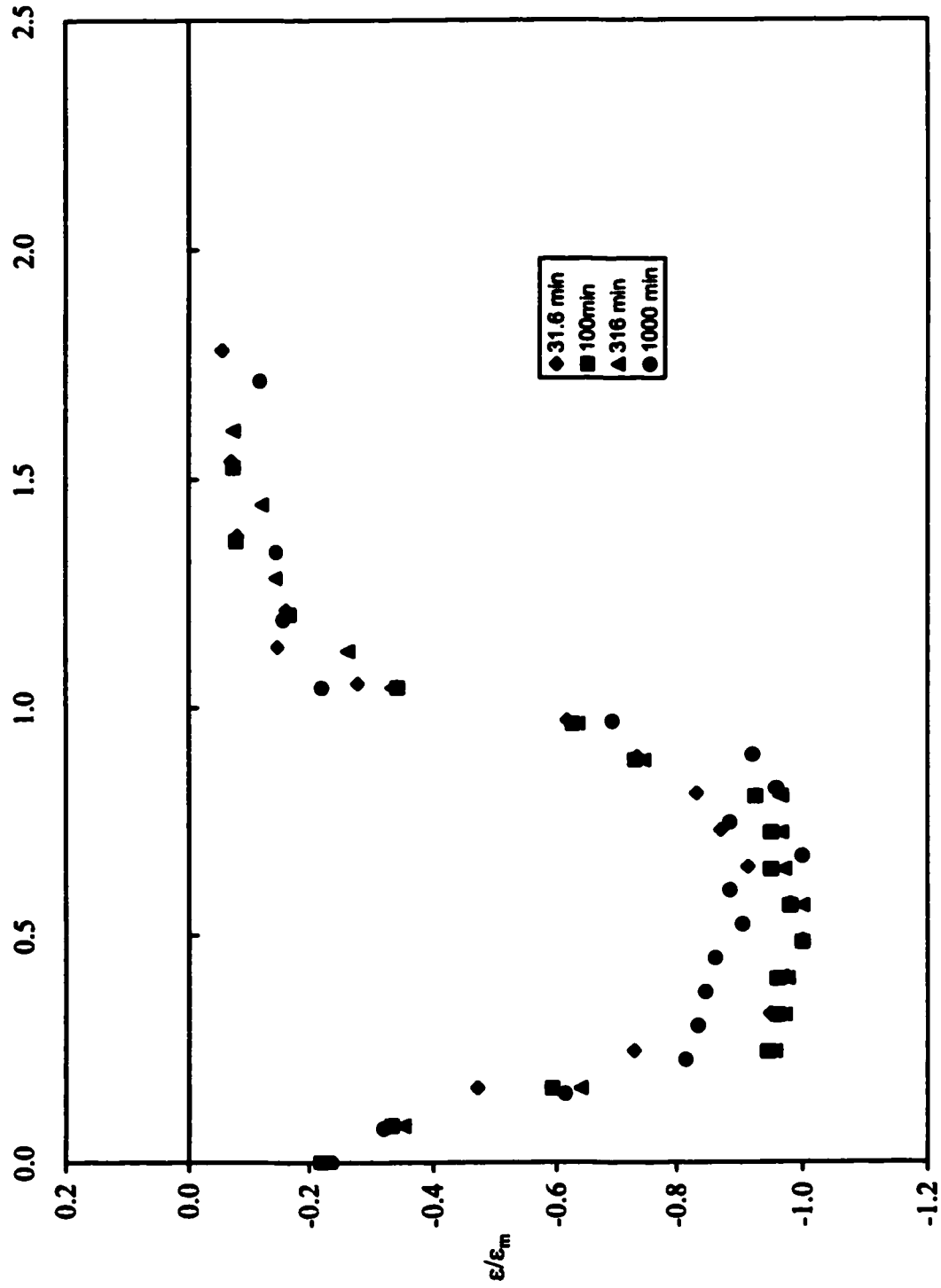

Fig. D-4 Dimensionless Scour Profile-Abt's test 31.

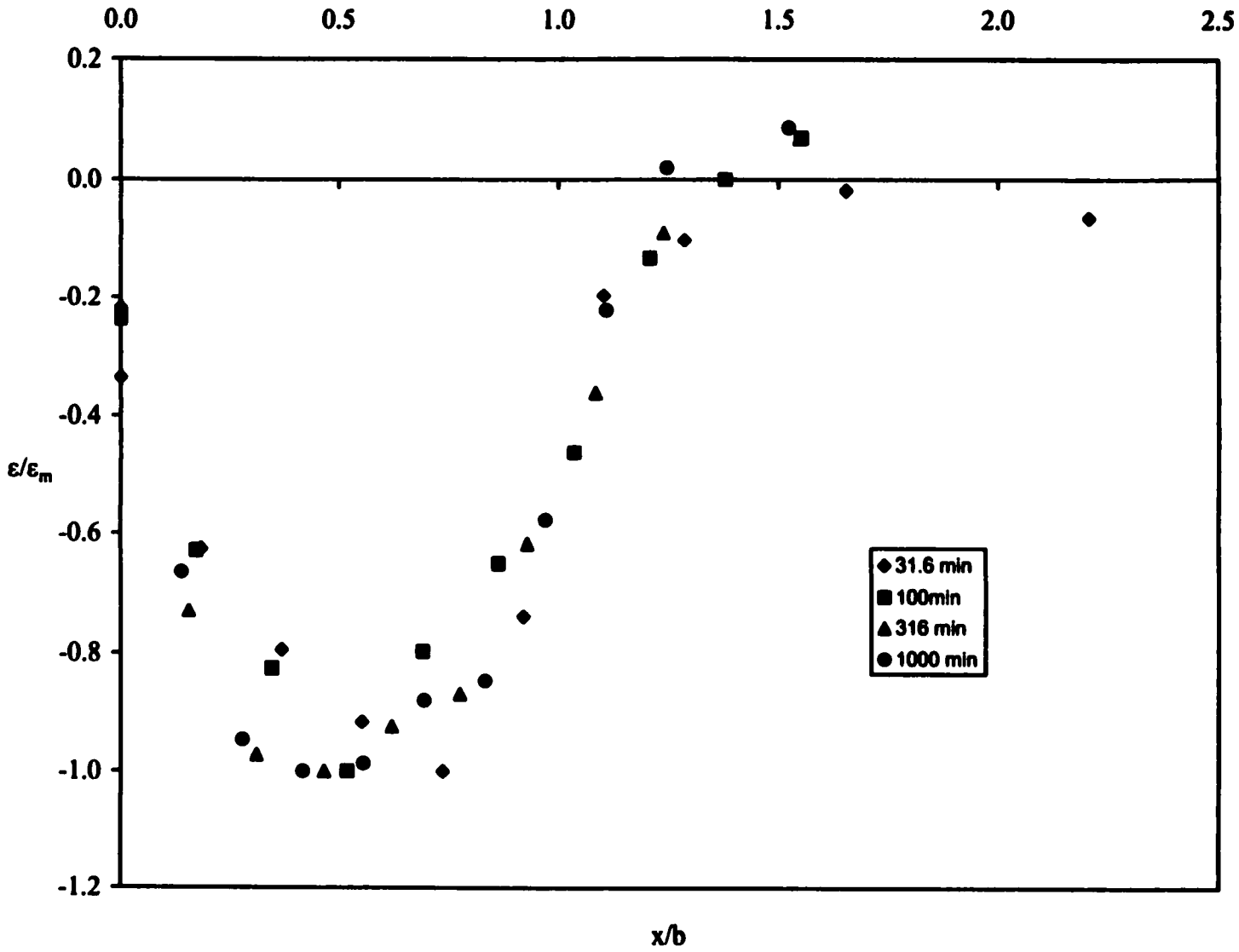

Fig. D-5 Dimensionless Scour Profile-Abt's test 33.

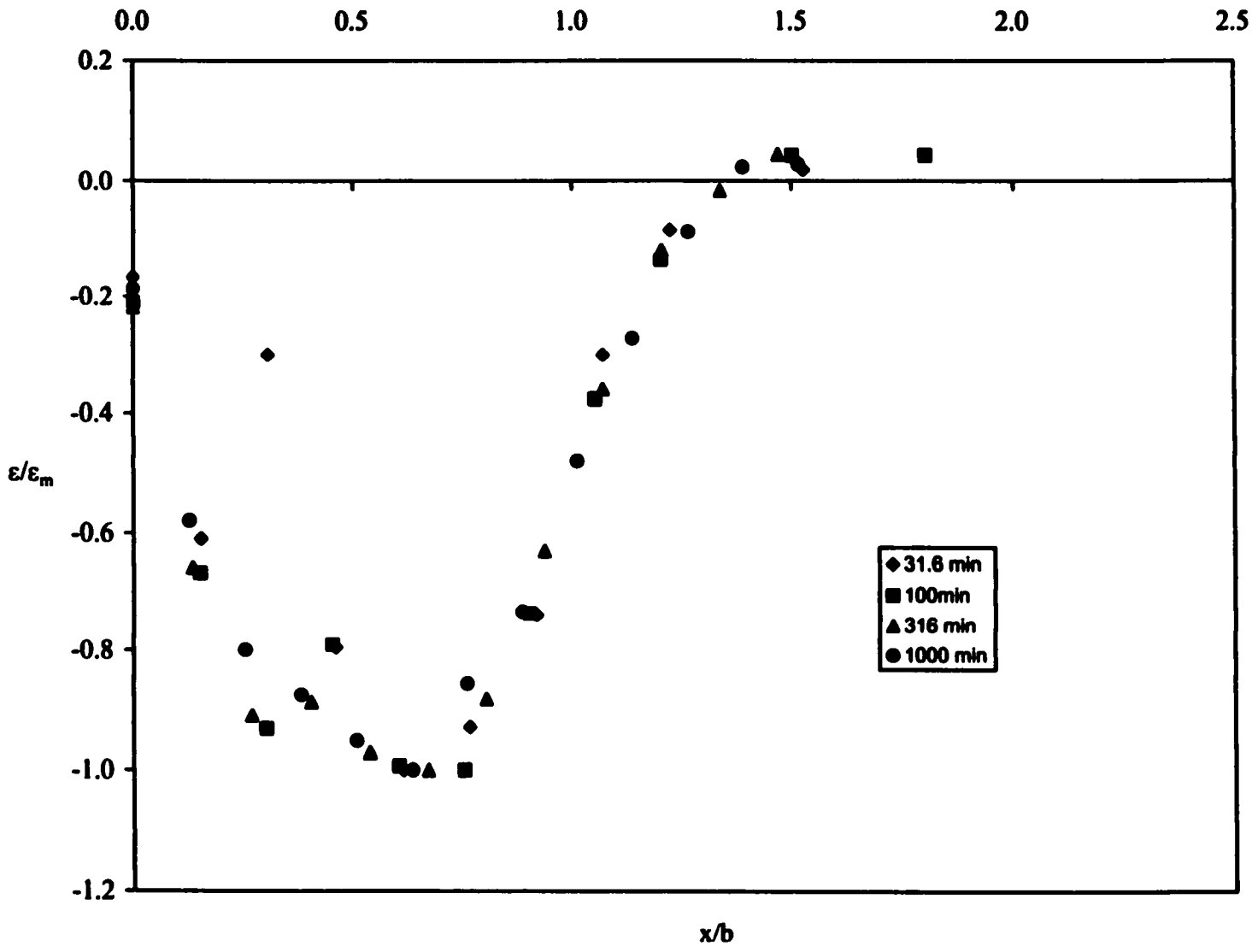

Fig. D-6 Dimensionless Scour Profile-Abt's test 34.

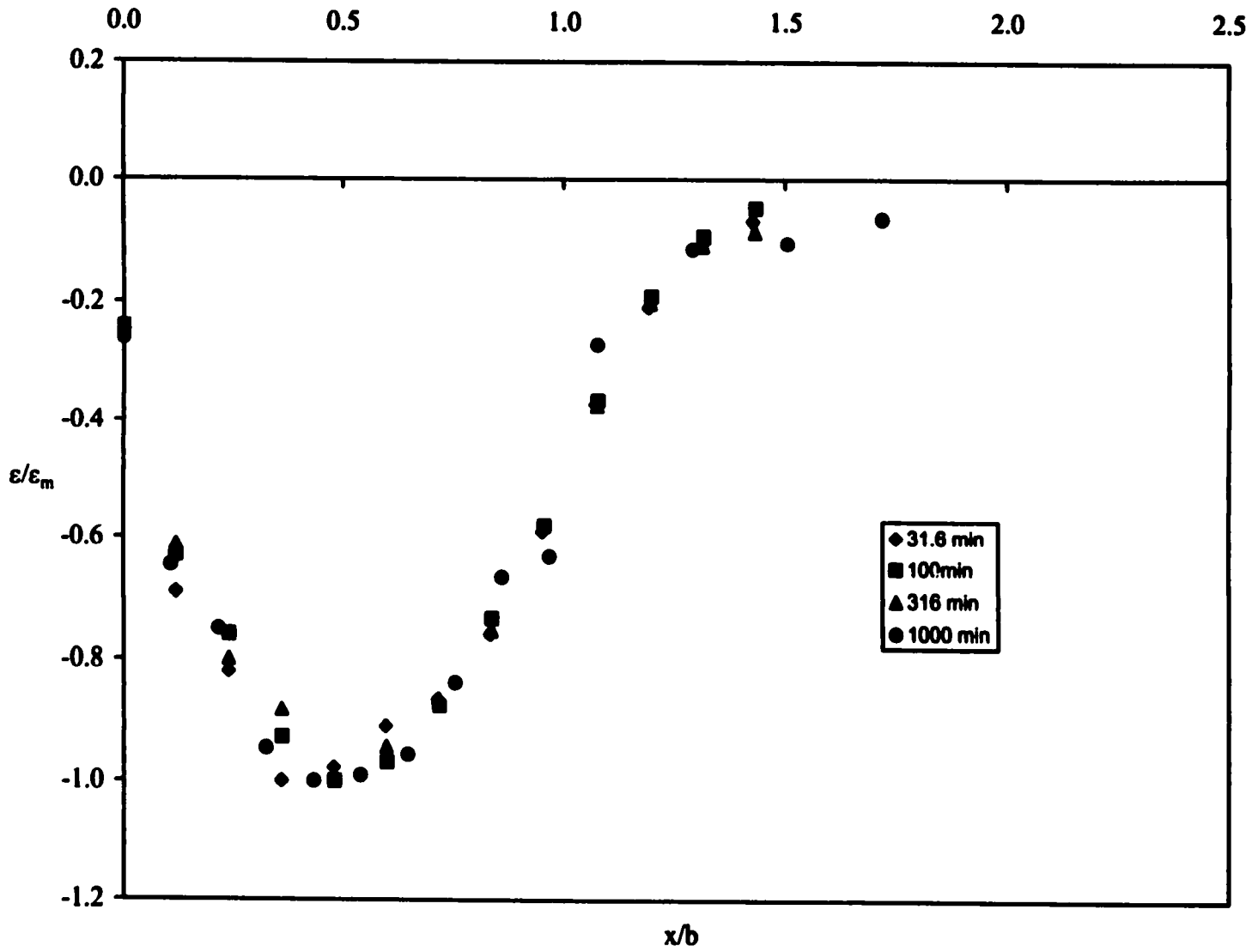

Fig.D-7 Dimensionless Scour Profile-Abt's test 35.

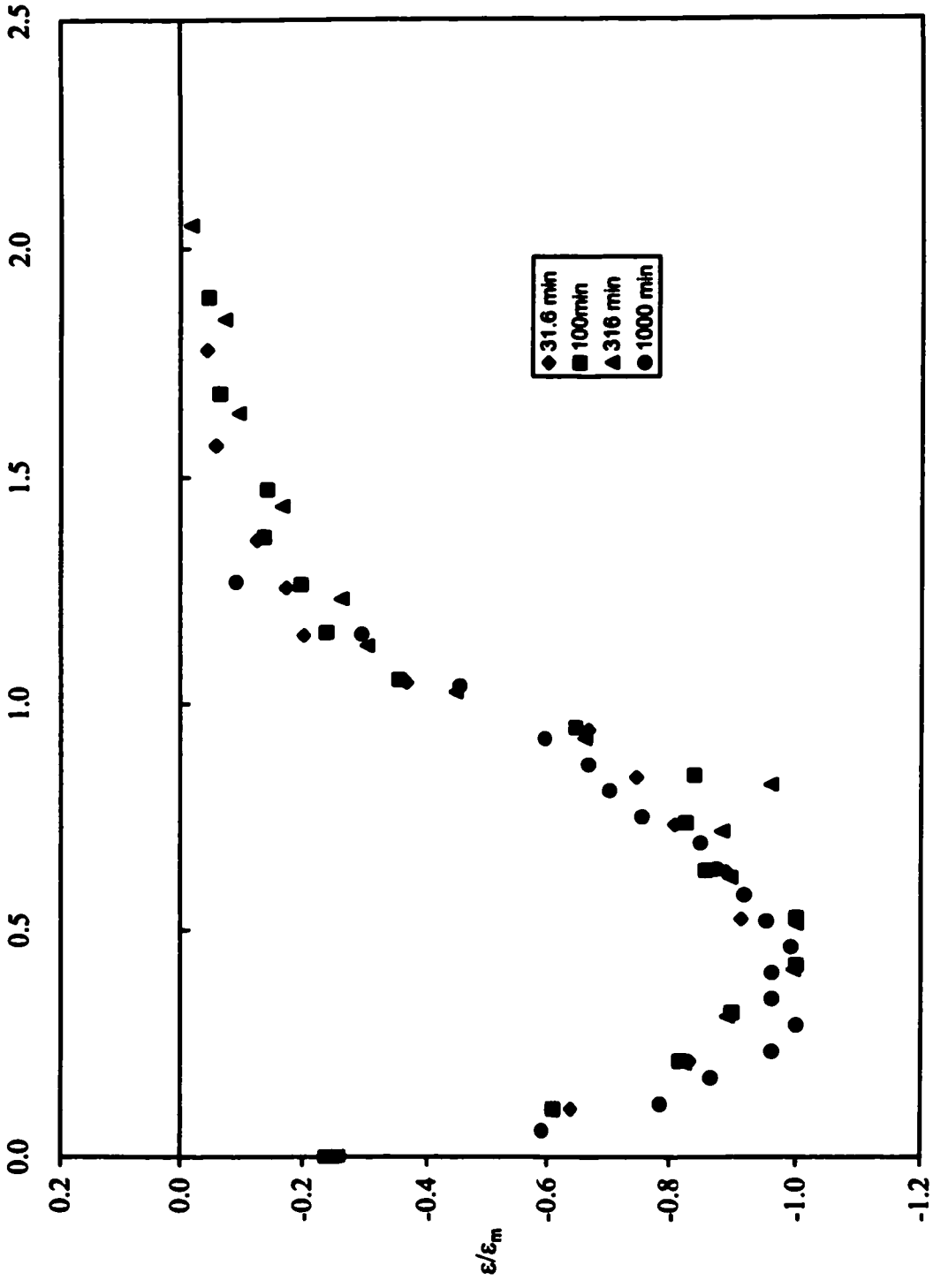

Fig. D-8 Dimensionless Scour Profile-Abt's test 36.

VITA AUTHORIS

Ye Liu was born in 1973 in Zhuolu, People's Republic of China. She obtained a Master degree in Engineering in 1997. She is currently a candidate for the Master degree of Applied Science at the University of Windsor, Canada.